SEAFLOOR MORPHOLOGY AND SEDIMENTARY PROCESSES IN KNIGHT INLET, BRITISH COLUMBIA

by

Ping Ren
B.Sc., Hangzhou University, the People's Republic of China, 1982

A Thesis Submitted in Partial Fulfilment of the
requirements for the Degree of

MASTER OF SCIENCE

in the School of Earth & Ocean Sciences

We accept this thesis as conforming
to the required standard

ACCEPTED
FACULTY OF GRADUATE STUDIES

[redacted]
DEAN

DATE Sept. 28/92

[redacted]
Dr. B.D. Bornhold, Supervisor (School of Earth & Ocean Sciences)

[redacted]
Dr. E. Van der Flier-Keller, Departmental Member (School of Earth & Ocean Sciences)

[redacted]
Dr. V. Tunnicliffe, Outside Member (Department of Biology)

[redacted]
Dr. B. Hart, External Examiner (Pacific Geoscience Centre)

University of Victoria

Supervisor: Dr. Brian D. Bornhold

ABSTRACT

This study focuses on the interpretation of seafloor morphology and sedimentary distribution, particularly as related to seabed currents - turbidity currents - in Knight Inlet, British Columbia, Canada. The study is based on acoustic imagery and sediment sampling in the upper part of the fjord and on a comparison with a nearby similar and well studied fjord, Bute Inlet.

The seafloor morphology map compiled in this study shows that while the upper part of Knight Inlet resembles in many respects other British Columbia fjords (e.g. Bute Inlet), it differs in that a great many channels emanate from the intertidal zone opposite the river mouths to coalesce ultimately into a few and finally one channel farther down-inlet. In Bute Inlet only one channel emerges opposite each of the two fjord-head rivers; these join a short distance down-slope to form a single incised channel. In both systems sand-transporting turbidity currents are responsible for creating a major channel system; in Knight Inlet these channels are up to 40 m deep and up to 300 m wide continuing 41 km down the inlet. The seafloor morphology can be divided into four zones which reflect not only seabed character but also the interpreted flow characteristics of turbidity currents.

Laboratory sediment analysis of 50 grab samples and 97 core subsamples shows a general distal fining in the upper part of Knight Inlet with sand and muddy

sands being confined essentially to the channel system.

A close relationship was found between turbidity current events, as measured by Turbidity Events Detectors installed between April 9, 1991 and October 16, 1991, and river discharge peaks on the Klinaklini River at the head of the inlet. Fluvial suspended matter concentrations associated with such floods are not believed to be sufficient to produce turbidity currents directly. Rather, it is believed that river mouth bars which accumulate during periods of low river flow are destroyed by the floods and the coarse sediments swept onto the adjacent steep, unstable delta front. Failures on the delta front give rise to the coarse-grained turbidity currents which continue down the inlet.

Calculated turbidity current velocities and densities, based on channel morphology, are between 60 and 400 cms^{-1} and 1.024 - 1.048 gcm^{-3}, respectively based on an assumed friction coefficient of 0.0029; these results are comparable to those obtained in Bute Inlet. Analysis of variations in turbidity current density ρ_t and sediment discharge Q_s shows that the turbidity currents erode the seafloor in Zone One and the upper part of Zone Two but deposit sediment on the seafloor in the lower part of Zone Two and in Zone Three. Thus the channel system in Zone Three must have been subjected to either an earlier period of intense erosion or, at the present time, to periodically large turbidity currents in order to account for the infilling of the channel in the distal part of the system.

Examiners:

[redacted]

Dr. B.D. Bornhold, Supervisor (School of Earth & Ocean Sciences)

[redacted]

Dr. E. Van der Flier-Keller, Departmental Member (School of Earth & Ocean Sciences)

[redacted]

Dr. V. Tunnicliffe, Outside Member (Department of Biology)

[redacted]

Dr. B. Hart, External Examiner (Pacific Geoscience Centre)

Table of Contents

LIST OF TABLES

Pages

LIST OF FIGURES

Pages

ACKNOWLEDGEMENTS

The author would like to express her appreciation to the many individuals who have made suggestions and aided in the development of this thesis. The author would first of all, like to thank my supervisor Dr. Brian Bornhold for his constant encouragement, patient advice, and complete moral support throughout the course of this thesis. The author would also like to thank Dr. Eileen Van der Flier-Keller for her advice and suggestions. Thanks are extended to the staff at the Pacific Geoscience Centre and in particular to V. Barrie, T. Forbes, I. Frydecky, B. Sawyer, R. Currie, G. Jewsbury, B. Hill and B. Macdonald.

The author would like to thank the crew of the CSS Vector (March 1990 and September 1991) for their assistance at sea. Financial support was from a grant to Dr. Brian Bornhold from the Natural Science and Engineering Research Council of Canada.

DEDICATION

To my parents.

SEAFLOOR MORPHOLOGY AND SEDIMENTARY PROCESSES IN KNIGHT INLET, BRITISH COLUMBIA

I. Introduction

Gravity resedimentation phenomena which are active on land (e.g., landslides, debris flows, debris torrents, rock slides) have been recognized as well in many different submarine environments, such as off deltas, in active tectonic areas, and on continental slopes (e.g. Prior and Bornhold, 1990; Nemec, 1990; Lu et al., 1991). They result in distinctive sea floor morphologies and sediment distributions and are often responsible for damage to seafloor cables, pipelines and coastal and offshore engineering structures (Prior and Bornhold, 1990). The best known case involving cable rupture is that of the Grand Banks earthquake and turbidity current which broke several seafloor cables in sequence on November 18, 1929 (Heezen and Ewing, 1952).

Fjords are an interface between glaciated continents and the oceans. They exhibit a broad range of environmental conditions and are ideal sites for the study of nearly every form of submarine slope failure and sediment gravity flow (Syvitski et al., 1987). The relationship between seafloor morphology and sediment transport is still poorly understood although research has been undertaken in some specific

fjords such as Bute Inlet, Kitimat Arm, Howe Sound, and South Bentinck Arm in British Columbia. As the relationships are complex, an understanding of the mechanics of rivers entering fjords, sediment flows (e.g. debris flows, inertia flows and turbidity currents) and the sea floor morphology which both affects and is modified by these processes, is required. Rivers carrying extremely heavy sediment loads build deltas at the heads of fjords; turbidity currents resulting either directly from bedload or indirectly from delta front slope failures can transport very large volumes of water and sediments into the fjord basin. In fjords, which are long, deep and narrow, turbidity currents can transport deltaic sediments many tens of kilometres from their source (Prior et al., 1987; Prior and Bornhold, 1988, 1989, 1990). Many factors, such as sea level changes, tectonic regime and glaciation can be important in determining sedimentary facies distributions in fjords.

This study aims to interpret the relationships among seafloor morphology, sedimentary facies distribution and mass-movement phenomena, principally turbidity currents, in Knight Inlet a major fjord in British Columbia. The seafloor morphology and associated distribution of sediments are described based on acoustic imagery and sampling. A previous investigation in another British Columbia fjord, Bute Inlet, is used as a principal reference for comparision in this study because it is similar to Knight Inlet in many aspects and has been well studied (Prior et al., 1987; Prior and Bornhold, 1988; Zeng et al., 1991).

This study may aid in understanding the controls on sedimentary processes in fjords in order to assess the possible hazards to coastal development and seabed

installations.

1. Overview of the Study

Knight Inlet is a fjord along the coast of mainland British Columbia, Canada with a length of 102 km and an average width of 3 km (Figure 1). The mid-inlet depth is 420 m; the maximum depth is 550 m. It has two sills, 74 and 110 km from the head of the inlet. Two rivers, the Klinaklini and the Franklin, flow into the head of Knight Inlet and control to a large measure the seafloor morphology in upper Knight Inlet through episodic floods and failures on the deltas of these two rivers. The study area encompasses the upper part of Knight Inlet from the head of the fjord to Kwalate Point, approximately 43 km down the inlet (Figure 2).

Various field and laboratory analytical techniques were employed to determine sedimentary facies characteristics of the sediments and their distribution. These include grab and core sampling, visual description and textural analyses. Seafloor morphology was mapped using sidescan sonar, high-resolution seismic profiling and echosounding. As well, the frequency of turbidity currents was determined through long-term deployment of a turbidity event detector (TED) within the northern part of the study area. Considerable geophysical data were obtained during a cruise in September 1988. A cruise in March 1990 obtained geophysical and echosounding data as well as grab samples. Core samples at several sites were taken and a TED installed on the seafloor outside the main submarine channel during

April 1991. Data from TED were retrieved in October 1991, and supplementary echosounding data were obtained during the same cruise.

Results from the mapping and analytical work are used to describe the seafloor morphology and sediment distributions and to estimate turbidity current transport trends and character along the seafloor in upper Knight Inlet.

2. Previous Work

Knight Inlet was visited by scientists as early as the 1950's (Pickard and Rodgers, 1959). It has not, however, been extensively studied. Most of the research has been limited to a study of the oceanographic features of the fjord, especially deep water properties, such as temperature, salinity and circulation (Pickard and Rodgers, 1959; Pickard, 1975). No studies have dealt with detailed seafloor morphology and the short-term sedimentary processes (especially turbidity currents), although a great deal of acoustic data (side-scan sonar and seismic) have been obtained in the area. Syvitski and Farrow (1983) only described the fjord-head delta of Knight Inlet. The study by Schafer et al. (1989) concentrated on the bio- and lithofacies of modern sediments in Knight Inlet. Syvitski et al. (1988) developed a theoretical model for the infilling of a basin by the progradation of a delta; this model has been used to simulate infilling processes for Knight and Bute inlets. It is, however, of relatively low precision and only useful for predicting very general basin infilling on time scales greater than a few hundred years.

(1). Fjords

Fjords developed during intense glaciation of dissected coastal plateaus and mountains of appropriate structure and are flooded structurally controlled U-shaped valleys that extend from a mountainous hinterland to the open ocean.

Fjords have narrow, deep basins (usually several hundred metres), steep-sided walls, one or more relatively shallow entrance sills of rock or morainal debris, and are fed by one or more rivers from fjord-head or fjord-side deltas that drain glacial water and sediments directly to the sea (Syvitski and Murray, 1981). They have a number of properties which allow for an ideal study of coastal sedimentation: (1) the steep sloping coastline eliminates complicated shoreline sedimentary environments (e.g. very few beach areas); (2) there usually is only one significant sediment source, i.e., the fjord-head river, with no significant external marine source due to the shallow entrance sill; (3) the narrow inlet shape restricts the spreading river jet, resolving the flow into essentially two dimensions (Syvitski and Murray, 1981); (4)they are a transition zone between the sea and the land so that they have properties of both the sea (deep water) and rivers (estuarine deltas in which gradients in suspended load and rate of sedimentation can be comparable to those of the Mississippi delta (Farrow et al., 1983); and (5) many fjords display dramatic evidence of submarine slope instability processes involving slides and debris flows, in which coarse sediments (sands and gravels) are often deposited long distances from available sources by turbidity currents which have been detected acoustically

(Hay et al., 1982) and directly monitored by in-situ mooring arrays (Prior et al., 1987).

(2). Turbidity Currents

Almost all fluid flows other than those of hemispheric proportions are produced by gravity, either directly or indirectly. One category of fluid gravity flow has traditionally been called density currents, of which those containing suspended sediments have been termed turbidity currents (Middleton, 1978). These are currents which result from gravity acting on the relatively small differences in density between different layers of fluid. Such density differences which generate density currents are commonly due to differences in water temperature, salinity and suspended sediment concentration. In theory, any difference in density within the body of water will result in the denser water sinking. If the bed is inclined, even with quite small slopes (e.g. less than 0.2°), this denser water will run forward along this slope and a density current is generated.

As Middleton (1978) has indicated, there is a fundamental distinction between turbidity currents and those density currents which involve only fluid properties. In the case of turbidity currents (dilute sediment gravity flows), gravity is acting on the sediment particles and thereby moves the fluid, whereas in pure fluid gravity flows, gravity acts on the fluid and moves it. In turbidity currents, the flow must first be initiated by some event, such as an avalanche (Bagnold, 1962), that takes a large

volume of sediment into suspension. A river with high sediment load can also generate turbidity currents during floods. The suspended particles are supported by the fluid, which therefore acquires a higher density than that of the surrounding sediment-free fluid. With the action of gravity, the effective density difference produces a lateral flow, which in turn produces turbulence in the fluid, tending to hold the sediment in suspension and thus preventing the turbidity current from becoming dissipated by deposition.

Turbidity currents are very common in fjords. As long as the sediment concentration exceeds the density of deeper water masses, turbidity currents form and carry the sediments long distances away from the shoreline over slopes as low as 0.03 degrees. In a classic study of Hardangerfjord, Norway, Holtedal (1965, 1975) noted the abundance of normally graded beds in his sediment cores. He assumed that the graded layers were deposited by turbidity currents and that the material gradually became finer with distance of transport. The turbidites were restricted to the eroded megachannels on the flat floors, as cores taken outside the central channel did not contain turbidite layers. Fifty percent of the sediment column within the basins of Hardangerfjord resulted from turbidity currents, with an average accumulation rate of 0.5 cma^{-1}.

Turbidity currents may be inferred from graded layers, but they seldom occur as single rare events (Syvitski et al., 1987). Therefore, interpreting their size and scales is very difficult. However, the morphology on the sea floor is the direct reflection of the sediment flows on the bottom. Some fjord basins are fed sediment

through one or two megachannels that have attained depths from 5 to > 25 m and widths of 100 to 1000 m (Gilbert, 1983; Syvitski and Farrow, 1983; Syvitski et al, 1983; Syvitski et al., 1984; Prior et al., 1986). In Knight Inlet, such 'megachannels' are incised 40 m into the sea floor (Syvitski and Farrow, 1983). These megachannels share some general characteristics (Syvitski et al., 1987; Syvitski and Farrow, 1988): (1)the channels are commonly found on slopes of less than 2°; (2)channel depth decreases with decreasing slope; (3)the channels are somewhat sinuous and may traverse the floor of the basin; (4) the proximal parts of the channels display near-vertical walls; and, (5)if a channel has been recently active, it will contain coarser sediment compared to the surrounding hemipelagic basinal muds.

As mentioned above, the difficulty with attempting to analyze turbidity currents is that there are many unknown parameters; the density, thickness, width, length, and composition are usually unknown or are highly uncertain (Komar, 1969). Since the late 1970's, using seafloor morphology and/or sediment distribution both vertically and longitudinally, some authors (e.g. Komar, 1969, 1970, 1975, 1985; Zeng et al., 1991) have tried to apply the general flow equations established in laboratory studies to reconstruct flow dynamics and scales (i.e. thickness and velocity) of natural turbidity currents with the help of seafloor acoustic surveys, sediment sampling, and *in situ* instrument packages.

Komar (1969) proposed an equation to calculate curves of average velocity versus density, the two principal unknowns of turbidity current flow, based on the channel cross section, radius of meander bends, and height difference between

opposite banks of submarine channels. This analysis was based on the observation that turbidity currents remain largely channelized in submarine canyons before debouching onto the deep sea floor. Zeng et al. (1991), using both channel morphology and sediment distribution, calculated the characteristics of average turbidity flows in Bute Inlet, and further compared the calculated results with *in situ* instrument records.

Chu et al. (1979) derived the general governing equations of turbidity current flow and developed a one-dimensional flow model. Although only the steady flow case is considered in detail, their study shows very interesting results. They demonstrated theoretically that four stages can be distinguished during the history of a turbidity current according to the variation in Froude number: (1)flow establishment; (2)uniform flow; (3)hydraulic jump; and, (4)flow decay. The progress of the flow is controlled by four parameters: sediment flux near the sea floor, the slope of the sea floor, turbulent entrainment of the overlying sea water, and the resistance force (stress) imposed on the flow by the sea floor. Obviously, the stress on the bottom determines the sediment distributions (grain size), which thus reflect the bottom stresses. A consideration of relationships among flow properties, sediment types and bedforms, will be undertaken in this study.

II. Geological Setting

1. Coastal Geomorphology and Geology of the Shoreline Rocks

The British Columbia Coast is a leading edge continental margin backed by rugged mountain ranges more than 3000 metres in elevation (McCann and Kostaschuk, 1987); its outstanding features are the numerous fjord inlets (Holland, 1976). The highest areas, such as Silverthrone Mountain, Mount Waddington and Mount Tiedemann which are adjacent to Knight and Bute inlets, maintain small ice caps and valley glaciers (Holland, 1976). The fjords, together with the associated narrow mountain valleys and marine channels, have developed in association with marked NW-SE and NE-SW trending structural lineaments. As well, there is a general rectilinear pattern to the coastal outline (Holmes, 1965). The headward reaches of most fjords are deep within the Coast Mountains and along their length water cascades over falls and down rock faces. Therefore fjord morphology is typically characterized by steep bedrock walls, smooth sediment floors except for the area of river deltas, deep basins, and shallow bedrock or bedrock and morainic sills (McCann and Kostaschuk, 1987).

Within the British Columbia Coastal area several morphogeological belts have been distinguished based on geological structure and morphology (Gabrielse and Yorath, 1989). Knight Inlet, like other mainland British Columbia fjords, lies on the Coast Belt which is a rugged, high relief region forming the Coast and Cascade

Mountains and composed largely of granitic and metamorphic rocks of the Coast Plutonic Complex along the west coast of the mainland (Douglas et al., 1970). Metamorphism in the Coast Belt ranges from greenschist to upper amphibolite facies and reflects deeper burial and substantially greater uplift during Cretaceous and Tertiary time than that experienced by adjacent belts. The Coast Plutonic Complex consists of numerous I-type foliated and non-foliated granitic plutons (Douglas et al., 1970). Bedrock composition and structure have controlled the fluvial sediments and morphology (Holland, 1976).

2. Glacial and Sea Level Changes

Pre-glacial valleys on the western side of the Coast Mountains were occupied by Pleistocene ice and served as escape routes for ice flowing westward to the sea from the high area of accumulation along the crest of the mountains (Holland, 1976; Bird, 1980). As ice left the valleys, fjords were invaded by the sea to produce the drowned fjord system of today (Holland, 1976). The presence of glaciers in the mountain catchments had, and continues to have, a marked effect on the hydrological and sedimentological regimes of most of the major rivers that enter the fjords (McCann and Kostaschuk, 1987). Mount Tiedemann (4000 m) and Silverthrone Mountain (3000 m) today control the drainage of the Klinaklini River, and further control to a great extent sedimentation in Knight Inlet.

Changes in sea level continued to take place along the west coast of British

Columbia during and since the Pleistocene (Holland, 1976). During much of the Tertiary the coastline remained in much the same general position as it is now. Despite the reduction of the land surface by erosion, the land stood relatively higher at the close of the Tertiary than it did at the beginning. Changes in sea level are variable from place to place for they involve the interplay of three factors of isostatic adjustments, tectonic movement and eustatic change (Holland, 1976; Bird, 1980; Clague et al., 1982).

Late Quaternary sealevel changes on the British Columbia coast have been established from studies of terrestrial and marine sediments and landforms (Clague et al., 1982). These studies indicate that the sealevel history of mainland British Columbia and eastern Vancouver Island is very different from that of the Queen Charlotte Islands and western Vancouver Island. On the British Columbia coast and eastern Vancouver Island, there was a rapid rise of submerged coastal lowlands between about 13,000 and 10,000 years ago. Emergence culminated about 6,000 - 9,000 years ago, depending on locality, when the sea, relative to the land, was 12 m or more lower than at present in some areas. During middle and late Holocene time, relative sea level rose on the mainland coast and at least locally on eastern Vancouver Island, resulting in inundation of coastal archaeological sites and low-lying terrestrial vegetation. Tidal records and precise levelling suggest ongoing submergence of at least part of this region.

These patterns of late Quaternary sealevel changes are attributed to complex isostatic response to downwesting and retreat of the late Wisconsin Cordilleran Ice

Sheet, to transfers of water from melting ice sheets to oceans, and to plate interactions on the British Columbia continental margin. It is believed that late Pleistocene and early Holocene crustal movements were dominantly isostatic (Clague et al., 1982).

Thus, a combination of three factors - isostatic adjustments, tectonic movement and eustatic fluctuations during and since the Pleistocene - has resulted in significant changes, demonstrated by beach deposits and Recent marine fossils at various heights above sea level. A post-Pleistocene land emergence of 175 m has been measured at Vancouver, 91 m at Victoria and 152 m at Campbell River (Holland, 1976). However, considering eustatic changes only it is currently believed that in stable regions in post-glacial time the sea has risen continuously, and this rising sea level has affected the British Columbia coast during the last 10,000 years (Bird, 1980). For example, this period witnessed a relative sea level rise of some 13 metres in Fraser River (about 300 km southeast of Knight Inlet) which affected the depositional evolution of the Fraser Delta by both vertical accretion and lateral progradation (Williams and Roberts, 1989).

3. Earthquakes

Earthquakes are generally considered to arise from stress releases due to sudden slips along geological faults. In the deep ocean they may cause slides and turbidity currents which can travel large distances, up to several hundred kilometres

(Pouls, 1988). Major earthquakes in the present century in North America have been mainly concentrated in a narrow belt related to the movement of oceanic plates relative to the America plate (Bird, 1980). The Nootka fault zone, whose projection intersects the America plate near central Vancouver Island, separates these oceanic plates into the Juan de Fuca and the Explorer plate and experiences left-lateral shear due to the different rates of subduction of the two plates (Cassidy, 1986). Knight Inlet lies on the America plate and close to the Explorer plate and the Nootka fault. Riddihough (1984) has suggested that the Explorer plate has stopped subducting, in an absolute sense, and is simply being over-ridden by the southwestward moving America plate.

III. Oceanographic Setting

1. Circulation

Superimposed on the obvious back-and-forth movement of tidal currents, there is a subtle flow termed estuarine circulation (Nichols and Biggs, 1985), which controls the depositional distribution of suspended sediments. The fresh water from the river flows outwards over the sea water which, due to its higher density, penetrates the fjord as a salt wedge along the bottom and underneath the seaward-flowing fresh water. The salinity of the surface layer increases from the head to the mouth, reflecting the mixing of salt water upward into the surface layer (Pickard, 1961). In order to replace the salt water carried seaward in the surface layer, there must be up-inlet flow of sea water at depth below the surface layer.

Data collected from Knight Inlet in 1956 (Pickard and Rodgers, 1959) showed that the water began as a highly stratified, two-layer system at the head and became nearly homogeneous in the outer basin. The fresh water was chiefly in the upper 20 m, though there was still a gradient in salinity below this. The fresh water has salt water mixed upward into it as it moves down the inlet. The upper layer eventually reaches a salinity close to that of sea water at the mouth of the fjord.

Bottom salinity in Knight Inlet is highest in the autumn and winter seasons and falls within an annual range of 31.10 to 31.25 $^{\circ}/_{oo}$ (Pickard, 1975; Schafer and et al., 1989) below 200 m. The bottom varies annually temperatures by less than 1°C

(Farrow et al., 1983).

2. Wind and Waves

The wind can affect water conditions in the inlet both through frictional stress causing surface drift and surface wave generation (Pickard, 1961). The frictional stress on the water surface, may influence the motion of the surface layer and thus may increase or decrease the surface-layer flow along the inlet. On average up-inlet wind of 8 ms^{-1} occur in Knight Inlet during July with down-inlet surface flows reversing to up-inlet, frequently for more than 24 hours (Pickard and Rodgers, 1959). The waves generated by the winds will cause mixing in the surface layer and tend to make the surface layer more homogeneous.

Data from the summer months of 1951 -1959 (Pickard, 1961) suggest that for about 80% of the time the wind speed does not exceed 6 ms^{-1} and wave heights are about 1 m. The wind direction is almost invariably along the length of the inlet, following the bends, and most often directed up-inlet. The along-inlet direction of the wind is a result of the channelling action of the steep sides of the fjord, with wind speed significantly affected by inlet width so that an increase of wind speed is often experienced in the narrower, steeper-sided reaches. In addition the wind speed is generally greatest near the mouth of the inlet and least near the head. The up-inlet wind is usually diurnal in character with 13 ms^{-1} in summer and 17 ms^{-1} in winter during storm events which can last from 2-16 days (Syvitski and Farrow, 1983),

springing up during the morning and dying away in the late evening (Pickard and Rodgers, 1959).

The waves in the inlet are all short-period (2- to 4-second) wind waves generated locally and progressing along the inlet. No data provide any indication of "swell" or long-period waves penetrating from the ocean (Pickard, 1961; Pickard and Stanton, 1980). The average diurnal wave height (h) is 1.2 m and wave length (λ) is 31.6 m; during storms these are 2.4 m and 56.2 m, respectively (Syvitski and Farrow, 1983).

3. Tide

The tides in British Columbia are semi-diurnal and markedly declinational; their range increases from south to north. There is little difference in tide between the mouth and head of the inlets (Pickard, 1961). Tides in Knight Inlet are of mixed semi-diurnal type with an average range of 4.0 m and a maximum range of 6.3 m at the Klinaklini delta (Syvitski, et al., 1987). This macrotidal environment results in a large expansive deltaic tidal flat (≈6 km) at the head of the inlet. The currents on the flood and ebb differ in direction by less than 180°, i.e. the flood mean direction is between 103° and 155° true while the mean ebb direction is between 270° and 285° true by Pickard and Rodgers (1959). No data about tidal currents in the upper part of inlet were found; some data were collected from two temporary stations on and near the inner sill in 1956 (Pickard and Rodgers, 1959). The maximum near-bottom

currents reached at the station 15 km up-inlet from the inner sill were 15 cms^{-1} on spring tides (Pickard and Rodgers, 1959; Farrow et al., 1983).

4. Rivers

The Klinaklini and Franklin rivers, the two main rivers entering Knight Inlet, originate from the adjacent upland area and flow into the head of the fjord forming the Klinaklini and Franklin delta complex (Figure 3) (Syvitski and Farrow, 1983). The Klinaklini River drains some of western Canada's largest ice-fields, in its 6462 km^2 drainage basin (Farrow et al., 1983; McCann and Kostaschuk, 1987) and its hydrologic cycle shows therefore a strong seasonal variation in discharge (Schafer et al., 1989). The Pacific ranges of the Coast Mountain rim the inlet at 1800-3000 m elevation (Syvitski and Farrow, 1983).

The Klinaklini and Franklin Rivers supply about 95% (85% and 10%, respectively) of freshwater input at the head of the inlet (Farrow et al., 1983) with the rest entering through small creeks along the remainder of the inlet's length (Freeland, 1980). The summer discharge maxima are typically two to three times higher than the annual average (Schafer et al., 1989). The freshwater source from melting snow reaches a maximum in June, and from glacial meltwater in early August (Syvitski and Farrow, 1983). The average annual freshwater discharge of the Klinaklini River ranges from 230 to 440 m^3s^{-1} with summer maxima of 680 to 1100 m^3s^{-1}, and winter lows of $\approx$ 50 m^3s^{-1} (Water Survey of Canada, 1979). The data from

the W.S.C. in 1990 and 1991 also show similar characteristics (see Chapter VII).

Klinaklini glacier is the closest and largest sediment source to the Klinaklini delta, lying 22 km upstream (Syvitski and Farrow, 1983). During the summer freshet suspended particulate matter concentrations decrease from more than 200 mgL^{-1} (may be more than 500 mgL^{-1}), at the head of the inlet to about 1 mgL^{-1} near its mouth, a distance of about 83 km. The highest concentration of suspended particles within the fjord is contained within the upper 50 m of the water column, and concentrations decrease with increasing water depth and distance along the fjord (Syvitski et al., 1988). There was evidence that an increase in the turbidity levels was found near the seafloor by Pickard and Giovando (1960). During the winter discharge minimum, suspended sediment loadings are low, about 1.5 mgL^{-1} (Farrow et al., 1983; Schafer et al., 1989) throughout the basin. The rate of sedimentation in Knight Inlet markedly exceeds that observed in many estuaries, due to: (1) resuspension being minimized in the comparatively deep and sheltered fjord basins; and (2) the flux of suspended particulate matter to the basin from the melting of snow and ice being exceptionally high during the spring and summer, especially near the fjord head (Schafer et al., 1989).

In the absence of any direct measurements the bedload through the Klinaklini River was calculated theoretically using both Einstein's (1950) and Bagnold's (1966) equations by Syvitski and Farrow (1983). Both equations predict that the Klinaklini carries a high bedload. In the summer maximum, estimated bedload reaches 1615 kgs^{-1} (Bagnold's equation) and 937 kgs^{-1} (Einstein's equation) and yearly mean

bedload is estimated as 536 kgs^{-1} (Bagnold's equation). In addition, Farrow et al. (1983) introduced a sedimentation model (suspended load) as $Q_s = 0.34Q_o^{2.05}$ (or $C_s = 0.34Q_o^{1.05}$) based on data from Howe Sound, where Q_s is the sediment discharge, in gs^{-1}, C_s is the sediment concentration, in gm^{-3}, and Q_o is the water discharge, in m^3s^{-1}. Using the average discharge (over 25 years) of the Klinaklini River of 330 m^3s^{-1}, sediment discharge is 49.5 kgs^{-1}, and yearly total sediment discharge is $1.56x10^9$ kga^{-1}.

IV. Methods

1. Field Techniques

Modern acoustic mapping and sampling techniques have been applied to the study of the seafloor morphology of fjord deltas (Prior et al., 1981; Prior et al., 1986; Prior et al., 1987; Kostaschuk and McCann, 1987; Prior and Bornhold, 1988, 1990). The seafloor morphology in the upper part of Knight Inlet was surveyed in 1988 using a 100 kHz, scale-corrected, sidescan sonar system at a 200 m range setting. Nineteen survey lines were completed over the study area (Figure 2); navigation data were obtained with a combination of Global Positioning System (GPS), Loran C and radar. Overlapping sidescan sonar swaths were used to construct a morphological map of the entire seafloor surveyed. Correlation of sidescan sonar imagery with echosounding and subbottom profiles reduces ambiguities in interpretation.

Bathymetry and shallow subbottom structure were obtained using a hull-mounted 3.5 kHz echosounder. In soft clays and silts the system is capable of penetration to 30 - 50 m below the sea floor with resolution of individual beds 1 m or less in thickness. Nineteen echosounding cross-lines were obtained in 1990, and twenty-two in 1991; navigation was by radar.

Surficial sediment samples were acquired using a Shipek grab sampler in March, 1990. Approximately 2 - 4 kg of sediment were retrieved from 50 locations (Figure 2) positioned by radar. Nine sediment cores (Figure 4 and 5) were obtained

using a 1000 kg piston corer in April, 1991; positions were determined by radar.

Turbidity currents were detected by a Turbidity Event Detector (TED), developed at the Pacific Geoscience Centre (P.G.C.), Geological Survey of Canada and installed in Knight Inlet from April 1991 to March 1992. Data were retrieved in October, 1991. TED is composed of a light-emitting diode (LED), a photo-diode detector, a computer which includes an analogue to digital convertor, and batteries. These components are housed in a glass sphere fixed in a steel frame. Flotation is provided by four glass spheres; the system is tethered using an acoustic release to a railway wheel on the sea floor. The detector stands about 2 m above the sea floor.

The operating principle of the TED system is that turbidity events cause temporary reduction in visibility in the water column close to the bottom. Therefore TED looks for pulses of reduced visibility and records some of the characteristics of these events. Simply, TED looks at the relative transmissivity of the water in a path between a LED source and a photo-diode detector. The measurement is made by pulsing the LED (rate 1/sec) controlled by the computer and charging two capacitors with the amplified output of the photo-diode. One capacitor is charged when the LED is on and the other is charged when the LED is off. The difference between the two capacitors is then measured. This technique compensates for background light levels. When the program detects a turbidity event it stores the minimum value during the event, the maximum value during the event and the duration of the event in seconds. The trigger algorithm utilizes a large circular buffer to detect events. It fits two lines to the data, a long line which gives background average transmissivity

levels, and a short line which gives the instantaneous value. An event starts when the slope of the short line is positive and the difference between the short and long line is greater than an operator set threshold. Once an event starts the system looks for peaks by checking consecutive slopes of the short line. When a peak is detected, a hold counter is set, if the hold counter expires without another peak detected the event is determined. The event is logged if the time difference between the start of the event and the end of the event is greater than an operator set threshold.

2. Sediment Laboratory Analysis

All laboratory analyses were performed in the Sedimentology Laboratory, Pacific Geoscience Centre. 50 grab and 97 subsamples from 8 cores were analyzed.

(1). Sample Fractionation

(a). Surficial Sediment Samples

Grab samples were brought into the laboratory and emptied into the drying pan and dried in 80°C ovens.

Sampling of dried samples occurred when no gravel was present and when the sample weight was greater than approximately 300 gms. The whole sample was weighed in large stainless steel bowls, then stirred well with a spatula. A subsample

of about 200 g was transferred to a second drying pan.

The weighed dry samples (subsamples) were then soaked overnight in a 10% solution of sodium hexametaphosphate. This dispersal procedure largely removes clay particles adhering to sand grains and breaks up aggregates of silts and clays.

Samples were then separated into their gravel, sand and mud components by wet sieving through W.S. Tyler brass sieves with stainless steel meshes of 2 mm and 0.063 mm (U.S. standard sieve mesh Nos. 10 and 230). Mud passing through the 0.063 mm sieve was retained in large beakers. A sample was washed until the water was clear. Mud was retained for all samples collected for this study. Larger shells or wood fragments were separated from sand by a 2 mm sieve. The shell, wood and sand fractions were placed in 80°C ovens to dry.

Following wet sieving, the mud from each sample, suspended in beakers of wash water, was concentrated by centrifuging. Samples were spun for 90 minutes at 2000 rpm in an I.E.C. Model K Industrial Centrifuge. Following each spin, the clear water was poured out and new muddy water added over the mud coating the bottom of the container. Eventually all mud from a sample was collected in one plastic bag, spun, and covering water poured out. Muds were then frozen and freeze-dried. The latter technique extracted the water from the sediment through sublimation, and provided a sample that was easily disaggregated.

The dried sand from each sample was weighed and percent data calculated. Weight of mud was determined by difference.

(b). Cores

A core section was taken from the cold storage room and split into a working and an archive half using a skill saw. The entire archive half was then stored in the cold room (4°C). Before collecting subsamples from the working half, core descriptions were made which included the measurement of the core length and colour and a detailed examination of the core including the consistency (soft or stiff), colour (gradations or changes with depth) and structure (lenses, laminae, shells, worm burrows and their depths and orientation in the bedding).

Following the descriptions, core subsampling was started. Each subsample, taken based on the core description, was obtained using a spatula and placed in a small 'whirl pak' bag; they were then frozen and freeze-dried. There were 97 subsamples collected from the 8 cores; gravel was found in 5 subsamples. Core #6 was not subsampled as it was disturbed in the field, and sand was found to be the only lithology in this core.

The freeze-dried samples were emptied into 250 ml beakers and weighed to 0.01 g. A tip of sodium hexametaphosphate was added to each beaker, with 150 ml distilled water. The samples were stirred and disaggregated using a rubber-tipped stirring rod, and then sonicated for 30 seconds.

The samples were separated into their gravel, sand and mud components by wet sieving, the same procedure as that described above. The gravel and sand fractions were weighed to 0.1 g and the mud calculated by the difference. The weight

percent data were calculated for each fraction.

(2). Textural Analysis

(a). Sand

A 2 m settling tube, with an internal diameter of 20 cm and filled with distilled water at room temperature was employed to determine textural characteristics of the sediment sand fraction. Following Stokes' law, the actual physical size or diameter of a grain is not determined, but instead the 'sedimentation diameter' which relates to the particle settling velocity (Gibbs et al.,1971) is ascertained, a function of particle size, shape and density (Galehose, 1971).

A sample is adhered to the bottom of an inverted plate (using Kodak Photo-flo 200) which is lowered to the water surface at the top of the tube. At the moment of contact the sand grains are released and fall through the water. They are collected on a suspended plate 2 m below the water surface, which is connected to a balance which records the cumulative weight over time.

Software developed at P.G.C. allowed the information to be fed directly to an IBM-PC microcomputer. A real-time curve is displayed on the screen and subsequent grain-size fraction results are derived based on the experimental work of Gibbs et al. (1971).

Each sample was split, using a micro-splitter, into two 2.0 g (+/- 0.1 g)

subsamples. Water temperature was recorded, and each of the two sample splits were run for 10.5 minutes. Heights on the cumulative curves from the two runs were averaged in the subsequent computer calculations.

(b). Mud

Grain size analysis of the clays and silts in the mud portion of the sample were analyzed using a Sedigraph (Micromeritics, 5000D, Particle Size Analyzer). This instrument records decreasing attenuation of an X-ray beam by particles, over time, establishing particle size through settling, as determined by Stokes' Law.

Mud samples were stirred and approximately 2 - 2.5 g of dried sample placed in a 50 ml beaker and mixed with 40 ml of 0.5% sodium hexametaphosphate solution. An ultrasonic probe was immersed in the liquid, and the sample sonicated for one minute to ensure complete dispersion of the clay particles. The beaker contents are placed within the operating cell to equilibrate with the compartment temperature. At the time a sample is run, temperature is recorded and the related 'rate' is set. The latter is a number which programs the Sedigraph to solve Stokes' Law for a particular fluid viscosity (Sarracino and Forbes, 1981). Samples are stirred by magnet and circulated through the glass cell until the computer is prepared to record the analysis. Once the computer is activated, and the Sedigragh is initiated, the circulation ceases, and recording of the beam attenuation begins. A sample is run until the reverse cumulative curve reaches the equivalent spherical diameter of

0.0004 mm, after about 40 minutes. Software completes sample statistics by extrapolating the slope to 0.0002 mm.

The mud fractions of 50 grab samples and 97 core subsamples were analyzed by Sedigraph. Information collected from Sedigraph analyses were merged with data from settling tube analyses.

(c). Gravel

The gravel fraction in core subsamples was analyzed using a series of size 16, 13.2, 8, 5.6, 4, 2.8, 2 mm sieves, with the 16 mm sieve at the top and a solid pan at the bottom. Each fraction was weighed and recorded to the nearest 0.01 g. There was no gravel found in grab samples. Only 5 core subsamples contained gravels. The results were merged with data from the Sedigragh and the settling tube and tabulations of complete grain size were obtained.

(3). Map Compilation

A seafloor morphology map (Figure 5) of the upper part of Knight Inlet was created based mainly on the sidescan sonar records, with 400 m swath width, obtained in 1988. The echosounding records (3.5 kHz) collected in 1988, 1990 and 1991 were used to supplement the sidescan data.

A scale 1:5000 was used for the first draft of the morphology map and 1:10000

for the second. The final map is at a scale of 1:10000.

The time difference between the side-scan sonar record and the ship's position (layback), which typically increases with increasing water depth, was corrected using the 1988 echosounding records. Such differences are generated due to the instrument being towed behind ship at a distance determined by the cable length and the ship's speed.

The bathymetric map (Figure 6) was made based on the data compiled on a Canadian Hydrographic Service field sheet prepared in 1958 (No.2253-L and No.2254-L). The contour lines were first drawn on the field sheet by hand at scale 2 inches = 1 nautical mile. Since this scale is not a standard map scale, the contours were digitized and processed using AUTOCAD software. A bathymetric map at a scale of 1:15000 was produced.

V. Seafloor Morphology

The Knight Inlet submarine channel system is 41 km long, sinuous in plan and very different from other inlets in British Columbia (e.g. Bute Inlet). Many channels emanate from the delta front and coalesce into a few and finally into a single channel farther down the inlet (Figure 4 and 5). The seafloor in the upper part of the inlet is characterized by a variety of distinctive morphologies which change both laterally and downslope. Four zones are identified according to the channel shapes and their development along the inlet (Figure 4 and 5).

1. Zone One

Zone One (Figure 4) is adjacent to the intertidal flats of the Klinaklini and Franklin river mouths. It extends about 6.3 km down-inlet to maximum water depths of 270 m (in the channel). The area from 0 m to about 100 m water depth (1 km long; average gradient 4.6°) (Syvitski and Farrow, 1983) was not surveyed in this study because of navigational concerns. This area was, however, described in detail by Syvitski and Farrow (1983).

Many channels, initially up to 500 m wide and 40 m deep (Figure 7 and 8), develop from the river mouth and merge several hundred metres downslope. No debris was found at the base of the slopes in the channels, although obviously situated close to the sediment source. These channels are mostly gullied and straight.

Having slightly different orientations, these channels coalesce at varying distances farther downslope. Some of these channels are believed to be offshore extensions of river distributaries (Syvitski and Farrow, 1983).

These multiple channels converge ultimately into a single sinuous channel (Figure 4 and 5). The overall sinuosity, a ratio of the channel length (11.6 km) to its valley length (6.3 km) (McGraw-Hill Encyclopedia of Science & Technology, 1982) is 1.84. Three consecutive down-inlet channel segments, covering the lower half of Zone One (Figure 5), are particularly sinuous. The sinuosity ratios are 2.59, 3.30 and 4.41, respectively; their average ratio is 2.08, the length of the total of three segments to the straight length between the first segment start-point and the third segment end-point. The average seafloor and the channel gradients are 2.07° and 0.94°, respectively. The channels are incised into the sea floor up to 40 m. Nearer the river mouth, the deeper the channel depth, the steeper the channel slope. When channel slope is 1.10°, for example, the channel depth is 40 m at 1.6 km from the river mouth; when the channel slope is 0.84°, the channel depth is 30 m at 5 km from the river mouth.

Near the mouth of the Franklin river at the east side of the upper part of this zone (Figure 5), sidescan sonographs reveal a smooth undulating surface consisting of hummocks, with 10 - 20 m relief, downslope-oriented ridges and narrow, smooth swales. Corresponding echosounding profiles (3.5 kHz) show a convex-upward sea floor (Figure 9) with small (up to 5 m high) hummocks. There are no channels in this area except for one close to the bedrock at the eastern edge of the inlet.

On the western side of the inlet a channel extends from one distributary of the Klinaklini River and continues southeastward along the westernmost edge of the inlet. The surrounding seafloor is very smooth (Figure 5).

Gullies (Figure 10, 11 and 12) and terraces (Figure 13 and 14) are present within the channels. Within the channels of Zone One are ubiquitous transverse bedforms which may indicate the flow direction and strength (Figure 14). Hand (1974) gave a relationship between wavelength λ and velocity of density flows U' as: $U' = \{[(g\lambda/2\pi)*(\Delta\rho/(\rho' + \rho)]\}^{1/2}$, where λ is wavelength, U' is velocity of density flows, g is gravitational acceleration, ρ and ρ' are densities of fresh water (from rivers) and mixed water (from the sea), respectively, and $\Delta\rho$ is density difference between them. Thus, the longer wavelengths reflect the stronger flow velocity. The transverse bedforms are sinuous with heights from 1 - 5 m and wavelengths of 25 - 100 m. In high-resolution seismic records, these bedforms do not appear as a quasi-stable undulating sequence of parallel-bedded strata as described by Bornhold and Prior (1990) from the Noeick River delta of British Columbia. Rather the bedforms in Knight Inlet appear to be a thin surficial unit which moves frequently as strong flows pass through the channel.

2. Zone Two

Zone Two (Figure 4), 4.2 km long with an average gradient of 0.47°, is characterized by a single sinuous channel. Between 240 m (270 m in the channel) and

305 m (335 m in the channel) water depth, this channel is 7.5 km long, 250 - 300 m wide, 30 m deep and has an average slope of 0.93°. Its average sinuosity is 1.79 (7.5 km / 4.2 km) with the ratio in the most curved segment (Figure 5) of 4.72.

Approximately halfway along this zone a small river, Sim River (Fig. 5), empties into the western side of the inlet. Two channels (23 -25 m deep) extend downslope from this river across a slope with 85 m relief and a gradient of 4.5°, joining the main channel farther eastward.

There are few features evident outside the channels except some hummocks and terraces around the active channels (Figure 5). On the north side of the above two channels and on the west side of the single main channel the seafloor is smooth as in Zone One. To the south side of these channels, the seafloor is undulating with hummocks 0.5 - 4 m in relief.

Prominent transverse bedforms can be found in the above two channels (Figure 5) and extend into the main single channel. The wave heights are 0.5 - 1 m, with wavelength increasing with distance. Single waves appear in the more proximal part of the zone and multiple waves in the more distal (Figure 13). The crests of the waves are more V-shaped in the upper part of the zone than in the lower (Figure 15 and 16); the wavelength is approximately 50 m. Farther eastward, at the prominent bend in the main channel, the bedforms can be seen again, with 0.5 - 1 m relief, 25 - 75 m wavelength (Figure 5).

Terraces created around the channel are considered evidence of the channel being deepened or shifted laterally. Figure 17 is a typical profile which shows a

channel being deepened and figure 18 is a sidescan sonograph which displays three terraces formed on the convex side of the channel bend. Clearly, this channel bend has migrated in the same direction over time, such that the channel is now more curved than before in this segment as the curve length has become longer. In other words, the channel curvature becomes smaller. These two figures are chosen from the same area of the prominent bend mentioned above. In addition, along the western bank of this bend, larger gullies, 100 - 125 m long are well developed along the channel wall.

In Zone Two the terraces are up to 300 m wide with 20 m relief, and are well developed on one side of the channel (Figure 19). Some terraces display arcuate erosional features (Figure 20) and others exhibit gullies (20 - 30 m relief) especially in the lower part of this zone. Two or more terraces developed on the same side of the channel are very common. Given that two or more terraces are developing along the north or west banks of the channel, the channel in this zone thus has a tendency to move southwards and eastward. In other words, the channel is tending to reduce its curvature.

As well, a few small-relief and irregular features, i.e. longitudinal ridges (100 - 350 m long and 1 - 4 m high) and hummocks (2 - 3 m relief), can be seen on the terrace surface and along the wall of the terrace in the straight lower reaches of this zone. Meanwhile some small spoon-shaped gullies (50 - 75 m in size and 6 - 7 m relief) are found at the westernmost terrace edge in the same area (Figure 5).

3. Zone Three

The channel, in Zone Three (21.1 km long) (Figure 4), has gradually lost its dominantly sinuous shape and is nearly straight, controlled by the sidewalls of the inlet. The sinuosity of the channel is 1.04 (21.9 km / 21.1 km) over its 21.9 km length. From 305 m to 494 m where the channel disappears, a variety of small (irregular depressions), medium (transverse bedforms, flutes) and large (channels and terraces) relief morphological features occur (Figure 5).

In the upper part of this zone, the channel is almost straight and is located approximately at the centre line of the inlet (Figure 5). The width of the channel varies from 150 to 225 m. Terraces (mostly 2 steps) are well developed on both sides of the channel, with widths up to 250 m. Transverse bedforms within the channel are 1 - 2 m high with 25 - 50 m wavelengths. Gullies can be seen along the walls of the terraces, indicating that these terraces are still active. The sea floor outside the channel is mostly hummocky with small relief features up to 2 m high and medium-size depressions up to 6 m deep and 250 m in diameter (Figure 5).

In some areas in the upper part of Zone Three, undercutting of the channel walls has led to accumulations of debris on the adjacent channel floor; incipient failure, as evidenced by shallow fractures (Bornhold, 1983), can be seen along the wall (Figure 20).

In the central part of the zone the channel is slightly curved, following the shape of the inlet, and then deflects to the eastern side of the inlet in the lower

reaches. The channel width is 75 - 300 m and the depth decreases to about 10 m.

Within the channel a crescent-shaped, concave-downslope depression (Figure 21) 25 m wide and 150 m long is present on the east side of the upper reaches of the channel in this zone. Similar features have been interpreted as flutes by Prior and Bornhold (1989, 1990) and attributed to turbidity currents (Nemec, 1990). Similar and larger flutes have been found in other British Columbia fjords such as on the Bear Bay fan delta in Bute inlet (Prior and Bornhold, 1989) and the Noeick River delta of the South Bentinck Arm (Bornhold and Prior, 1990). In general such flutes are more commonly formed outside the channel in Knight Inlet (Figure 22, 23 and 24), especially along the eastern side of the channel.

Some transverse mega-ripples or ridges (up to 100 m long) are developed on the seafloor to the west of the channel (Figure 23). The distances between them are up to 50 m. As well, a complex zone of criss-crossing mega-ripples or ridges, making a network-shape, occur between the central and the lower parts of the zone. Many other depressions (0.5 - 2 m deep), such as abandoned small channels, small relief terraces (1 - 2 m), large shallow swales, small rounded or irregular depressions (0.5 m deep, up to 7.5 m long), are present in the middle and lower part of Zone Three (Figure 24 and 25).

In the lower part, the channel shifts first from the east side to the west side of the inlet, then continues close to the northern edge of the inlet and finally disappears at the end of the Zone Three (Figure 5). Meanwhile the channel depth varies from 10 m to 0 m. All features outside the channel (e.g., swales, hummocks,

ridges, scars and terraces) have reliefs less than 1 m suggesting that turbidity currents have significantly diminished energy at this point (Figure 26).

Near the bedrock wall along the south side of the inlet, a tongue-shape depression, about 625 m long, 150 m wide and less than 1 m deep, is found (Figure 27). This appears to be the remnant of a channel created by channelized flow at an earlier time. Beyond the northern boundary of this abandoned channel, mega-ripples or dunes are present. They are about 200 m long (their heights are not clear) with about 50 m wavelengths.

Along the north and south sides of the inlet, several debris fan features have developed in this lower part (Figure 28 and 29). One of these, from the Ahnuhati Valley, forms part of the north side of the channel so that sediments, from the adjacent high relief fjord wall, pour out directly into the channel; as a result, the channel has been diverted away from the edge of the inlet wall (Figure 5). An abandoned channel (less than 1 m deep) with a very shallow (0.5 m) and curved channel-like depression within it can be seen on the seafloor at the fan's down-stream edge (Figure 30).

4. Zone Four

Zone Four, which displays no morphological evidence of strong bottom flows is 11.6 km long (Figure 5). The water depth varies from 494 m to 520 m (at Kwalate Point) with a gradient of 0.13° (Figure 31). In the lowermost part of the zone, starting

about 1 km from Kwalate Point, many blocks (up to 60 m in diameter) are present on the smooth seafloor. They are not, however, believed to have been created by flows from up-inlet. Bornhold and Prior (1989) have presented two possible explanations for their origin including upward growth under the effects of gas hydrate formation or partial remolding and collapse of the sediment fabric caused by seismicity; their origin is still debated, however, (Lewis and Bentkowski, 1991) and further work is required.

The following table (Table 1) summarizes the characteristics of the four morphological zones and figure 32 shows the longitudinal profile both within and outside the channel in the upper Knight Inlet.

Table 1. Summary of seafloor morphology characteristics.

zones	Zone 1	Zone 2	Zone 3	Zone 4
water depths (metres)	0 - 270(C*) 0 - 240(S#)	270 - 335(C) 240 - 305(S)	335 - 494(C) 305 - 494(S)	494 - 520 (C & S)
slopes (degrees)	0.94° (C) 2.07° (S)	0.47° (C) 0.93° (S)	0.40° (C) 0.52° (S)	0.13° (C & S)
number of channels	many	one	one	none
channel shapes	braided	sinuous	nearly straight	
sinuosity of channels	1.84	1.79	1.04	
main features	channels, swales, gullies, transverse bedforms, hummocks	channel, terraces, transverse bedforms, hummocks, ridges	channel, flutes, swales, terraces, ripples, small relief depressions	smooth seafloor

*: C means the data in the channel.

#: S means the data from the outside of the channel.

VI. Sediment Types

Fifty grab samples were collected in zones one, two, three and four and nine cores in zones one, two and three (Figure 2 and 4). In general, surface sediments in Knight Inlet are clays, muds, muddy sands and sand, with most of the sea floor covered by clays and muds. The classification of sediment types in this study is based on the classification scheme of Shepard (1954) (modified by Pettijohn et al., 1972) (Figure 33).

By analyzing all of the surface grab samples, it can be seen clearly that the sediment distribution in the upper part of Knight Inlet displays distal fining of sediments (Table 2). Figure 34 shows an example of grab samples taken from and outside the channel. Silts dominate Zone One, the delta front, and clays occur in Zone Four, farthest from the fluvial source (Prior and Bornhold, 1989). Zones two and three are thus transition zones with sediments varying from silts to clays. Muddy sands and sands are found only within the channels.

It is not surprising to find that gravels do not occur in these surface grab samples, even in those obtained from the channel. Because the samples were collected in March, the winter season (as mentioned above, Chapter III), the environment of sediment deposition was relatively tranquil, which means that no large water and sediment discharges were introduced into the inlet. As a result, fine suspended sediments were able to accumulate uninterrupted by episodic sand-transporting turbidity currents. The samples collected within the channels in March,

1990 are undoubtedly finer than if they had been collected in the summer season. This conclusion is supported by the facies evident in the cores taken in April of 1991.

Table 2. Distributions of Sediment types within four the morphological zones.

zones / sediments	Zone 1	Zone 2	Zone 3	Zone 4
samples	17, 18*, 19, 20, 21*, 22, 23,24, 25, 26, 27, 28, 29, 30	31*, 32, 33*, 34, 35*, 36, 37, 38, 39	11, 12*, 13, 14, 15, 16*, 40, 41, 42, 43A, 43*, 44, 45, 46, 47, 48, 49, 50*	1, 2, 3, 4, 5, 6, 7, 8, 9, 10
sand	4%	13%	5%	2%
silt	58%	43%	39%	38%
clay	38%	44%	56%	60%
types	mud	mud	clay	clay

*: these samples are excluded from the statistics above as they are from the channels.

As figure 5 shows, cores #5 and #9 (END91A-05, END91A-09 with 5.21 m and 4.36 m lengths, respectively) (Figure 35 and 36) are from outside of the channel, cores #1, #3 and #4 (END91A-01, END91A-03 and END91A-04: 5.18 m, 5.16 m and 2.84 m long, respectively) (Figure 37, 38 and 39) are from near the edge of the channel and cores #2, #6, #7 and #8 (END91A-02, END91A-06, END91A-07 and END91A-08: 2.46 m, 4.18 m, 3.35 m and 3.66 m long, respectively) (Figure 40 and 41) are from within the channel. Among them cores #2, #3 and #4 were taken in Zone One, core #1, #5, #6 and #7 from Zone Two, and core #8 and #9 from Zone Three. TED was installed close to core #6, but was outside the channel.

For those cores obtained outside the channel, including those from the edge of the channel, they contain mostly soft and homogenous grey clays and muds (including only 0.5% sand on average) with sandy lenses (up to 3 cm in size), interstratified sandy and muddy layers and sand layers (up to 5 cm thick) (Figure 35 and 37). Most of sand layers are normally graded with sharp lower boundaries and gradational upper boundaries.

In cores #5 and #9, there are normally graded sand layers (up to 5 cm thick) sitting in the dominantly soft and homogeneous muddy unit. For those cores closest to the edge of the channel (cores #1, #3 and #4), sediments are comprised mainly of soft, homogeneous clays with vague or slight stratification (Figure 37, 38 and 39). Graded sand layers (up to 6 cm thick) and interstratified sandy and muddy laminae (from less than 0.25 cm to 1.5 cm thick) also occur. Bioturbation is found between 0 cm and 150 cm in these three cores. No bioturbation is evident in cores #2, #6, #7

and #8, as they all come from the channel. However, it was unexpected that no bioturbation occurred in cores #5 and #9 since both come from outside the channel, from much farther away from the channel edge. It may be that turbidity currents bring organic material to the vicinity of the channel which encourages the development of benthic and burrowing fauna.

For cores #2, #6, #7 and #8 from the channel, they consist mainly of medium-to-coarse or fine-to-medium massive sands in which clays are less than 0.1% on average. Gravel (up to 9 mm diameter) was found at 1.37 m depth in core #2 from Zone One close to the fluvial sediment source (Figure 40). The gravels are mixed with poorly sorted medium-to-coarse sands and continue to the bottom of the core, for a total thickness of about 1.14 m. Between 1.64 m and 1.83 m depth, mud blocks (up to 4 cm in size) occur. These are interpreted to have been deposited by turbidity currents rather than debris flows as in general there is insufficient fine-grained matrix for the deposit to be of debris flow origin (Middleton, 1978); the clay content in this part of the core is no more than 0.1 percent.

Above this mixed gravel-sand layer, there are three prominent sand layers, 38 cm, 24 cm and 25 cm thick. The shallowest layer is finest (Figure 40). The deepest layer (38 cm thick on the bottom) is comprised of medium-to-coarse well-sorted sands. Occasionally, small mud clasts occur within this unit. The middle layer (24 cm thick) consists of medium-to-coarse reversely graded sand. As mentioned in the chapter on Seafloor Morphology (Chapter V), transverse sand waves are well developed within this area of the channel. Thus this type of reversely graded

deposition may be interpreted as the result of sand waves migrating down-inlet driven by turbidity currents (Blatt et al., 1972). The third layer (25 cm thick) is also reversely graded with fine-to-medium sand, and contains larger mud clasts (up to 6 cm in size) of the same material as in the overlying homogeneous mud unit. On the top of the core, the surficial unit is about 50 cm thick and consists of very soft and homogeneous clays. It is noteworthy that the gravels throughout the core are graded, i.e. fining-upward. The maximum grain sizes vary from 8.0 mm at the bottom to 2.0 mm at the top. Meanwhile, the peak values in the frequency distribution of grain sizes also show the same trend through core #2 (Figure 42).

Core #6 was disturbed in the field and was not analyzed in the laboratory. The core consists, however, only of sand. Cores #7 and #8 are also mainly comprised of sands (99% and 95%, respectively), except on their tops, which consist of less than 20 cm of silty clays (Figure 41). These surficial thin muddy layers are evidence of fine sediment deposition within the channel during the spring - a relatively quiescent period during which turbidity currents are infrequent (Syvitski et al., 1988; Prior and Bornhold, 1989; Bornhold and Prior, 1990). In core #7, (figure 41), from 5 cm to the bottom of the core, sediments consist of fine-to-medium homogeneous sands. A very thin (0.3 cm) clayey layer is present on the top of the core and a 4.7 cm thick layer of very fine silts occur between 0.3 cm and 5 cm depth. Similarly, a 5 cm thick layer of very soft clay occurs at the top of core #8. A gradational clayey silt layer, about 15 cm thickness, is located between 5 cm and 20 cm depth. Below a core depth of 20 cm the column consists of very fine sands.

By comparing the cores from outside the channel in these three zones, it has been found that cores in Zone One contain primarily graded laminar and interstratified sediments; cores from Zone Two have less interstratified structures and instead consist of individual graded sandy layers; and core #9 in Zone Three consists of even fewer sandy layers and, instead is made up of massive muddy units displaying vague stratification. In comparison, the cores within the channel display diminishing grain size with the distance from the river mouths, i.e. sands become finer with distance from the head of the inlet.

The above results indicate that coarser sediments are deposited principally in the channel as a result of strong turbidity currents. Turbidity currents are confined principally to the channel but can spill out of the channel onto the adjacent seafloor as evidenced by the interstratified sandy and muddy sequences from the sides of the channels.

VII. Turbidity Events

Turbidity events were detected by the TED installed in Knight Inlet (Figure 5 and 43) from April 9, 1991 to October 16, 1991. Data retrieved from TED indicate that the events actually occurred only in August, from August 8th - 30th, when there were 19 events recorded. Figures 44 and 45 display these 17 main events; turbidity values presented are arbitrary uncalibrated measurements conveying relative turbidity.

Earthquakes must be considered as a possible trigger for turbidity events. Records for earthquakes located in the Knight Inlet region (50°N - 52°N, 125°W - 127°W) from March to November 1991 were obtained from the Pacific Geoscience Centre; the results are presented in Table 3. It is notable that, while a 1.5 Richter scale (5 km depth) earthquake was recorded on April 20, four days after TED was deployed, no event was detected. When turbidity currents were active in August, no earthquakes were recorded.

As turbidity currents are density currents, they may be created when the bulk density of seawater due to sediment concentration exceeds that of ambient seawater. In Knight Inlet, with increasing river discharge, the sediment discharge and concentration also increase. Thus yearly floods could lead to excess seawater density due to sediment load, thereby generating turbidity currents. The formula $C_s = 0.34Q_o^{1.05}$ (see above) expresses such a trend. If Q_o is 100 m^3s^{-1}, for example, C_s will be 42.8 gm^{-3}; and if Q_o is 1000 m^3s^{-1}, C_s will be 480 gm^{-3}.

Table 3. Earthquakes located in the Knight Inlet region (50.0 -52.0N, 125.0 -127.0W) from March to November 1991.

LAT (N)	LONG (W)	DATE (D/M/Y)	TIME (hr/m/s)	MAG (M_L)	DEPTH (km)
50.909	-126.499	20/04/1991	05/17/372	1.5	5.00
51.520	-125.995	25/09/1991	07/39/493	1.4	5.00
50.701	-125.717	25/09/1991	18/31/038	1.2	5.00
50.437	-125.719	02/10/1991	19/46/451	1.5	5.00

By comparing the water discharge data from the Klinaklini River in 1991 with the events recorded, a very good correlation was apparent. The discharge was less than 200 m^3s^{-1} from January to April, then increased beginning in May and had maximum values of more than 1000 m^3s^{-1} in August, and then decreased significantly beginning in September (Figure 46). Detailed daily discharge variation from April 1 to September 23 is shown in Figure 47, with the turbidity events shown in the same figure. It is clear that the events followed exactly the three peak discharge values in August: August 8th - 9th: 1110 - 1180 m^3/s, August 16th - 17th: 1030 m^3/s, and August 28th - 30th: 760 - 799 m^3/s. The estimated concentrations C_s would be 571 gm^{-3}, 495 gm^{-3} and 380 gm^{-3}, following the three maxima in water discharge Q_o,

respectively. The strengths of the turbidity events decreased as the river discharge decreased. This fact can be seen by comparing the difference between the background turbidities and maximum turbidities in the figure 46 and 47.

A similar relationship between turbidity events and river discharge also occurred in Bute Inlet (B.D. Bornhold, unpublished data). Figure 48 and 49 display the events, recorded by the TED, and river discharge variations in Bute Inlet from May 15 to October 17, 1989, respectively. The only difference is a time lag: all events occurred one to two days later than the discharge peaks.

As for seafloor slope failures, they can be generated by earthquakes, floods and by slope undercutting by turbidity currents; thus failures can give rise to further turbidity currents and to an intensification of their sediment concentration (and thus their density and velocity). Inspection of the sidescan sonographs from upper Knight Inlet revealed relatively few slope failures; a few were evident along channel banks where the sediments consisted of soft muddy materials. The muddy blocks within the sand layers of core #2 may be good evidence for such channel bank failures.It is felt that most turbidity currents are created as a result of floods in the two rivers (Klinaklini and Franklin). Local slope failures (due to undercutting by turbidity currents), contribute to these currents and strengthen them.

VIII. Discussion

1. Flow Properties

Based on previous investigations of seafloor morphology, sediment distribution and bottom currents in other fjords, it is apparent that turbidity currents are important agents of sediment transport and erosion in Knight Inlet (Prior et al., 1987). From the Turbidity Event Detector data turbidity currents occur most frequently in summer, related to snow and particularly ice melt in the drainage basins of the Klinaklini and Franklin Rivers. This relationship is demonstrated by the close correlation between river floods and the timing of turbidity currents, usually in August. The velocity and competence of such flows is more difficult to determine, however; installation in fjord bottom channels of instrumentation capable of measuring flow velocities of near-bottom currents is particularly hazardous (Prior and Bornhold, 1990). For this reason, an attempt is made to estimate the strength of these flows using a combination of information derived from the seafloor morphology and from sediment properties and distribution.

Average flow properties of turbidity currents may be evaluated indirectly from the channel morphology using the general equations related to turbidity currents and from the hydraulic interpretation of sediment properties (Komar, 1969; Zeng et al., 1991). Several techniques will be used and compared in order to obtain the best estimate of flow properties in Knight Inlet.

(1). Equations Based on Channel Morphology

The principal difficulty in attempting to determine the flow velocities of turbidity currents is that usually too many of the necessary parameters are unknown. In the past attempts have been made to estimate flow velocities by applying a modified form of the Chezy equation, $u = C(RS)^{1/2}$ (Komar, 1969), in which u is the average flow velocity, R is the hydraulic radius (approximately equal to the mean depth in a wide channel), S is the bottom slope and C is the Chezy drag coefficient. This semi-empirical equation, developed for steady uniform river flow, was modified for application to turbidity currents by Middleton (1966):

$$u = \sqrt{\frac{8}{f(1+\alpha)} \frac{\rho_t - \rho}{\rho_t} gdS} \qquad (1)$$

where ρ and ρ_t are the density of water and the turbidity current, respectively, g is the acceleration due to gravity, d is the thickness of the flow, f is the Darcy-Weisbach friction factor, and α is a factor. Komar (1969) gave the equation as:

$$u = C \sqrt{\frac{\rho_t - \rho}{\rho_t} gRS} \qquad (2)$$

where C is Chezy coefficient. Zeng et al. (1991) used the expression:

$$u = \sqrt{\frac{(1+\alpha)}{C_f}\frac{\rho_t - \rho}{\rho_t} gHS} \qquad (3)$$

where C_f is the friction coefficient and H is the average flow body thickness, when they estimated the flow velocity of turbidity currents in Bute Inlet.

A comparison of the above three equations shows that they differ principally in the expression of the drag coefficient C; $C=\{8/[f(1+\alpha)]\}^{1/2}$ in Middleton's equation and $C=[(1+\alpha)/C_f]^{1/2}$ in Zeng et al.'s equation. As Komar(1969) pointed out, C is determined from empirically derived tables for stream flow and any extension in range beyond their intended use can lead to appreciable errors. Thus the expressions developed by Middleton and Zeng are more suitable for estimating flow velocity accurately. In Middleton's equation f= 0.04 andα=0.43, so C=11.83; in Zeng et al., C_f= 0.0029 to 0.01 and α=0.42, so C=22.13 to 11.92. Thus when C_f=0.01 in Zeng et al. (1991) C has nearly the same value as in Middleton's equation.

In this study the equation of Zeng et al. is chosen, based on the assumption that turbidity currents in Knight Inlet are similar to those in Bute Inlet. Knight Inlet and Bute Inlet are similar in many respects: they are both fed by rivers originating from adjacent icefields (Farrow et al., 1983), which carry large volumes of coarse sands and gravels to extensive deltas at the heads of each inlet (Syvitski and Farrow, 1983); both fjords are deep (400 - 600 m) and have long upper basins uninterrupted by sills; both inlets display a complex system of incised channels.

Coefficients C_f and α are re-examined in order to obtain the most appropriate results. Most authors have used α=0.43, while for unexplained reasons Zeng et al.,

(1991) used $\alpha = 0.42$; The author has used a value of $\alpha = 0.43$. Zeng et al. (1991) have adopted a value of C_f of 0.0050. As pointed out by Komar (1977) C_f is highly uncertain; while earlier estimates were between 0.0035 and 0.0050 (Johnson, 1964; Komar, 1969, 1971, 1977), he feels that these values are higher than would be expected for channelized flows. A comparison of results using several values of this coefficient is presented below. As well, many authors (e.g. Chikita, 1990) have used the coarsest 5% or both 5% and 15% (e.g. Komar, 1987) of the grain size distributions to determine flow properties of turbidity currents; Zeng et al. (1991) used the coarsest 10%; in this analysis the grain size of the coarsest 5% and 10% have been used to facilitate comparison with these previous studies. It should be pointed out again that flow characteristics are highly susceptible to the choice of friction coefficient.

Parameters H and S can be obtained from the geometry of channels. The density of turbidity currents ρ_t, however, is generally unknown; velocity u, therefore, cannot be determined by equation (1) or (3) alone. Komar (1969) developed another equation, a surface slope equation to address this problem. The equation was created based on the assumptions that most turbidity currents remain channelized and that the channel is full. Under the influences of the Coriolis force and centrifugal force, the cross-channel profile will be developed such that there will be a difference in the heights of the levees that occur on the each side of the channel. The equation was expressed as:

$$\frac{u^2}{R_b} + 2u\Omega\sin\phi = \frac{\rho_t - \rho}{\rho_t}\frac{g\Delta H}{W} \qquad (4)$$

in which R_b is the radius of curvature of the channel, ΔH is the difference in height of the levees (based on observed internal structures, Figure 8 and 12), and W is the width of the channel (cross-channel distance from levee to levee). These parameters are all obtainable from the morphology of the channel and are illustrated by Komar (1969). The Ω is angular speed of rotation of the earth (0.00075 cms^{-1}), ϕ is the latitude of the channel (50.85° - 51° for Knight Inlet). Since ρ, the density of water (1.023 gcm^{-3} as mean seawater density in Knight Inlet as used for Bute Inlet by Zeng et al. 1991), is known, only velocity u and the density of the turbidity currents ρ_t remain to be determined.

Obviously, a fundamental assumption that the channel is curved should be satisfied when using this surface slope equation. Fortunately, the main channel in Knight Inlet is curved throughout most of its length (Fig. 4, 5), so Komar's surface slope equation (4) can be used to evaluate the flow velocity and density in Knight Inlet. Combining the equations (3) and (4), the flow velocity u and flow density ρ_t can thus be determined.

(2). Thickness of Channelized Flows

In the equations, parameter H, an average thickness of the flow body of turbidity currents, is assumed to be equal to the depth of the channel (Komar, 1969).

However, the flow thickness may be greater or less than the depth of the channel in nature (Zeng et al., 1991). The shaping of the upper portions of submarine channels is controlled largely by erosion at the turbidity current heads, and channel depths there usually reflect the thickness of the turbidity current heads (Middleton and Southard, 1984). As known from experiments, turbidity currents are comprised of the head, neck and body (Middleton 1966; Komar, 1972, 1977); the thicknesses of the head is usually larger than that of the body of the flow.

In Knight Inlet, there was little morphological evidence of flows overspilling the channel (cf. spillover lobes in Bute Inlet: Zeng et al., 1991), but some sand deposition was found in cores collected from the edge of the channel. These sandy intervals indicate that flows occasionally overspill the channel sides. Such units are less than 6 cm thick and are deposited as thin layers or lenses. In cores located farther from the channel, 350 -1500 m, sandy layers are even thinner (less than 5 cm) and the frequency of sandy layers is significantly diminished. Thus the flows may occasionally overspill the channel but most flow thicknesses are not much greater than the channel depth. It is assumed, for this analysis, that most turbidity currents filled but did not significantly overflow the channel.

As mentioned above (Chapter V. Seafloor Morphology), in Zone One many nearly straight channels develop from the river mouth and finally enter the main southeastward-flowing sinuous channel. Before joining the main channel, these channels cross a very steep slope (3.4° on average). It is difficult to determine an *absolute value of the channel depth because every channel has its own shape and all*

of them start near the river mouth such that many individual factors (e.g. localized slope failures, wind waves, etc.) may act on them.

Another way to estimate the flow body thickness is related to the size of bedforms in the channel (Yalin, 1972; Allen, 1982; Zeng et al., 1991). This method has been used to evaluate the depth of fluvial flows (Allen, 1982), and the maximum thickness of turbidity currents in Bute Inlet (Zeng et al., 1991). The ratio of wavelength to thickness is between 1 and 7 generally (Allen, 1982; Yalin, 1972); the ratio of 1 was used in Bute Inlet (Zeng et al., 1991). In Knight Inlet, the wavelength varies between 25 and 100 m throughout the length of the channel system. Thus there does not appear to be a consistent change along the channel, as would be expected, and therefore this relationship does not appear to be suitable.

(3). Flow Velocities and Densities

The mean flow velocity of turbidity currents can be estimated from the geometry of channels by solving equations (3) and (4), or by using bottom sediment grain size information (Komar, 1985, 1987; Zeng et al., 1991).

By solving equations (3) and (4), based on the geometric data from the three zones, mean velocities and densities of turbidity currents in several cross-sections along the inlet, which could be measured directly from the geomorphology map and seismic profiles, have been estimated. The results using $C_f=0.0029$ are shown in Table 4. It is clear that the velocities of turbidity currents reach maximum values

Table 4. Channel geometry and flow properties in Knight Inlet.

zone number	water depth(m)	H (m)	W (m)	S	ΔH (m)	R (km)	u(cms^{-1}) C_f=0.0029	ρ_t (gcm^{-3})	Qs (kgs^{-1})
1	190	18.0	180	0.060	7.5	13.300	382	1.026	$6.05x10^4$
1	230	20.0	175	0.010	12.0	1.445	356	1.037	$2.84x10^5$
2	285	40.0	250	0.0025	11.0	1.125	340	1.048	$1.38x10^6$
2	307	28.0	225	0.0099	11.5	2.695	406	1.036	$5.42x10^5$
2	308	25.0	250	0.0123	9.5	4.095	315	1.030	$2.24x10^5$
2	310	22.5	270	0.0123	10.0	3.750	246	1.028	$1.22x10^5$
2	335	12.5	200	0.0083	3.0	3.500	156	1.028	$3.18x10^4$
3	338	15.0	150	0.0051	4.0	1.435	116	1.027	$1.70x10^4$
3	422	11.5	150	0.0059	4.0	1.280	74	1.025	$4.16x10^3$
3	457	10.0	150	0.0107	2.0	4.300	58	1.024	$1.42x10^3$
3	491	5.0	200	0.0082	2.0	2.160	37	1.024	$6.03x10^2$

(about 4 ms^{-1}) in Zone Two. Whereas the slopes diminish from Zone One to Zone Two, the turbidity current densities and channel depths increase while the velocities decrease slightly. The interpretation is that velocities are maintained through erosion of the channel and incorporation of additional sediment into the turbidity currents, compensating in large part for the diminishing slope. Average channel depths are only 18 m in zone 1 but deepen to 40 m in the proximal part of Zone Two. Passing from Zone Two to Zone Three, velocities, densities and channel depths all diminish as the slope decreases.

The estimated results of velocities of turbidity currents using $C_f = 0.0028$, 0.0030, 0.0040 and 0.0050 are presented in Table 5. Obviously, the results using $C_f = 0.0040$ and 0.0050 are unacceptably small while those of $C_f = 0.0029$ and 0.0030 are the most plausible.

In order to obtain the most acceptable values, the flow velocity was also estimated using the bottom sediment grain size information. The formula used (Van Tassell, 1981; Komar, 1985, 1987; Zeng et al., 1991) is:

$$u = \frac{U_*}{\sqrt{C_f}} = \frac{W}{B\sqrt{C_f}} \qquad (5)$$

where W is the settling velocity of the fastest falling particles in suspension, U_* is shear velocity, and B is a factor relating the settling velocity of the particles and the shear velocity. As in Bute Inlet (Zeng et al., 1991), $B = 1$ is used in this study. C_f has the same values as above. The parameter W is estimated by using Gibbs et al. (1971)

Table 5. Comparison of flow velocities under different C_f's.

zone number	water depth(m)	u(cms^{-1}) C_f=0.0028	u(cms^{-1}) C_f=0.0029	u(cms^{-1}) C_f=0.0030	u(cms^{-1}) C_f=0.0040	u(cms^{-1}) C_f=0.0050
1	190	3310	382	203	36	20
1	230	-80*	356	43	4	2
2	285	-43*	340	34	3	2
2	307	-116*	406	74	8	4
2	308	-521*	315	94	12	6
2	310	-525*	246	83	11	6
2	335	-443*	156	66	10	5
3	338	-82*	116	34	4	2
3	422	-96*	74	27	4	2
3	457	102	58	40	10	6
3	491	80	37	24	5	3

* Sign indicates an unreasonable result.

empirical equation:

$$W=\frac{-3\eta+\sqrt{9\eta^2+gr^2\rho_f\,(\rho_s-\rho_f)\,(0.015476+0.19841r)}}{\rho_f\,(0.011607+0.14881r)} \qquad (6)$$

where W is velocity in cms^{-1}; η is dynamic viscosity of the fluid in poises, g is the gravitational acceleration (cms^{-2}), r is the sphere radius in cm, ρ_s and ρ_f are the density of the fluid ($gcm^{-3)}$ and sphere (gcm^{-3}), respectively.

In order to compare with the results estimated from channel geometry, the same C_f values and the coarsest 5% and 10% grain sizes are used in the calculation. The final results are shown in Table 6 and Table 7. When $C_f=0.0040$ and 0.0050, velocities inferred from both coarsest 5% and 10% of grain sizes are quite small. Meanwhile, results from $C_f=0.0028$ can not be compared with the corresponding results from the channel geometry. Apparently, the calculation using $C_f=0.0029$ results in the closest match between values, as seen by comparing Table 5 with Table 6 and Table 7. Thus, it is probable that the values in Table 4 are the most appropriate upper limit values and those in Table 6 and Table 7 are the lower limit values. Because all surface samples were collected in winter, leading to grain sizes which are finer than those carried by turbidity currents originating at the mouths of the river, the coarsest 5% of the grain size distributions may be more reflective of the turbidity current dynamics.

It must be noted that velocity inferred from grain sizes of 0.9640 cm and 0.9130 cm result in unacceptably high velocities of 13 - 14 ms^{-1} (Table 6 and 7) with $C_f=0.0028$ - 0.0030. These results are generated by an overestimation of settling

Table 6. Flow velocities inferred from coarsest 5% of the grain size distribution.

zone number	samples	grain size (cm)	u(cms^{-1}) C_f=0.0028	u(cms^{-1}) C_f=0.0029	u(cms^{-1}) C_f=0.0030	u(cms^{-1}) C_f=0.0040	u(cms^{-1}) C_f=0.0050
1	#18	0.0167	38	38	37	32	29
	#21	0.0240	63	62	61	52	47
	core 2	0.0768	231	227	223	193	173
		0.0549	166	163	160	139	124
		0.0755	227	223	220	190	170
		0.3060	711	699	687	595	532
		0.9640	1460	1435	1411	1222	1093
		0.9130	1415	1390	1367	1184	1059
	core 3	0.0235	62	60	59	51	46
		0.0202	50	49	48	42	38
		0.0241	64	62	61	53	48
		0.0272	74	73	72	62	56
	core 4	0.0121	23	23	23	20	18
		0.0126	25	25	24	21	19
		0.0293	81	80	79	68	61
		0.0255	68	67	66	57	51
		0.0315	89	87	86	74	67
		0.0282	78	76	75	65	58
2	#31	0.0594	179	176	173	150	134
	#33	0.0141	30	29	29	25	22
	#35	0.0119	23	22	22	19	17
	core 7	0.0209	53	52	51	44	39
		0.0279	77	75	74	64	57
		0.0407	120	118	116	100	90
		0.0424	125	123	121	105	94
	core 1	0.0186	45	44	43	37	33
		0.0223	57	56	55	48	43
		0.0244	65	63	62	54	48
3	#12	0.0420	124	122	120	104	93
	#16	0.0124	24	24	24	20	18
	#43,#50	0.0153	34	33	33	28	25
	core 8	0.0242	64	63	62	53	48
		0.0264	71	70	69	60	53

Table 7. Flow velocities inferred from coarsest 10% of the grain size distribution.

zone number	samples	grain size (cm)	u(cms^{-1}) C_f=0.0028	u(cms^{-1}) C_f=0.0029	u(cms^{-1}) C_f=0.0030	u(cms^{-1}) C_f=0.0040	u(cms^{-1}) C_f=0.0050
1	#18	0.0146	31	30	30	26	23
	#21	0.0210	52	52	51	44	40
	core 2	0.0568	171	168	166	143	128
		0.0470	140	138	136	117	105
		0.0645	195	192	188	163	146
		0.1551	428	421	414	358	320
		0.8220	1331	1308	1286	1113	996
		0.7241	1235	1213	1193	1033	924
	core 3	0.0199	49	48	47	41	37
		0.0176	41	41	40	35	31
		0.0225	58	57	56	49	34
		0.0249	66	65	64	55	50
	core 4	0.0107	19	19	19	16	14
		0.0110	20	20	19	17	15
		0.0267	73	71	70	61	54
		0.0255	68	67	66	57	51
		0.0283	78	77	75	65	58
		0.0245	65	64	63	54	49
2	#31	0.0503	151	148	146	126	113
	#33	0.0123	24	24	23	20	18
	#35	0.0109	20	19	19	17	15
	core 7	0.0156	35	34	34	29	26
		0.0248	66	65	64	55	49
		0.0350	101	99	97	84	75
		0.0381	111	109	107	93	83
	core 1	0.0156	35	34	34	29	26
		0.0191	46	45	45	39	35
		0.0207	52	51	45	43	39
3	#12	0.0366	106	104	103	89	79
	#16	0.0113	21	21	20	16	16
	#43, #50	0.0122	24	23	23	20	18
	core 8	0.0227	59	58	57	49	44
		0.0243	64	63	62	54	48

velocity, W, as Gibbs et al. (1971) pointed out when grain sizes (sphere diameters) are greater than 0.5 cm.

2. Turbidity Current Dynamics

(1). Generation of Turbidity Currents

As mentioned earlier when the first measured turbidity events occurred in Knight Inlet in the summer of 1991, the measured water discharge of the Klinaklini River reached its annual maximum value of 1180 m^3s^{-1} with its corresponding sediment discharge of about $6.7x10^2$ kgs^{-1} estimated from Farrow et al.'s empirical formula (1983). This value of suspended sediment discharge is similar to the value $6.03x10^2$ kgs^{-1} estimated for the terminal end of the channel in Zone Three (see Table 4 bottom line). The sediment concentrations implied by these discharges are, however, very different. The former reflects a concentration of 571 gm^{-3} while the latter is equivalent to 1629 gm^{-3}; thus suspended sediments from the rivers could only represent a fraction of the suspended sediments found in the turbidity currents. If the estimated concentration from Farrow et al.'s formula is close to reality, the turbidity currents measured in 1991 cannot be generated by such suspended sediment concentrations caused by floods. These concentrations are insufficient to overcome the seawater density stratification at the head of the inlet. The only possible explanation is that the delta front experienced slope failures due to the sudden delivery of large volumes of coarse sediment to the steep delta foreslope. The coarse sediments making up river mouth bars, which had accumulated since the previous year's floods would be swept onto the delta foreslope by the summer floods as

bedload. Failure of these unstable sediments would give rise to debris flows and, through increasing bulk water density due to the addition of sediment, to turbidity currents.

In other words, river mouth bars accumulate during low discharge periods, particularly through the winter. In latest spring and summer, during periods of snow and ice melt, discharge increases several fold, destroying the river mouth bars and carrying the sandy sediments onto the steep slopes at the head of the inlet. The resultant turbidity currents have sufficient momentum to erode the sea bed, creating prominent incised channels, adding sediments to the turbidity current and thereby increasing their velocity even more.

(2). Frequency of Turbidity Currents

Such turbidity currents in Knight Inlet can only be generated during the late spring and summer seasons, related to snow and ice melt and rainfall. The frequency of the currents is probably dependent on the flood strength and on the accumulation of river mouth sediments between flood events. This relationship, in both Bute and Knight Inlets is, however, unclear. While earthquakes are potentially another important factor in triggering such failures and turbidity currents they were not observed in Knight Inlet; the small earthquakes in the area had no discernible effect on the seafloor sediments.

(3). Turbidity Currents Processes

If slopes and initial suspended sediment concentrations are sufficiently great, turbidity currents will erode the sea floor incorporating more sediment, thus increasing their densities and velocities; as slopes diminish, sediment will be deposited, the suspended matter concentration will decrease, along with the velocity, and eventually the turbidity current will cease. The channel wall failures found in Knight Inlet are clear evidence of this erosion by turbidity currents in the upper part of the system. Thus the density of turbidity currents (ρ_t) in the channel can be indicative of whether erosion or deposition will occur. In Table 4, it can been seen clearly that the densities of turbidity currents (ρ_t) vary along the channel.

From Zone One to Zone Two, ρ_t increases steadily, and sediment discharge Q_s increases as well, indicating erosion. When ρ_t and Q_s reach their peak values, the channel depth has attained its greatest value of 40 m. Past this erosional section of the channel, ρ_t and Q_s start to decrease to the terminal end of the channel, and the channel depth decreases from 40 m to 5 m. Thus deposition is inferred along the more distal part of the channel as the turbidity currents wane. In the main part of Zone Two, however, ρ_t and Q_s do not decrease very significantly, except at the beginning of depositional part of the channel and the most distal part of Zone Two. At the beginning of the depositional part, ρ_t suddenly drops from 1.048 $g(cm)^{-3}$ to 1.036 $g(cm)^{-3}$, and Q_s from $1.38x10^6$ kgs^{-1} to $5.42x10^5$ kgs^{-1}, which results in the channel depth diminishing rapidly: from 40 m to 28 m. This transition represents the

change in turbidity current behaviour from erosion of the bed to deposition of sediments onto the bed. Near the end of Zone Two, Q_s drops from 1.22×10^5 kgs^{-1} to 3.18×10^4 kgs^{-1}, a reduction of 9×10^4 kgs^{-1}, although ρ_t has not changed. This drop marks the current's loss of vigour as the velocity is only about 1.6 ms^{-1}.

These two big drops in Q_s have different characters in which ρ_t has decreased significantly during the first but displays no change during the second. This phenomenon indicates that the coarsest sediments mainly settle to the bottom during the first drop so that the ρ_t experiences a major change. In the second, however, the uniform finer sand settles more gradually with the steadily decreasing thickness of the current from 22.5 m to 12.5 m, so that the ρ_t exhibits no significant change.

Since the channel exists in a zone that is appears to be one of deposition it is inferred that the channel must have undergone erosion during an earlier period of more vigorous turbidity currents or is today occasionally eroded by extremely strong turbidity currents.

Generally speaking, the channel lying within Zone One and the upper part of Zone Two is in an erosional state; within the lower part of Zone Two and all of Zone Three deposition occurs. Turbidity currents in the erosional area erode the channel and enhance their own strengths - the development stage; passing to the depositional area they drop their coarse sediments first - maintenance stage; with diminishing energy they drop even finer sand - waning stage before disappearing altogether beyond the end of the channel.

3. Knight Inlet and Bute Inlet

Bute Inlet includes a 70 km long sedimentation system which has been mapped and studied in detail (Zeng et al., 1991; Prior et al., 1987). Turbidity currents originate at the head of the fjord on the submerged delta front of two rivers, the Homathko and Southgate. They move downslope for about 30 km (41 km in Knight Inlet) within a single large channel, spill onto a depositional area and finally spread out over a low-relief distal splay area that passes 55 km downslope onto a flat basin floor (Zeng et al., 1991).

Knight Inlet is quite similar in many respects to Bute Inlet, although the Knight Inlet channel system differs from Bute Inlet in that many channels emerge from the delta front and coalesce into a few and finally one channel farther down the inlet. The mean velocities of turbidity currents in Bute Inlet (Zeng et al., 1991), based on channel morphology, are in the range of 160 - 425 cms^{-1} in the upper part of the incised channel and 66 cms^{-1} in the lower channel. Calculated current densities range from 1.048 to 1.028 gcm^{-3}. The turbidity currents monitored in 1986 using submerged instrument packages exceeded 32 m in thickness in the upper part of the incised channel, where the maximum measured velocity was 330 cms^{-1} and the densities of the monitored flows were estimated at 1.03 - 1.025 gcm^{-3}. These results are quite close to the results obtained in Knight Inlet: the maximum estimated velocity, based on the channel morphology, is 406 cms^{-1} in the upper part of the Knight Inlet channel and 116 - 58 cms^{-1} in the lower channel; the density of currents

range from 1.048 to 1.024 gcm^{-3}.

IX. Conclusions

1. Turbidity currents are a major mechanism of sediment transport in Knight Inlet. They have constructed a widespread, complex (up to 40 m deep, 300 m wide and 41 km long) incised channel system similar in many respects to those observed in other British Columbia fjords (e.g. Bute Inlet).

2. The detailed seafloor morphology map created in this study, based on acoustic imagery, has shown that the channel system is different in some respects from Bute Inlet. Many channels emanate from the delta front and coalesce into a few and finally into a single channel farther down the inlet. In Bute Inlet single channels emerge from each of the two rivers and combine downslope to form a single main channel.

3. Four sedimentation zones have been identified according to the channel shapes and their development along the inlet. Zone One is represented by many multiple channels; Zone Two by one single very sinuous channel; Zone Three by a less curved single channel; and Zone Four by smooth flat sea floor.

4. Laboratory sediment analyses (50 grab and 97 subsamples from 9 cores) show that

the sediment distribution in the upper part of Knight Inlet displays distal fining. Muddy sands and sands are found only within the channel.

5. Data from the Turbidity Event Detector (TED) installed in Knight Inlet from April 9, 1991 to October 16, 1991 indicate that the events occurred only in August, from August 8th -30th, when 19 events were recorded. These events had no relationship at all with earthquakes but were closely related to floods on the Klinaklini River. It was evident that the turbidity events followed exactly the three peak discharge values (also annual maximum values) on August 8th - 9th, 16th - 17th, and 28th - 30th. A similar relationship was also observed in Bute Inlet.

6. Using the method of Zeng et al. (1991) (based on the channel morphology) employed in Bute Inlet and assuming a friction of 0.0029, calculation of turbidity current velocity and density in Knight Inlet was undertaken. The maximum calculated velocity of turbidity currents thus reached about 400 cms^{-1} in the upper part of the channel and about 60 - 110 cms^{-1} in the lower channel; the densities of the currents are in the range of 1.024 to 1.048 gcm^{-3}. These results are comparable with the results obtained in Bute Inlet.

7. Suspended sediment concentration in Klinaklini River is quite small, based on Farrow et al.'s empirical formula, so that it is impossible to generate turbidity currents through excess surface water density, even during floods. The only apparent

mechanism to generate turbidity currents associated with periods of river flooding is by delta front slope failures of river mouth bars, which accumulate during lower discharge periods, particularly through the winter, are eroded and their coarse sediment deposited rapidly on the unstable steep delta foreslope.

8. The channel in Zone One and the upper part of Zone Two is in an erosional area, in which turbidity currents are continuing to increase velocity, density and thickness; in the lower part of Zone Two and all of Zone Three, deposition occurs reflecting the gradual waning of turbidity currents.

9. The channel system must have experienced earlier erosion or continues to be occasionally eroded by extremely strong turbidity currents such that deposition is now occurring in a previously incised channel bed. For the sake of the flow analysis presented in this study, it has been assumed that the flows are in equilibrium with present morphology. Clearly, a spectrum of turbidity current magnitudes exists, such that occasional energetic flows can erode channels in areas which subsequently experience deposition.

10. This study has clearly shown that major turbidity currents are closely related to river floods, and that they are not generated directly by suspended sediments carried by rivers. These conclusions can aid in understanding the controls on sedimentary processes in fjords and in assessing the possible hazards to coastal development and

seabed installations.

Bibliography

Allen, J.R.L. (1982) Sedimentary structures: their character and physical basis. Elsevier, Amsterdam, 663pp.

Bagnold, R.A. (1962) Auto-suspension of transported sediment---turbidity currents. Proceedings of the Royal Society of London, Series A, Vol.265, No.1322, p.315-319.

Bagnold, R.A. (1966) An approach to the sediment transport problem from general physics. U.S. geological Survey, Prof. Pap. 422-I, 37pp.

Bird, J.B. (1980) The natural landscapes of Canada, a study in regional earth science (2nd Edition). John Wiley & Sons Canada Limited, Toronto, 260pp.

Blatt, H., Middleton, G. V. and Murray, R.C. (1972) Origin of sedimentary rocks. Prentice-Hall, Inc., Englewood Cliffs, New Jersey, 634pp.

Bornhold, B.D. (1983) Sedimentation in Douglas Channel and Kitimat Arm. Canadian Technical Reports in Hydrography and Ocean Sciences, Vol.18, p.88-114.

Bornhold, B.D. and Prior, D.B. (1989) Sediment blocks on the seafloor in British Columbia fjords. Geo-marine Letter, Vol.9, p.135-144.

Bornhold, B.D. and Prior, D.B. (1990) Morphology and sedimentary processes on the subaqueous Noeick River delta, British Columbia, Canada. In: Coarse-Grained Deltas (Edited by A. Colella and D. B. Prior), Special Publication Number 10 of the International Association of Sedimentologists, Blackwell Scientific Publications, p.169-181.

Cassidy, J.F. (1986) The 1918 and 1957 Vancouver Island earthquake. M.Sc thesis, Vancouver, 143pp.

Chikita, K. (1990) Sedimentation by river induced turbidity currents: field measurements and interpretation. Sedimentology, Vol.37, p.891-905.

Chu. F.H., Pilkey, W.D. and Pilkey, O.H. (1979) An analytical study of turbidity current steady flow. Marine Geology, Vol.33, p.205-220.

Clague, J.J., Harper, J.R., Hebda, R.J. and Howes, D.E. (1982) Late Quaternary sea levels and crustal movements, coastal British Columbia. Canadian Journal of Earth Sciences, Vol.19, p.597-618.

Douglas, R.J.W., Gabrielse, H., Wheeler, J.O., Stott, D.F. and Belyea, H.R. (1970) Geology of western Canada. In: Geology and Economic Minerals of Canada (Edited by Douglas, R.J.W.), Queen's Printer, Ottawa, p.365-488.

Einstein, H.A. (1950) The bed-load function for sediment transportation in open channel flows. U.S. Dept. Agriculture, Soil Conservation Service, Technical Bulletin 1026, 78pp.

Farrow, G.E., Syvitski, P.M.S. and Tunnicliffe, V. (1983) Suspended particulate loading on the Macrobenthos in a highly turbid fjord: Knight Inlet, British Columbia. Canadian Journal of Fisheries Aquatic Sciences, Vol.40, p.273-288.

Freeland, H.J. (1980) The hydrography of Knight Inlet, B.C., in the light of long's model of fjord circulation. In: Fjord Oceanography (Edited by H.J. Freeland, D.M. Farmer and C.D. Levings), Plenum Press, New York, p.271-276.

Gabrielse, H. and Yorath, C.J. (1989) DNAG#4. The Cordilleran Orogen in Canada. Geoscience Canada, Vol.16, No.2, p.67-83.

Galehose, J.S. (1971) Sedimentation analysis. In: Procedures in Sedimentary Petrology (Edited by R.E. Carver), Wiley-Interscience, New York, p.69-94.

Gibbs, R.J., Matthews, M.D. and Link, D.A. (1971) The relationship between sphere size and setting velocity. Journal of Sedimentary Petrology, Vol. 41, No.1, p.7-18.

Gilbert, R. (1983) Sedimentary processes of Canadian arctic fjords. In: Sedimentology of fjords (Edited by Syvitski, J.P.M. and Skei, J.M.). Sedimentary Geology, Vol.36, p.147-175.

Hand, B.M. (1974) Supercritical flow in density currents. Journal of Sedimentary Petrology. Vol.44, No.3, p.637-648.

Hay, A.E., Burling, R.W. and Murray, J.W. (1982) Remote acoustic detection of a turbidity current surge. Science, Vol.217, p.833-835.

Heezen, B.C. and Ewing, M. (1952) Turbidity currents and submarine slumps, and the 1929 Grand Banks earthquake. American Journal of Science, Vol.250, p.849-873.

Holland, S.S. (1976) Landforms of British Columbia, a physiographic outline. Bulletin 48, 138pp.

Holmes, D.L. (1965) Principles of Physical Geology (2nd Edition). Thomas Nelson, Great Britain, 1288pp.

Holtedal, H. (1965) Recent turbidites in the Hardangerfjord, Norway. Colston Research Society Proceeding, Bristol, Vol.17, p.107-141.

Holtedal, H. (1975) The geology of the Hardangerfjord, west Norway. Norges Geology Unders., Bull 36 (323): p.1-87.

Johnson, M.A. (1964) Turbidity currents. Oceanographic Marine Biological Annual Review, Vol.2, p.31-43.

Komar, P.O. (1969) The channelized flow of turbidity currents with application to Monterey deep-sea fan channel. Journal of Geophysics Research, Vol.74, p.4544-4558.

Komar, P.O. (1970) The competence of turbidity current flow. Geological Society of America Bulletin., Vol.81, p.1555-1562.

Komar, P.O. (1971) Hydraulic jumps in turbidity currents. Geological Society of American Bulletin, Vol.82, p.1477-1488.

Komar, P.O. (1972) Relative significance of head and body spill from a channelized turbidity current. Geological Society of America Bulletin, Vol.83, p.1151-1156.

Komar, P.O. (1975) Supercritical flow in density currents: a discussion. Journal of Sedimentary Petrology, Vol.45, p.747-749.

Komar, P.D. (1977) Computer simulation of turbidity current flow and the study of deep-sea channels and fan sedimentation. In: The Sea (Edited by E.D. Golderg, I.N. McCave, J.J. O'brien and J.H. Steele), John Wiley & Sons, Inc., New York, Vol.6, p.603-621.

Komar, P.O. (1985) The hydraulic interpretation of turbidites from their grain sizes and sedimentary structures. Sedimentology, Vol.32, p.395-407.

Komar, P.O. (1987) Selective gravel entrainment and the empirical evaluation of flow competence. Sedimentology, Vol.34, p.1165-1176.

Kostaschuk, R.A. and McCann, S.B. (1987) Subaqueous morphology and slope processes in a fjord delta, Bella Coola, British Columbia. Canadian Journal of Earth Science, Vol.24, p.52-59.

Lewis, T.J. and Bentkowski, W.H. (1991) Blocky sediments in Bute and Knight inlets, British Columbia. Current Research, Part A, Geological Survey of Canada, Paper 91-1A, p.303-308.

Lu, N.Z., Suhayda, J.N., Prior, D.B., Bornhold, B.D., Keller, G.H.. Wiseman, Wm. J., Jr., Wright, L.D. and Yang, Z.S. (1991) Sediment thixotropy and submarine mass movement, Huanghe Delta, China. Geo-Marine Letters Vol.11, p.9-15.

McCann, S.B. and Kostaschuk, R.A. (1987) Fjord sedimentation in Northern British Columbia. In: Glaciated Coasts (Edited by Duncan M. Fitzgerald & Peter S. Rosen), p.33-50, Academic Press, Inc., 364pp.

McGraw-Hill Encyclopedia of Science & Technology (5th Edition), (1982), Toronto, Vol.11, p.684-686.

Middleton, G.V. (1966) Small-scale models of turbidity currents and the criterion for auto-suspension. Journal of Sedimentary Petrology, Vol.36, No.1, p.202-208.

Middleton, G.V. (1978) Chapter 8. Sediment Gravity Flows. In: Mechanics of sediment movement (2nd Printing with Corrections and Additions) (Edited by John B. Southard), Massachusetts Institute of Technology, p.8.1-8.20.

Middleton, G.V. and Southard, J.B. (1984) Mechanics of sediment movement. Lecture Notes for SEPM Short Course, No.3, 401pp.

Nemec, W. (1990) Aspects of sediment movement on steep slopes. In: Coarse-Grained Deltas (Edited by A. Colella and D. B. Prior), Special Publication Number 10 of the International Association of Sedimentologists, Blackwell Scientific Publications, p.29-73.

Nichols, M.M. and Biggs, R.B. (1985) Estuaries. In: Coastal Sedimentary Environments (2nd Edition)(Edited by R.A. Davis), Springer-Verlag, New York, p.77-186.

Pettijohn, F.J., Potter, P.E. and Siever, R. (1972) Sand and sandstone. Springer-Verlag, New York, 618pp.

Pickard, G.L. and Rodgers, K. (1959) Current measurements in Knight Inlet, British Columbia. Journal of Fisheries Research Board of Canada, Vol.16, p.635-678.

Pickard, G.L. and Giovando, L.F. (1960) Some observations of turbidity in British Columbia inlets. Limnology and Oceanography, Vol.5, No.2, p.162-170.

Pickard, G.L. (1961) Oceanographic features of inlets in the British Columbia mainland coast. Journal of Resources Board of Canada, Vol.18, No.6, p.907-999.

Pickard, G.L. (1975) Annual and longer term variations of deepwater properties in the coastal waters of southern British Columbia. Journal of Fisheries Research Board of Canada, Vol.32, p.1561-1578.

Pickard, G.L. and Stanton, B.R. (1980) Pacific fjords---a review of their water characteristics. In: Fjord Oceanography (Edited by H.J. Freeland, D.M. Farmer and C.D. Levings), Plenum Press, New York, p.1-51.

Pouls, H.G. (1988) Seafloor stability. In: Marine Geotechnics, London UNWIN HYMAN, p.344-436.

Prior, D.B., Wiseman, W.J., Jr. and Bryant, W.R. (1981) Submarine chutes on the slopes of fjords deltas. Nature, Vol.290, p.326-328.

Prior, D.B., Bornhold, B.D. and Johns, M.W. (1986) Active sand transport along a fjord-bottom channel, Bute Inlet, British Columbia. Geology, Vol.14, p.581-584.

Prior, D.B., Bornhold, B.D., Wiseman, W.J. and Lowe, D.R. (1987) Turbidity current activity in a British Columbia fjord. Science (Reprint series), Vol.237, p.1330-1333.

Prior, D.B. and Bornhold, B.D. (1988) Submarine morphology and processes of fjord fan deltas and related high-gradient systems: modern examples from British Columbia. In: Fan Delta: Sedimentology and Tectonic Settings (Edited by W. Nemec and R.J. Steel), Blackie and Sons, Glasgow, p.125-143.

Prior, D.B. and Bornhold, B.D. (1989) Submarine sedimentation on a developing Holocene fan delta. Sedimentology, Vol.36, p.1053-1076.

Prior, D.B. and Bornhold, B.D. (1990) The underwater development of Holocene fan deltas. In: Coarse-Grained Deltas (Edited by A. Colella and D. B. Prior), Special Publication Number 10 of the International Association of Sedimentologists, Blackwell Scientific Publications, p.75-90.

Riddihough, R.P. (1984) Recent movements of the Juan de Fuca Plate system. Journal of Geophysics Research, Vol.89, p.6980-6994.

Sarracino, L. and Forbes, T. (1981) Sedimentology laboratory manual. Unpublished Manual, Pacific Geoscience Centre, Geological Survey of Canada, 58pp.

Schafer, C.T., Cole, F.E. and Syvitski, J,P.M. (1989) Bio- and lithofacies of modern sediments in Knight and Bute Inlet, British Columbia. Research Report, The Society of Economic Paleontologists and Mineralogists, Vol.4, p.107-126.

Shepard, F.P. (1954) Nomenclature based on sand-silt-clay ratios. Journal of Sedimentary Petrology, Vol.24, p.151-158.

Syvitski, J.P.M. and Murray, J.W. (1981) Particle interaction in fjords suspended sediment. Marine Geology, Vol.39, p.215-242.

Syvitski, J.P.M., Blakeney, C.P., and Hay, A.E. (1983) SAFE: sidescan sonar sounder profiles. In: Sedimentology of Arctic Fjords Experiment: HU82-031 data report, v.1 (Edited by Syvitski, J.P.M. and Blakeney, C.P.), Can. Data Pep. Hydrogr. Oc. Sci. Vol.12, p.16-1 - 16-49.

Syvitski, J.P.M. and Farrow, G.E. (1983) Structures and processes in bayhead deltas: Knight and Bute Inlet, British Columbia. Sedimentary Geology, Vol.36, p.217-244.

Syvitski, J.P.M., Lamplugh, M. and Kelly, B. (1984) Fjord morphology. In: Sedimentology of Arctic Fjords Experiment: HU83-028 Data Report, Vol.2 (Edited by J.M.P. Syvitski), Can. Data Rep. Hydrogr. Oc. Sci. 28: p.20-1 - 20-27.

Syvitski, J.P.M., Burrell, D.C. and Skei, J.M. (1987) Fjords: processes and products. Springer-Verlag, New York, 379pp.

Syvitski, J.M.P., Smith, J.N. and Calabrese, E.A. (1988) Basin sedimentation and growth of prograding deltas. Journal of Geophysical Research, Vol.93, p.6895-6908.

Syvitski, J.P.M. and Farrow, G.E. (1988) Fjord sedimentation as an analogue for small hydrocarbon-bearing fan deltas. In: Deltas: Sites and Traps for Fossil Fuels (Edited by M.K.G. Whateley and K.T. Pickering). Geological Society Special Publication, p.1-23.

Van Tassell, J. (1981) Silver abyssal plain carbonate turbidite: flow characteristics. Journal of Geology, Vol.89, p.317-333.

Williams, H.F.L. and Roberts, M.C. (1989) Holocene sea-leave change and delta growth: Fraser River delta, British Columbia. Canadian Journal of Earth Science, Vol.26, No.9, p.1657-1666.

Yalin, M.S. (1972) Mechanics of sediment transport. Pergamon Press Ltd., Oxford, 290pp.

Zeng, J.J., Lowe, D.R., Prior, D.B., Wiseman, W.J., Jr., and Bornhold, B.D. (1991) Flow properties of turbidity currents in Bute Inlet, British Columbia. Sedimentology, Vol.38, p.975-996.

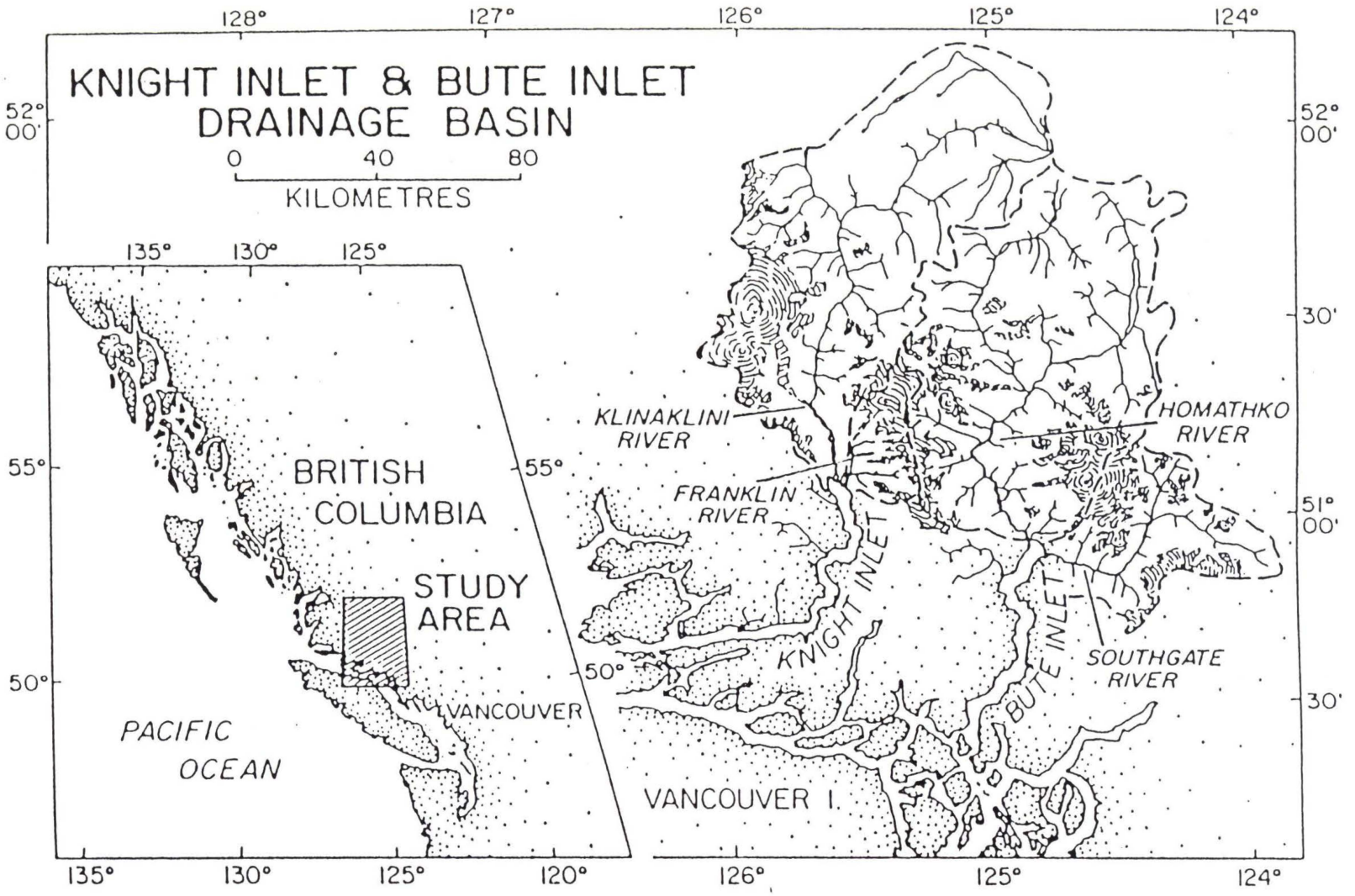

FIG. 1. Location of the study area and major drainage basins of Knight and Bute inlets, British Columbia, Canada.

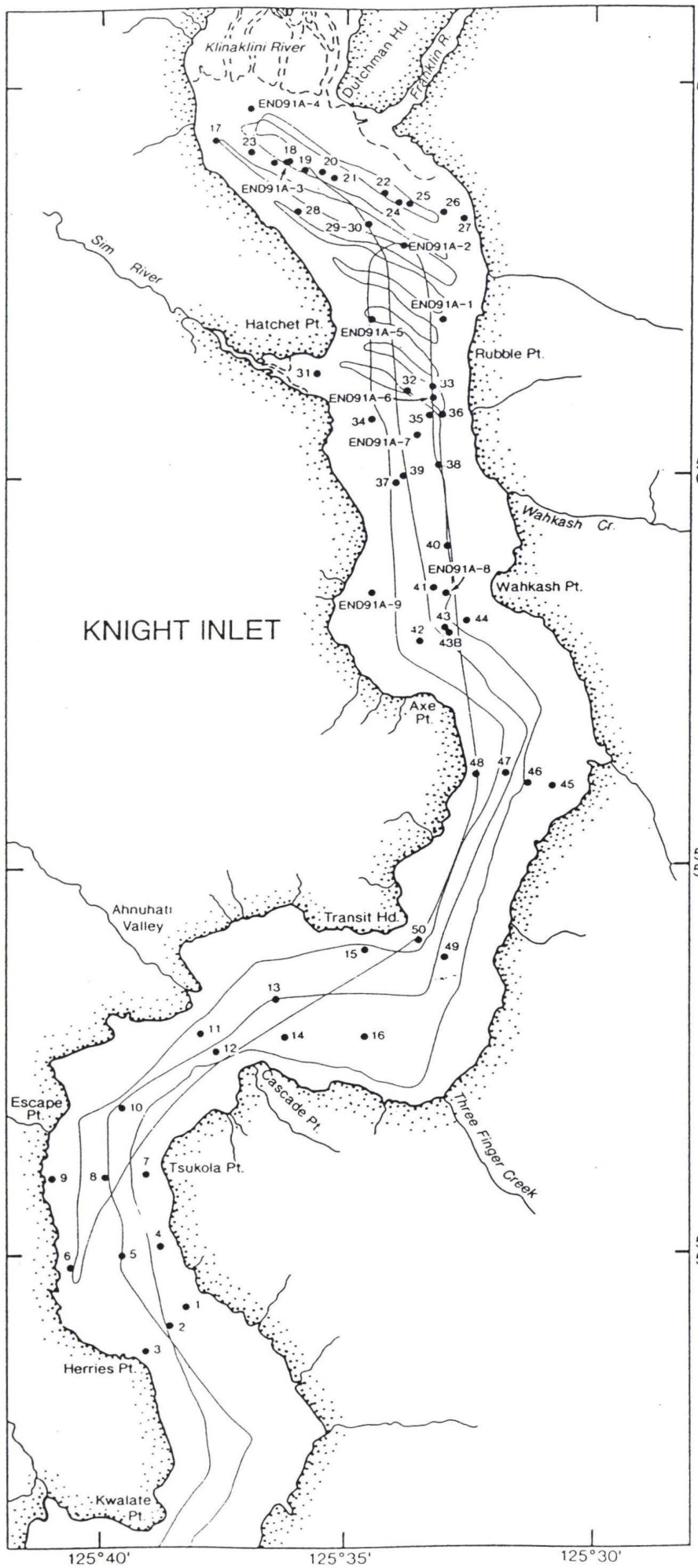

Figure 2. Sample distribution and geophysical survey tracklines within the study area.

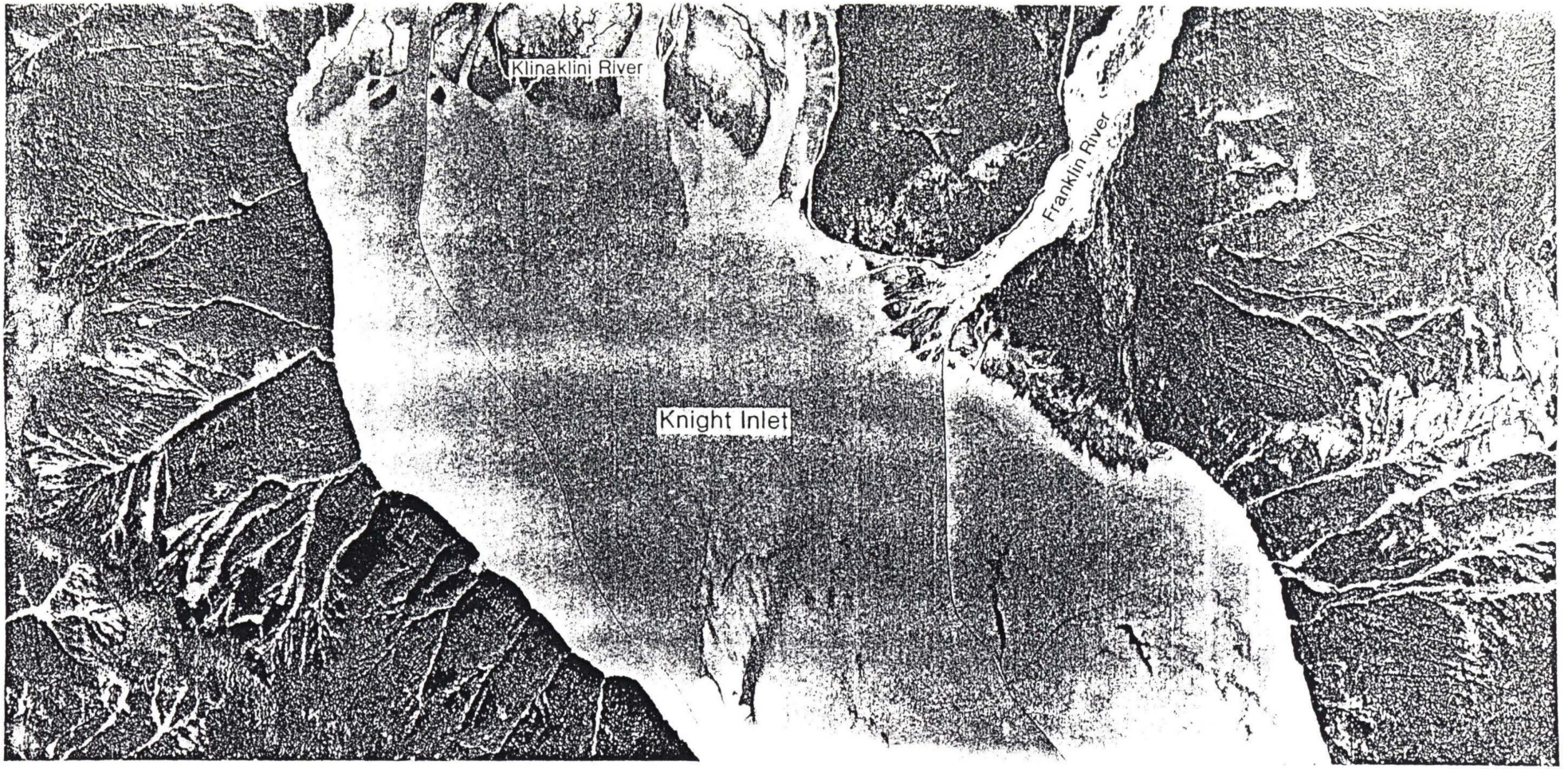

Figure 3. Klinaklini and Franklin rivers at the head of Knight Inlet.

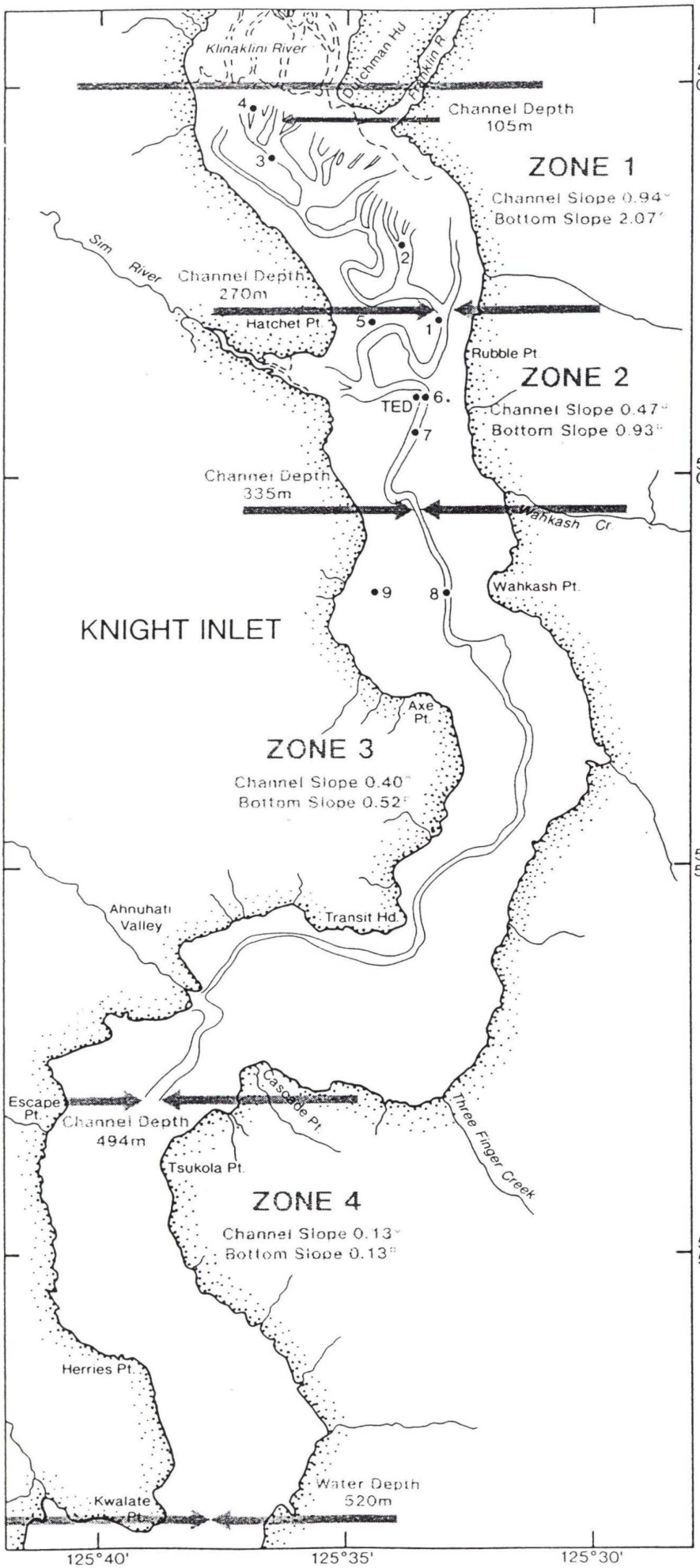

Figure 4. Configuration of the channel system and the four seafloor morphology zones.

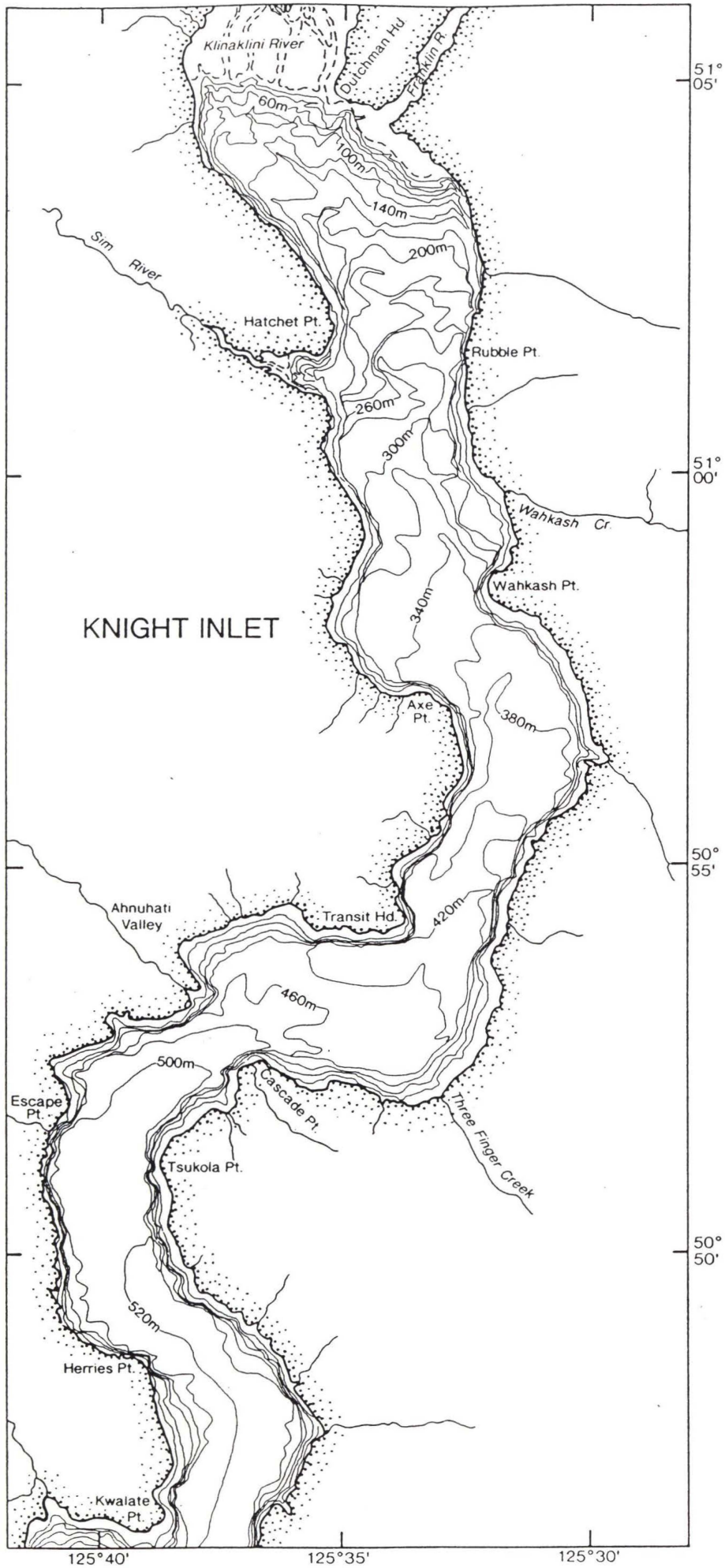

Figure 6. Bathymetric map of Knight Inlet within the study area (20 m intervals).

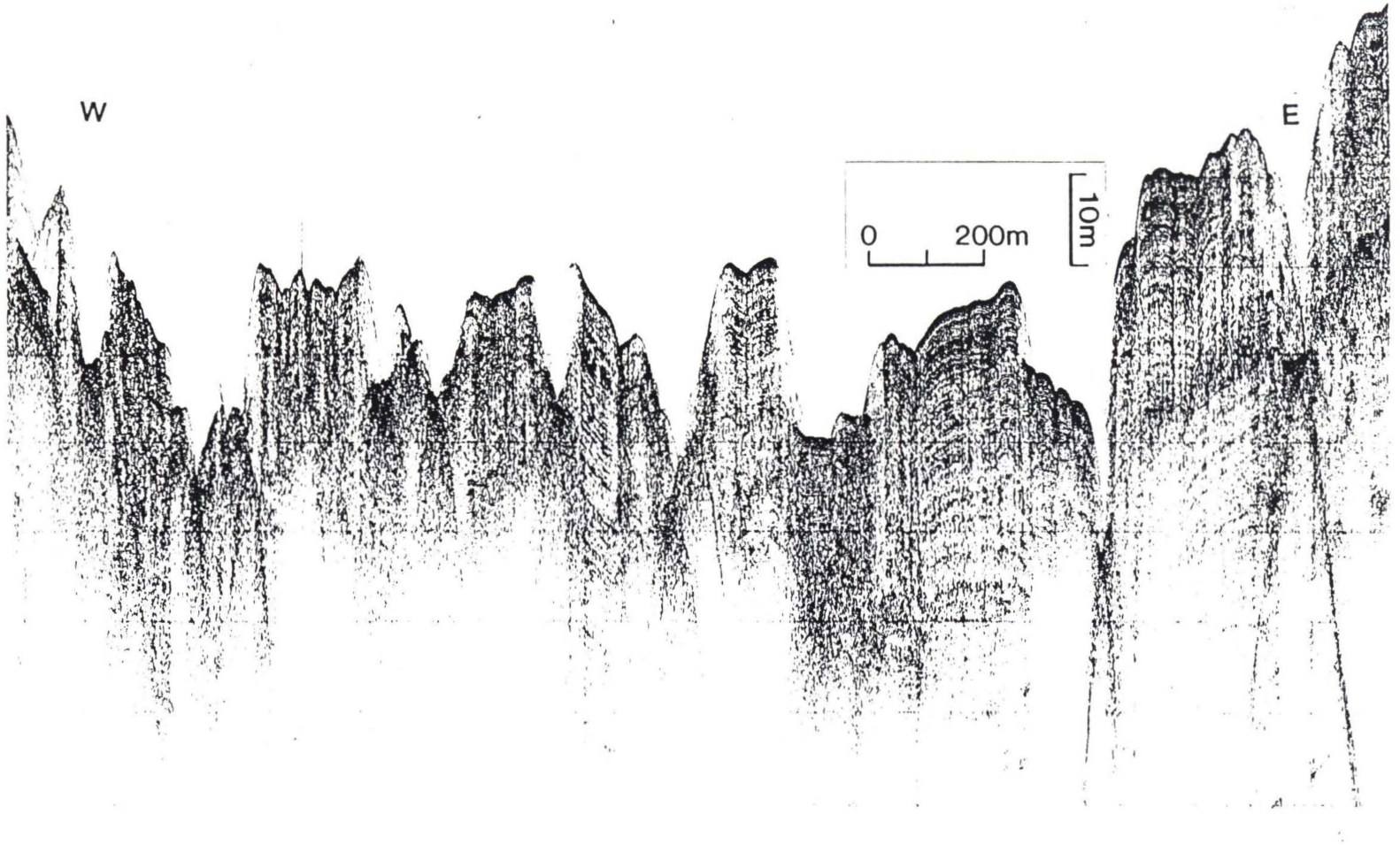

Figure 7. Echosounding profile showing the abundance of channels near the Klinaklini River mouth.

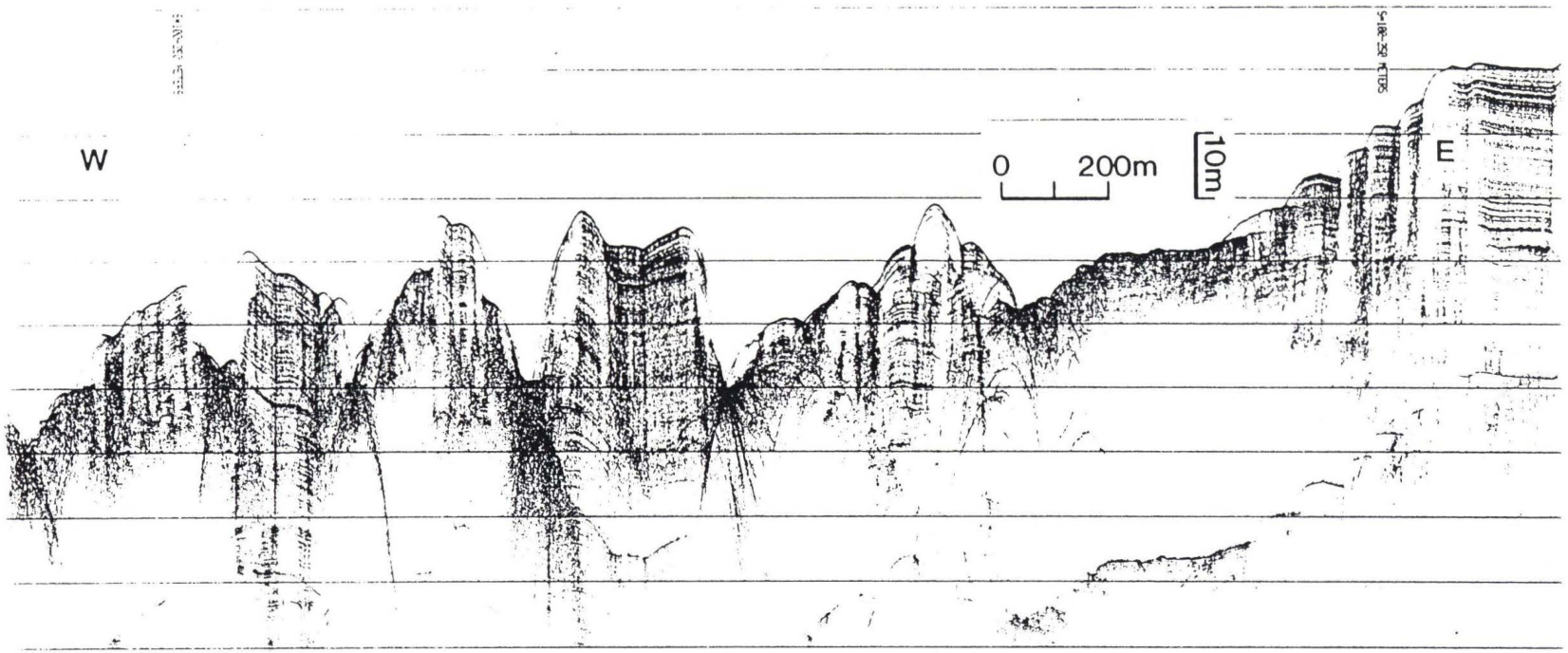

Figure 8. Echosounding profile showing the abundance of channels near the Franklin River mouth.

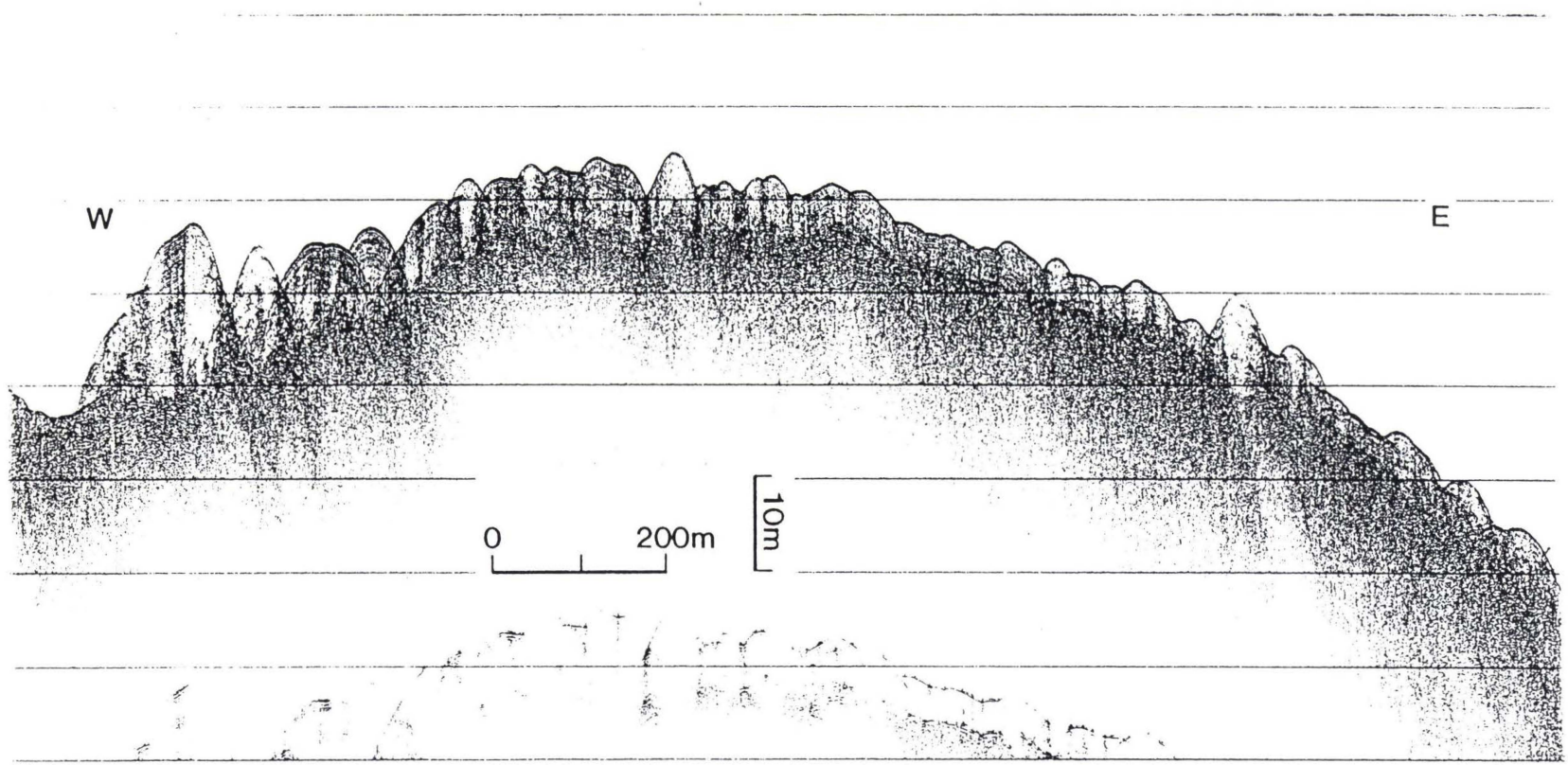

Figure 9. Echosounding profile showing the area near the head of the inlet to the east of the Franklin River mouth.

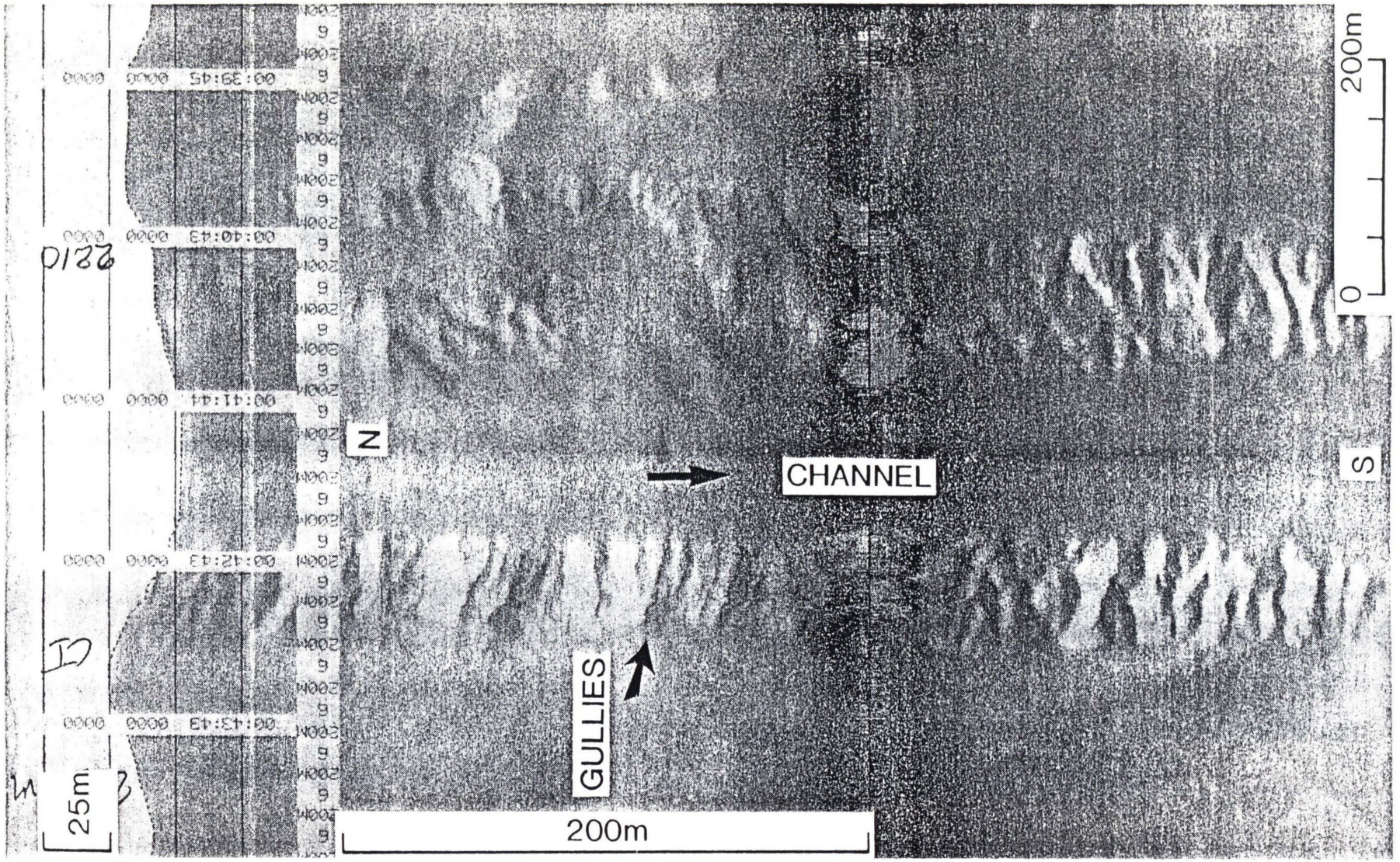

Figure 10. Sidescan sonograph showing one particular gully in the upper part of Knight Inlet.

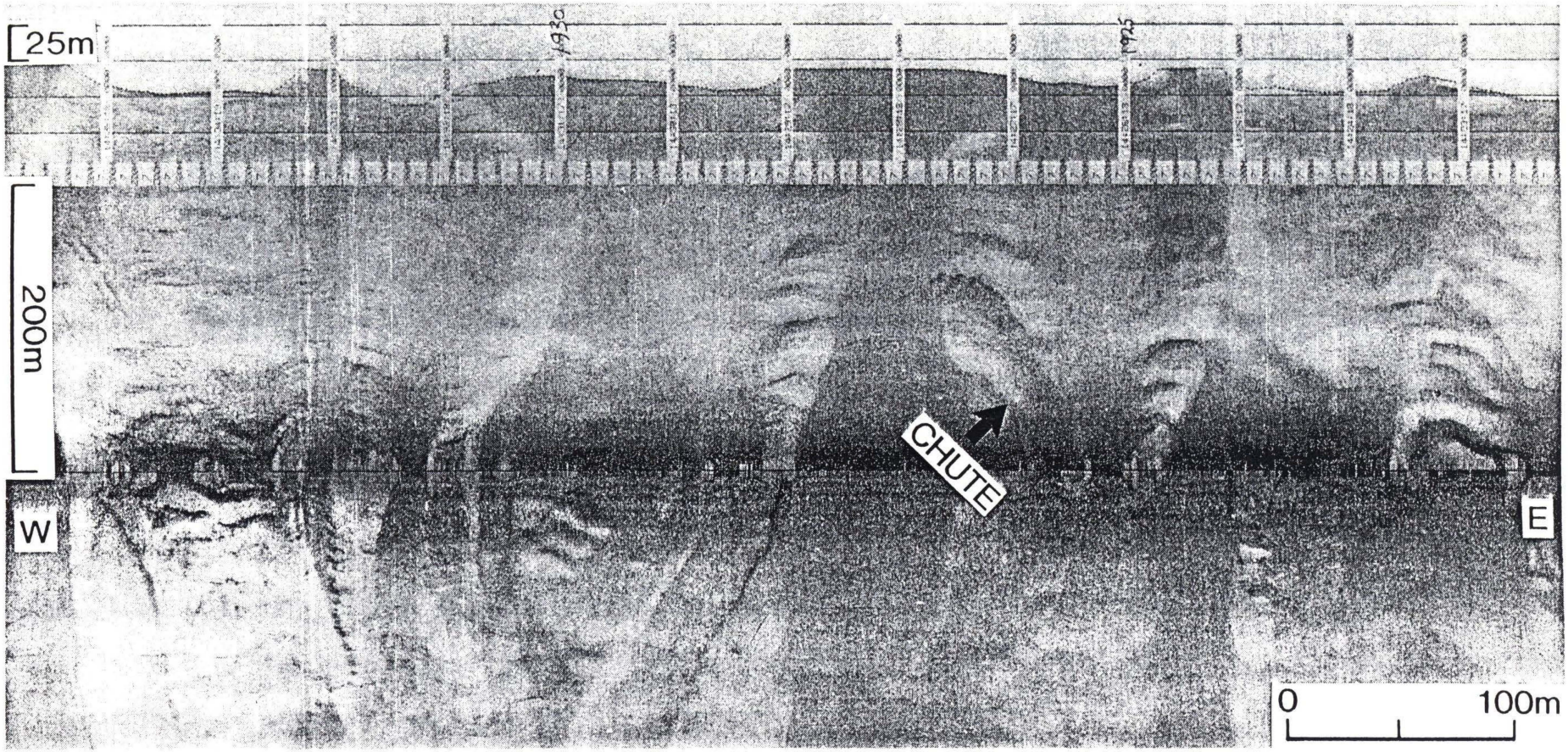

Figure 11. Sidescan sonograph showing several channels with gullies in Zone One.

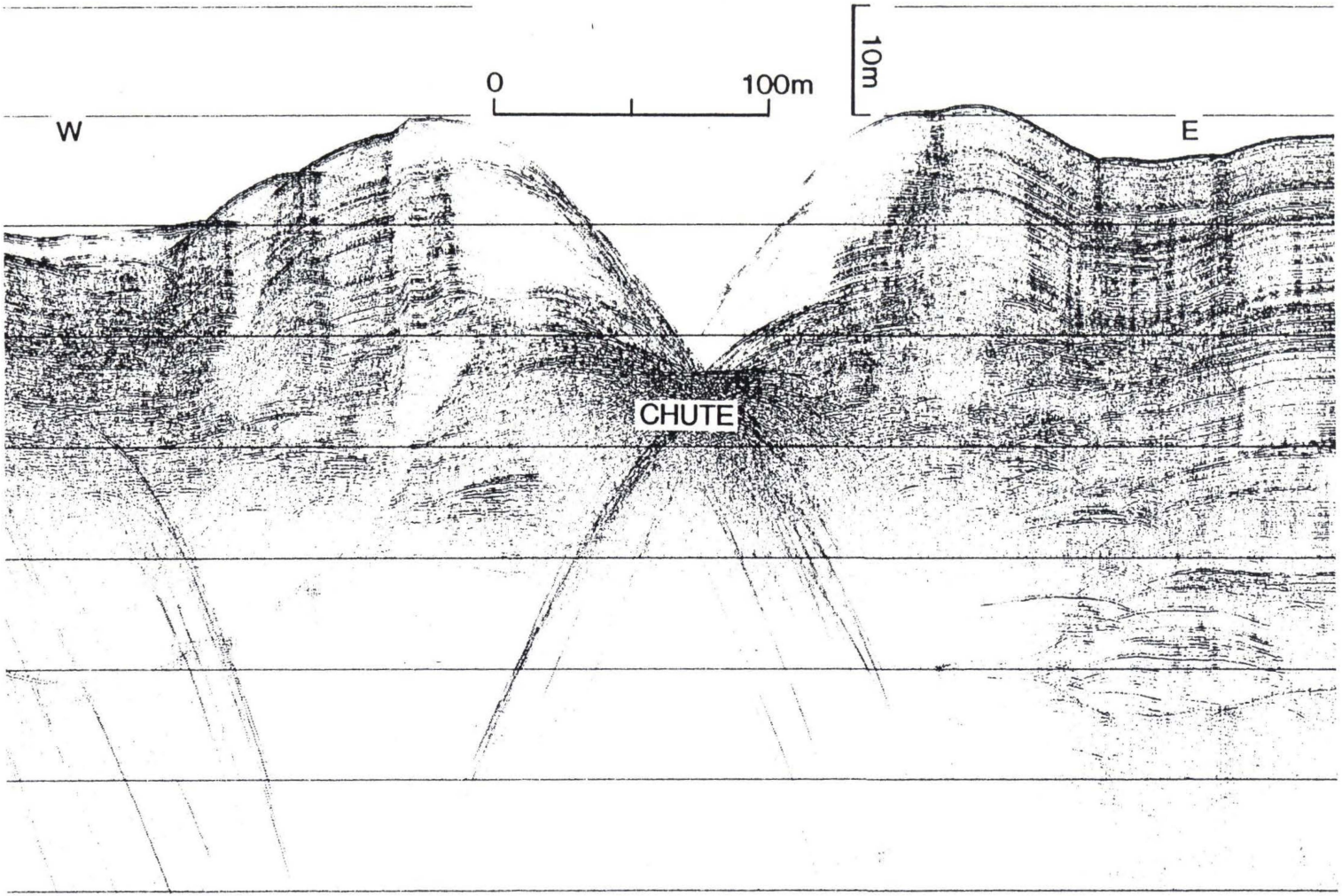

Figure 12. Echosounding profile displaying the cross-section of a channel with gully in Zone One .

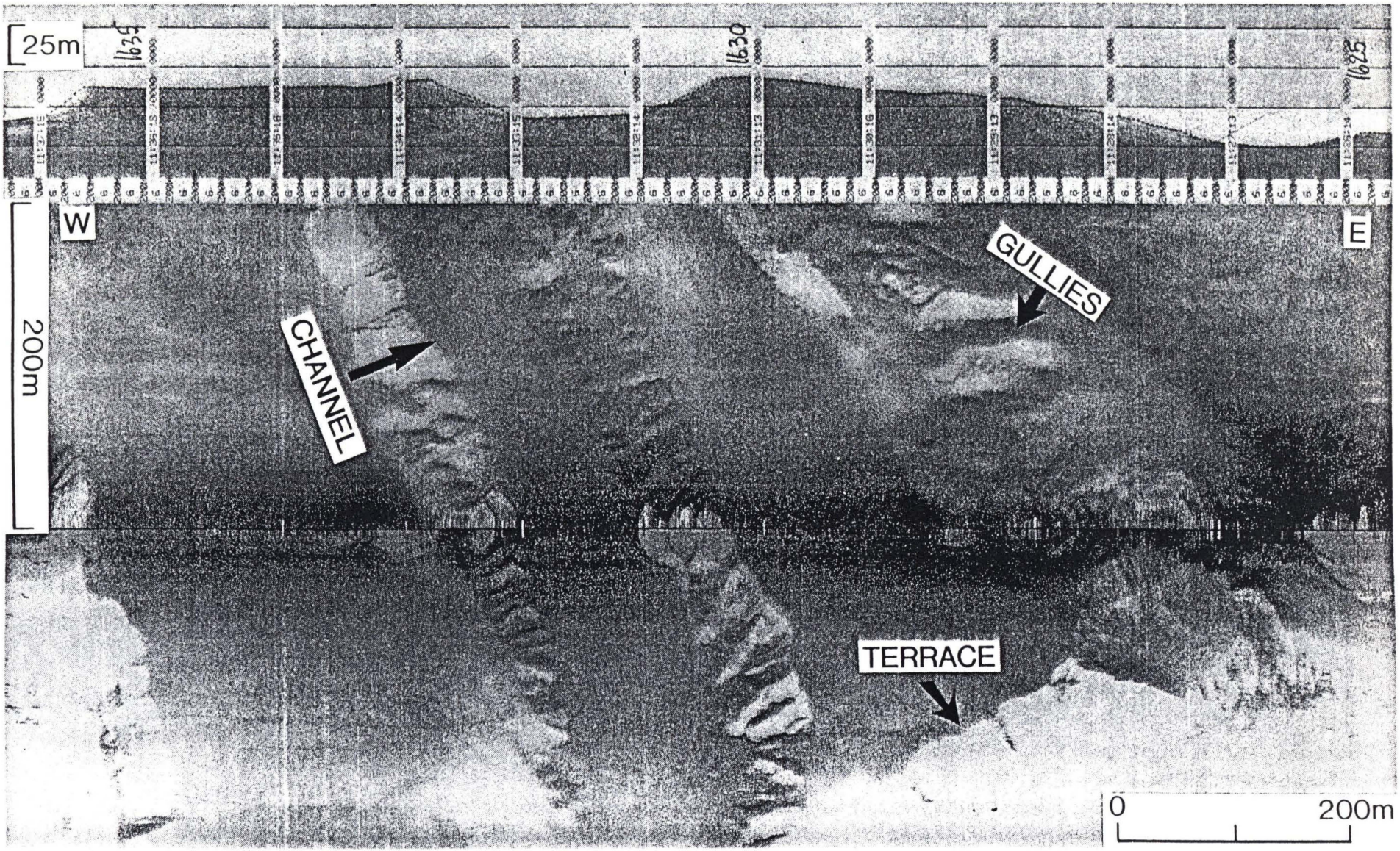

Figure 13. Sidescan sonograph of a terrace in Zone One .

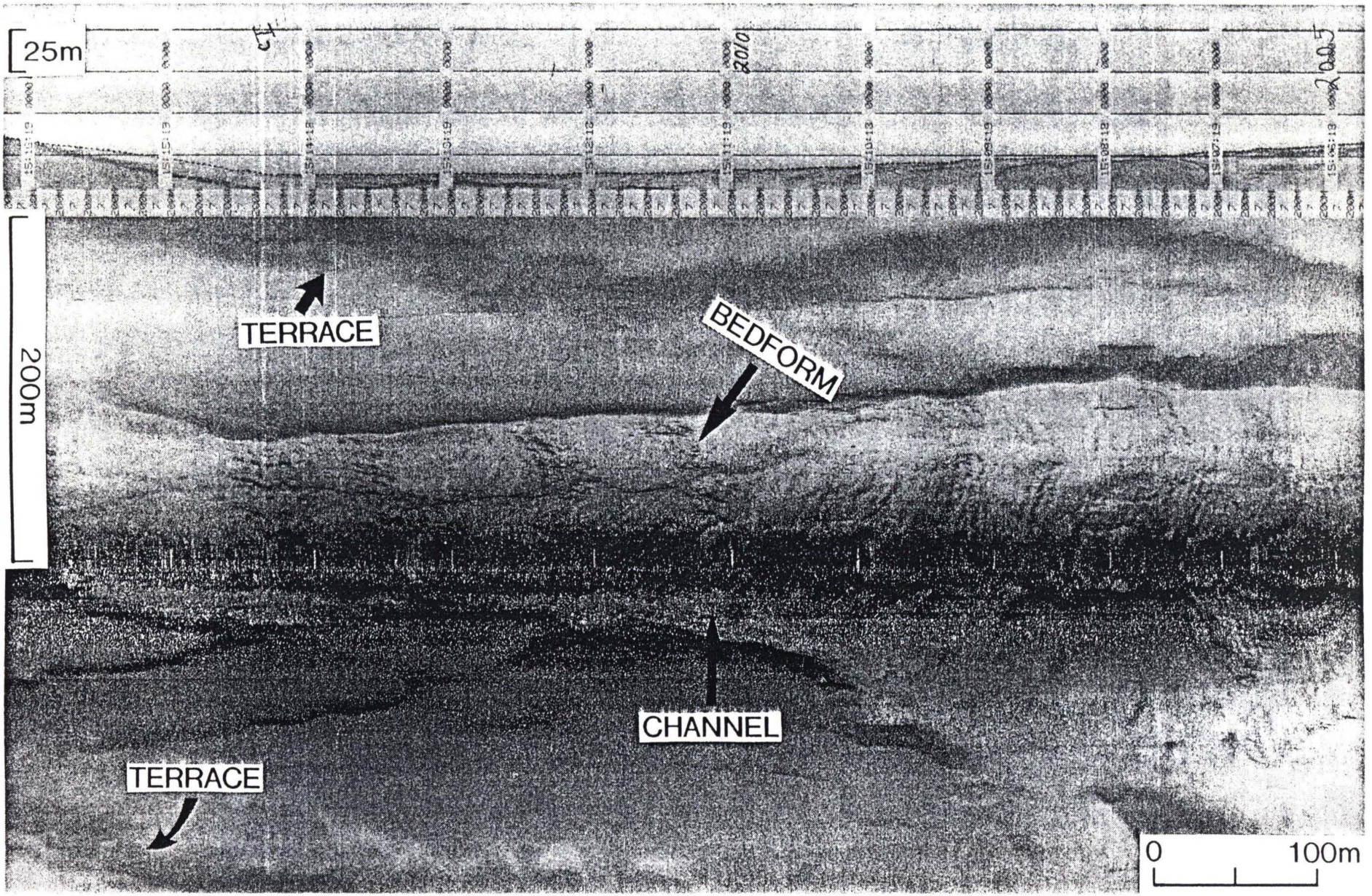

Figure 14. Sidescan sonograph displaying bedforms within the channel and terraces long the edges of the channel.

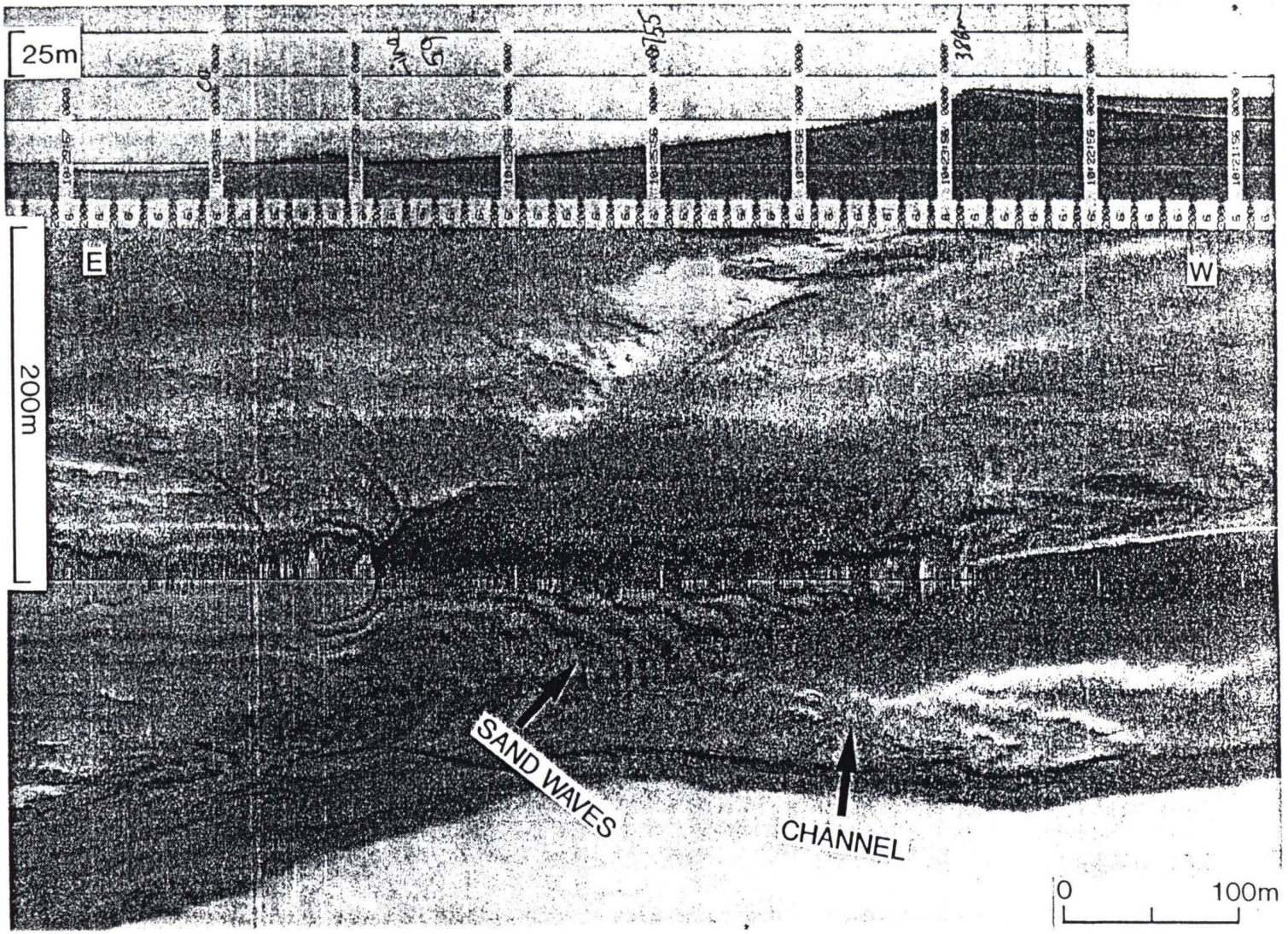

Figure 15. Bedform shapes and sizes varying along the slope as displayed on sidescan sonograph.

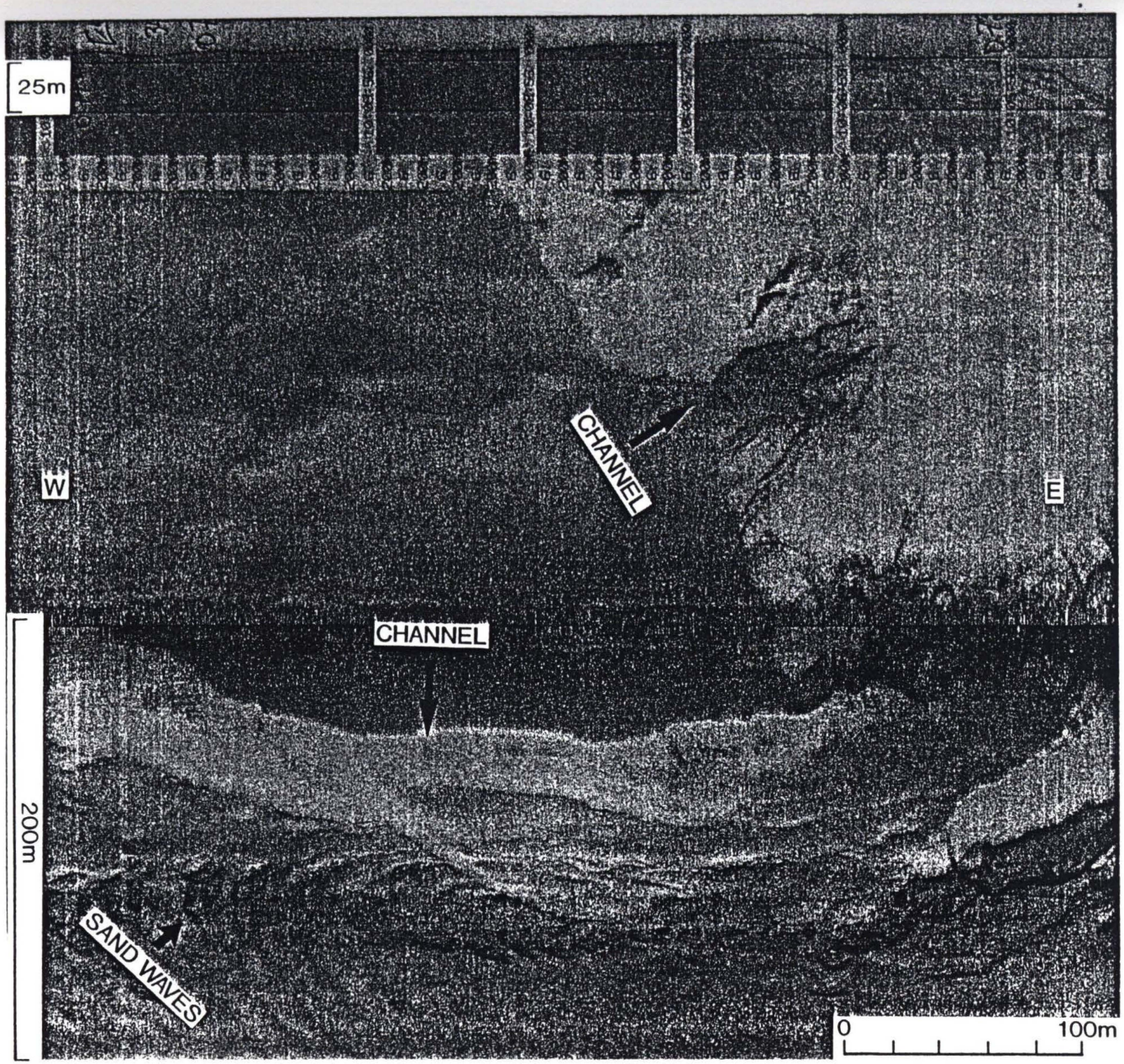

Figure 16. Bedform shapes and sizes varying along the slope (Continuing Figure 15), and two channels merging at the right hand side.

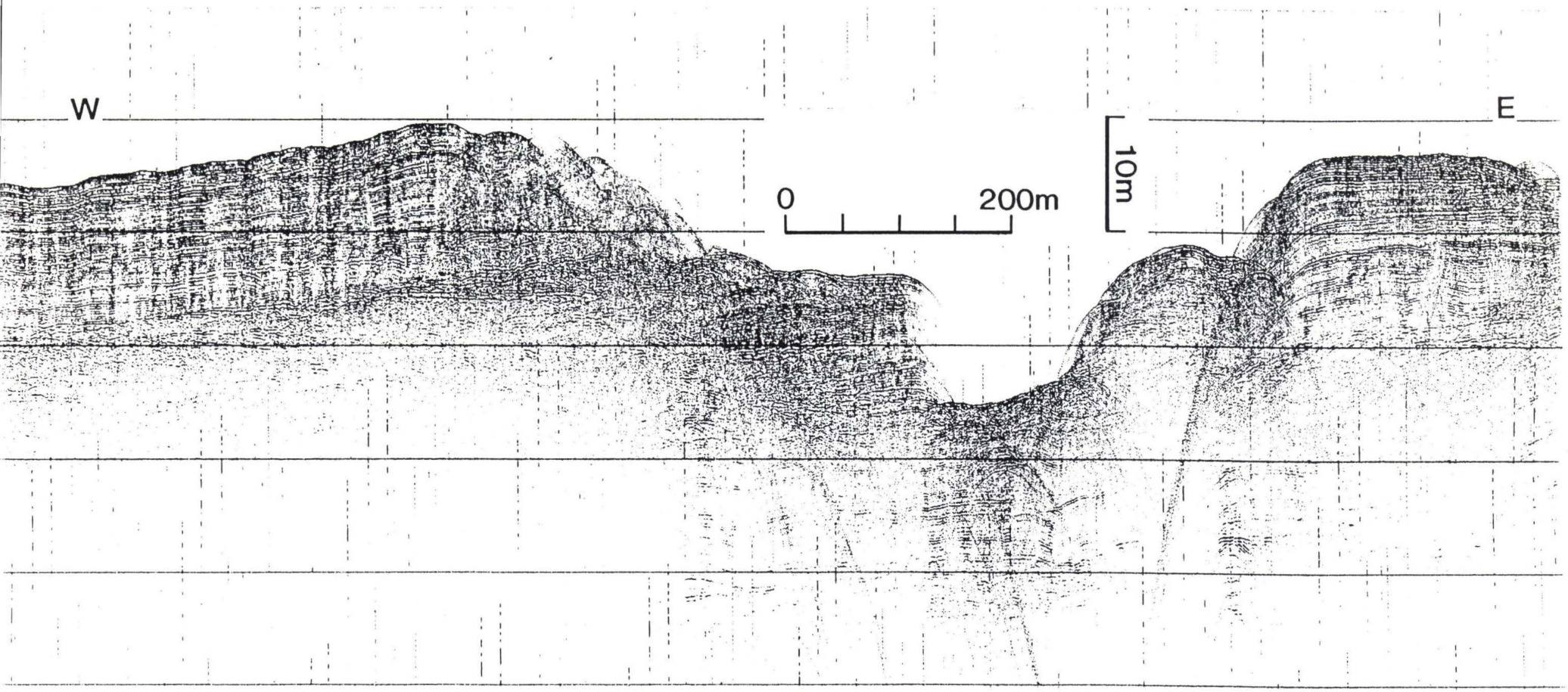

Figure 17. Echosounding profile showing a cross-section of the terrace around the channel.

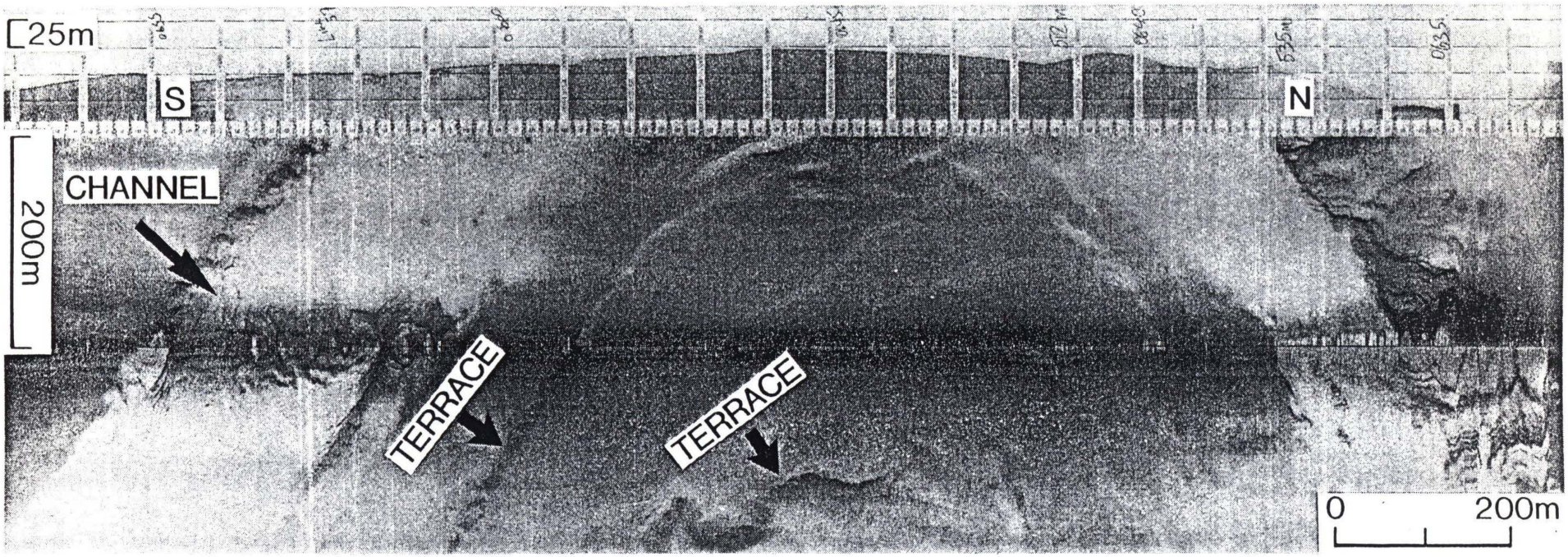

Figure 18. Sidescan sonograph showing a channel bend with several terraces on the convex side.

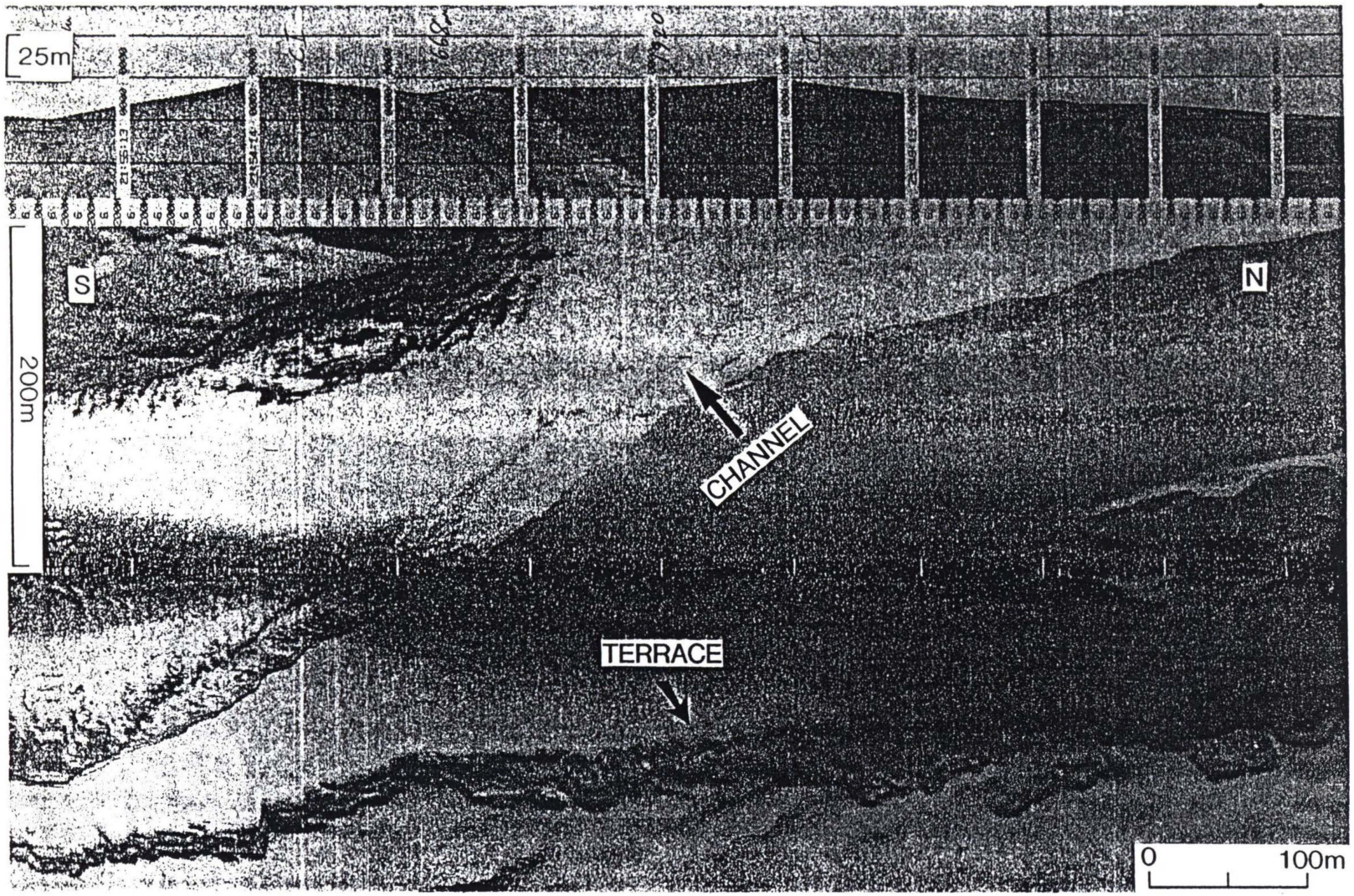

Figure 19. Sidescan sonograph displaying the terrace with arcuate erosional features developed on one side of the channel.

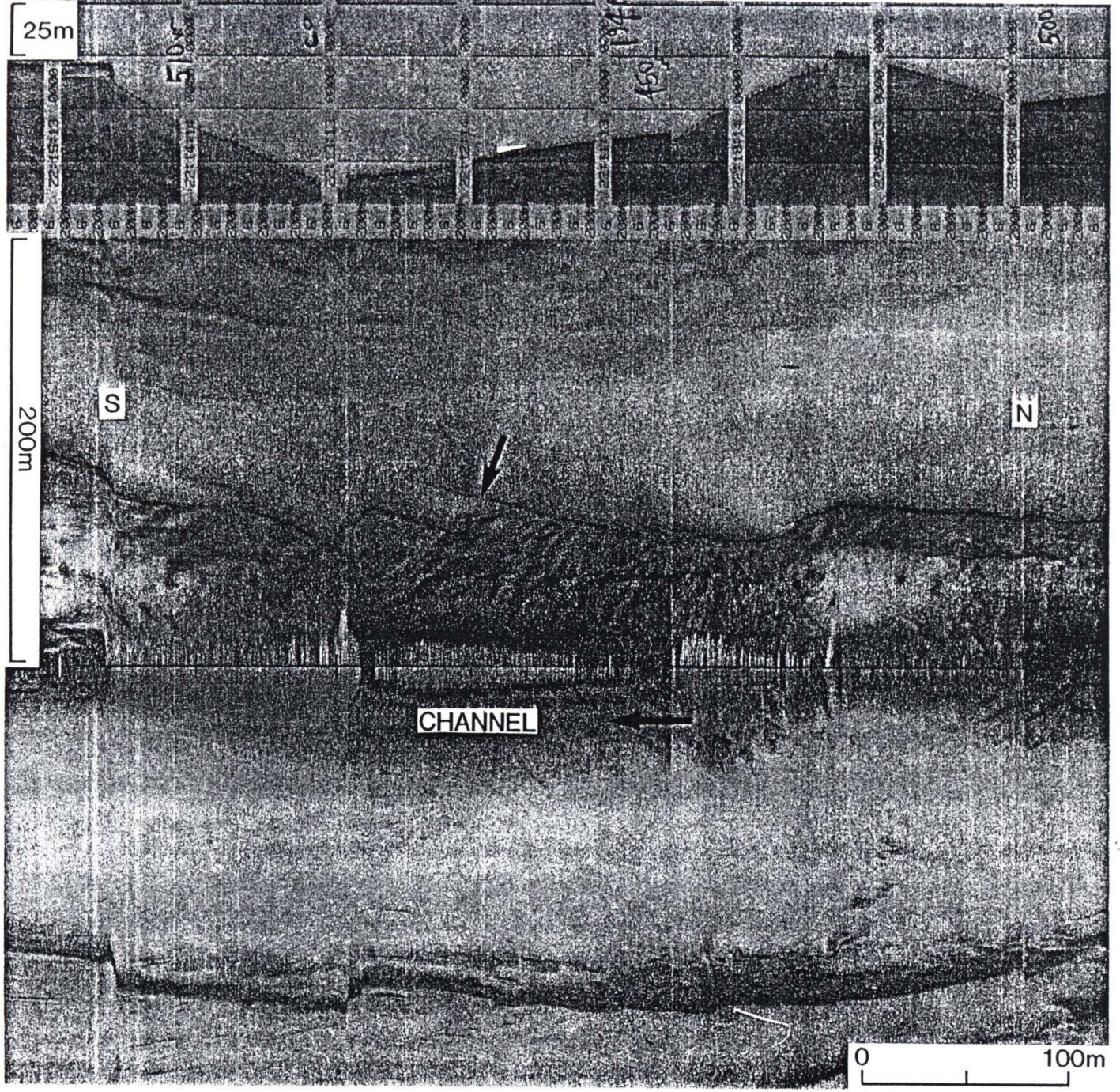

Figure 20. Channel wall at the point of incipient failure (see thin dark line) shown along the channel edge on the sidescan sonograph.

Figure 21. A large flute displayed on the sidescan sonograph.

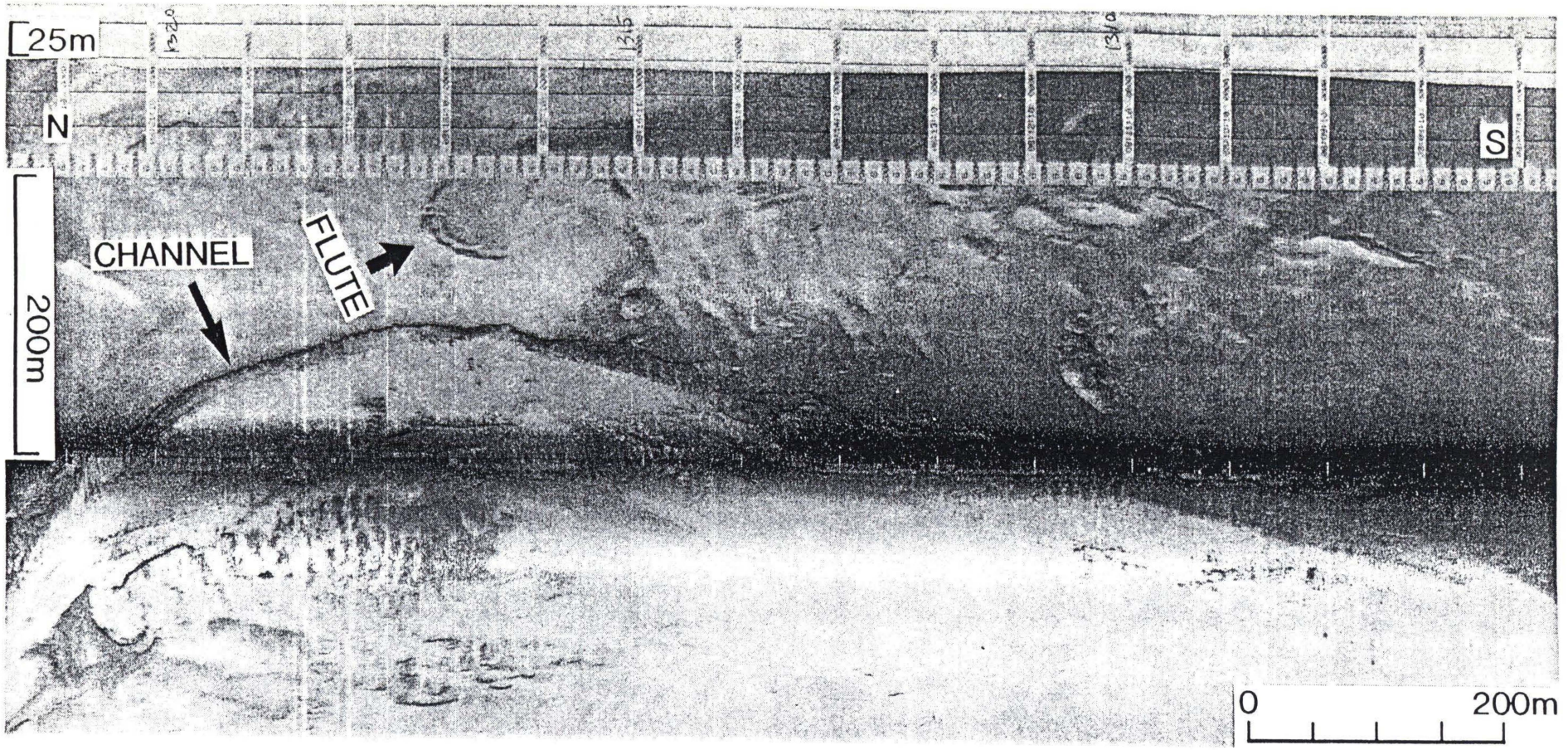

Figure 22. Sidescan sonograph showing a flute developed outside the curved channel.

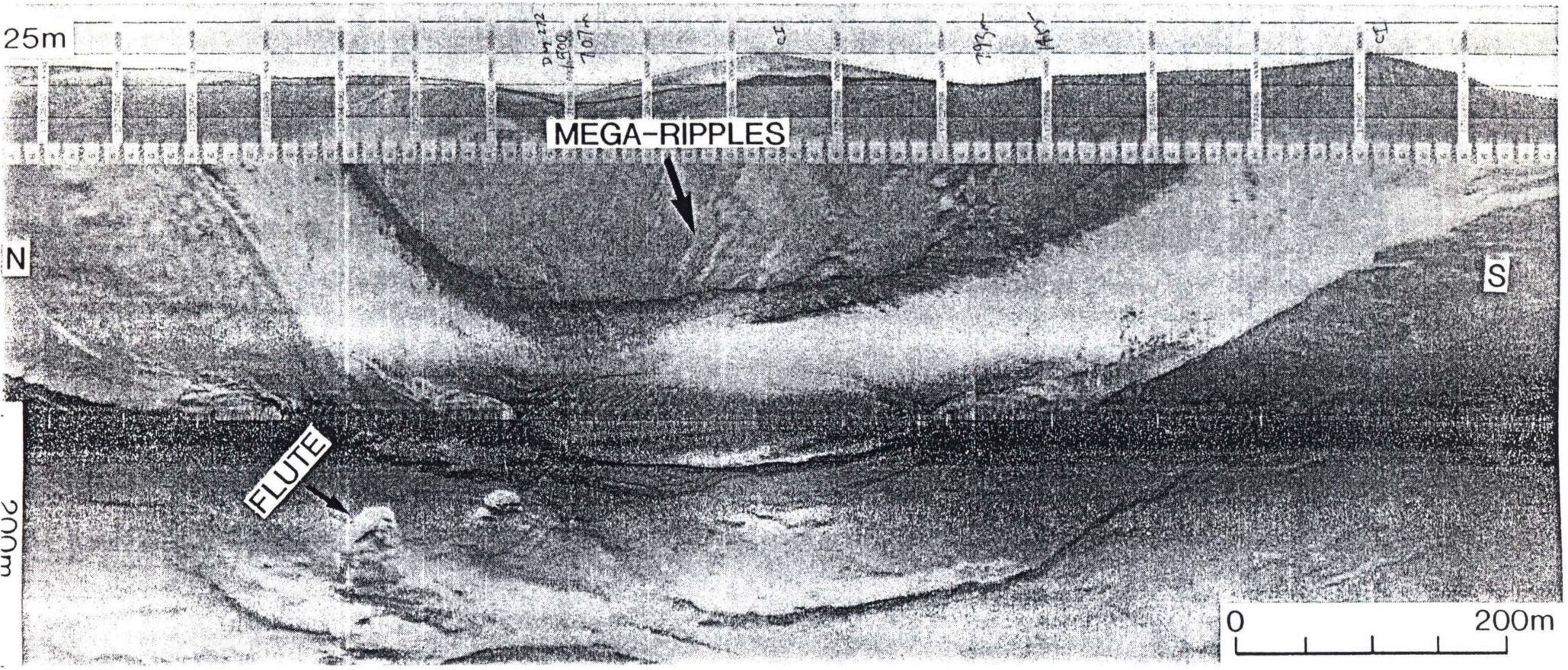

Figure 23. Sidescan sonograph showing transverse mega-ripples developed on the convex side of the channel and a flute on the concave side.

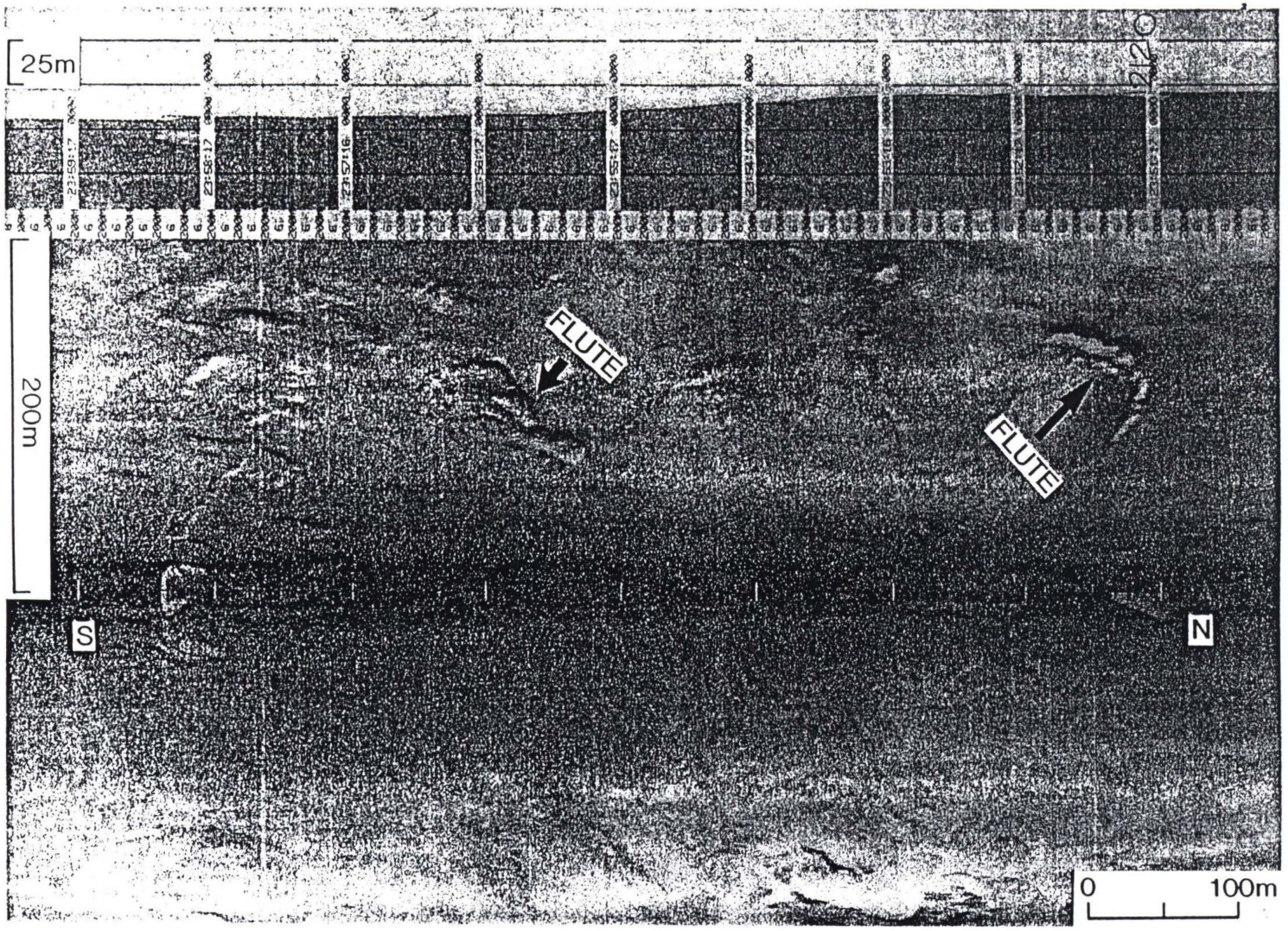

Figure 24. Several flutes (including three overlapped flutes in the mid-part of the sonograph), and low-relief depressions displayed on the sidescan sonograph.

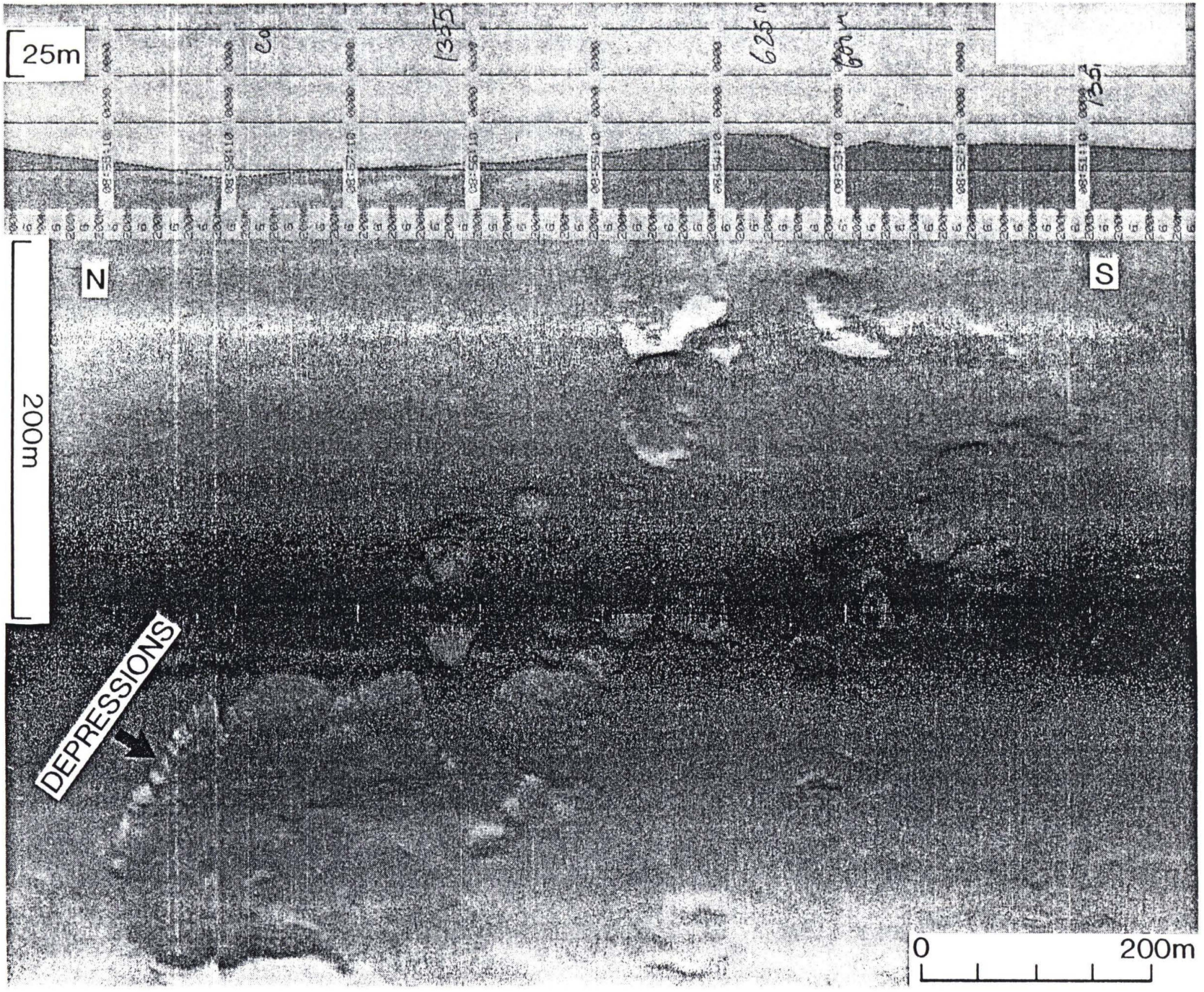

Figure 25. Large swales and small rounded depressions shown on the sidescan sonograph.

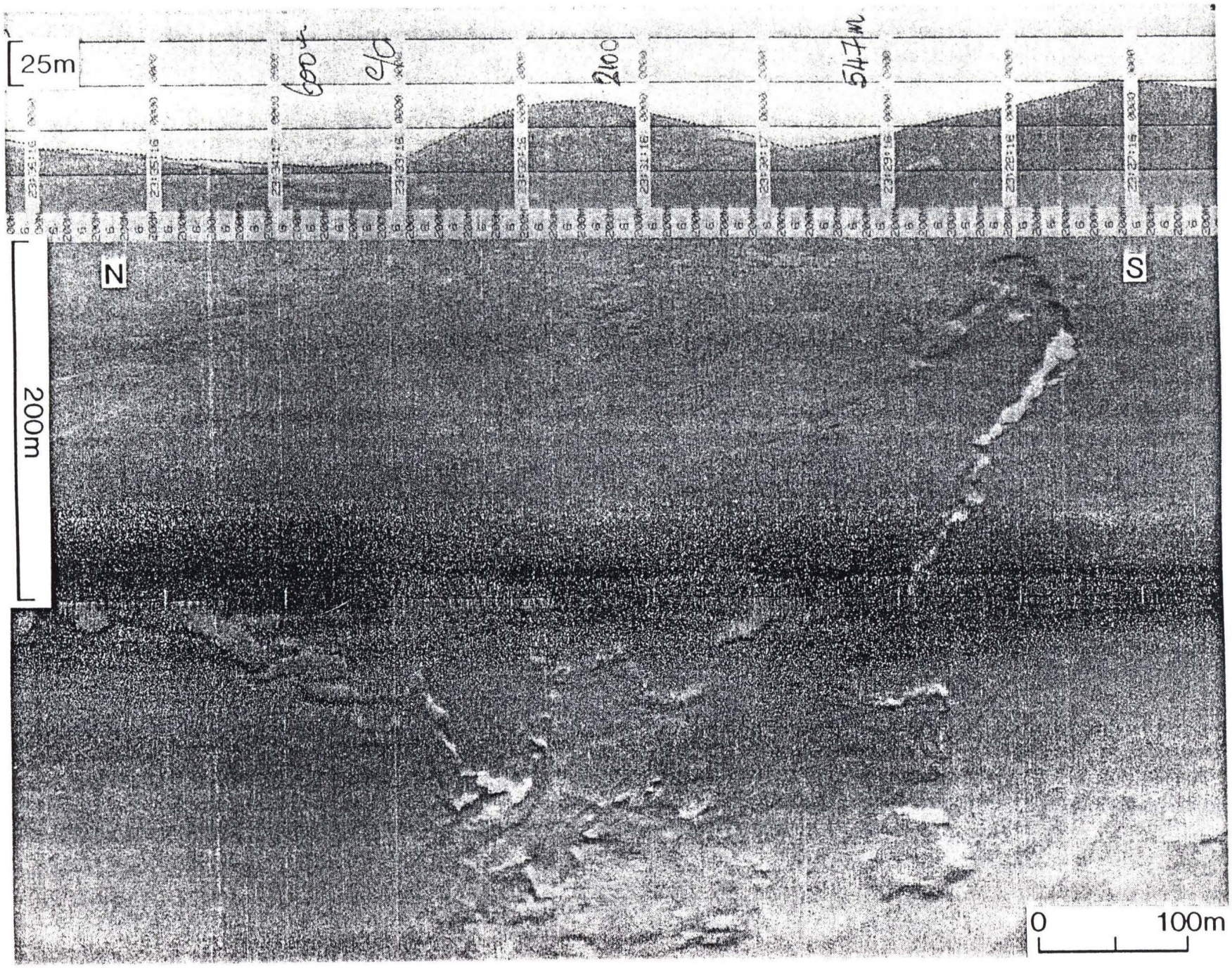

Figure 26. Small irregular relief features (less than 1 m) on the sidescan sonograph.

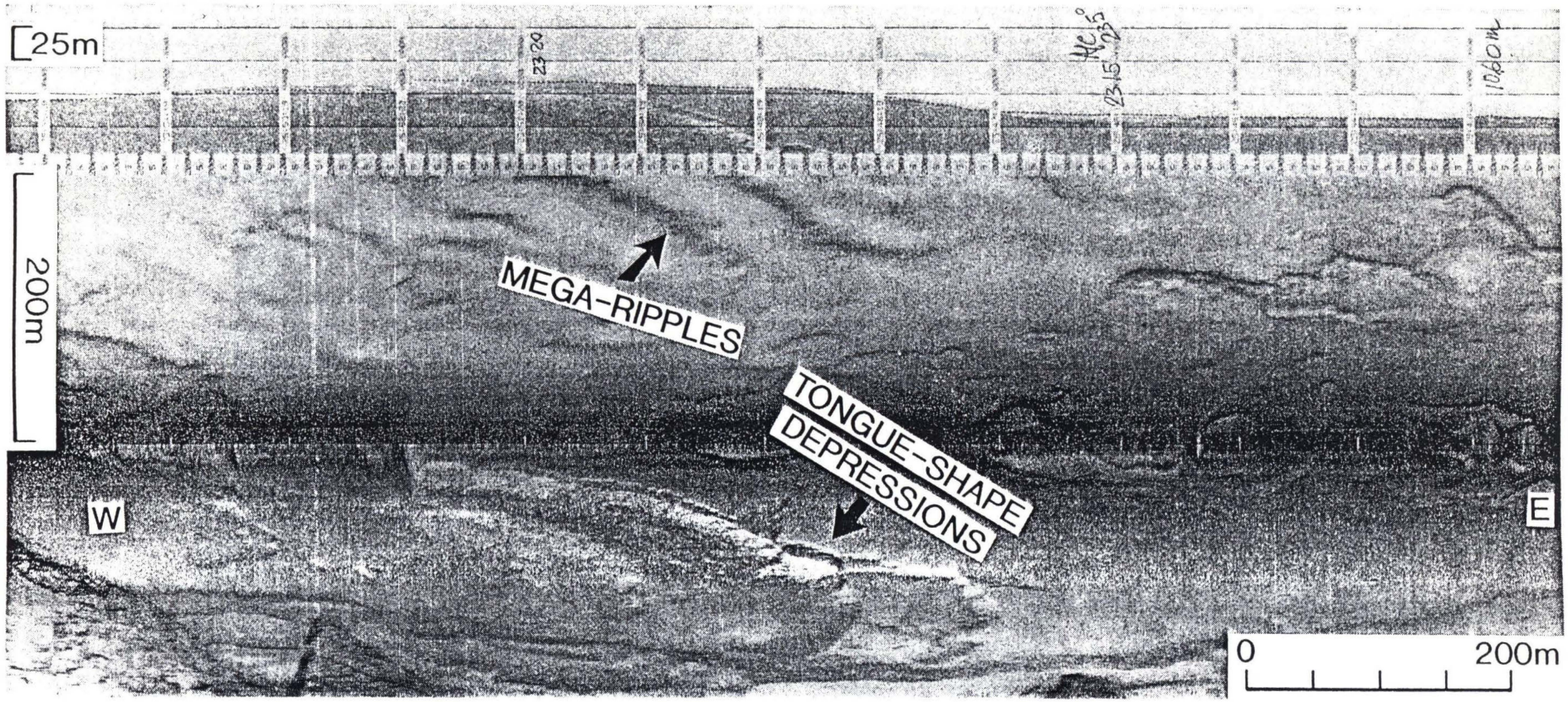

Figure 27. A tongue-shape depression (at the bottom), mega-ripples (at the top) and several small irregular depressions shown on the sidescan sonograph.

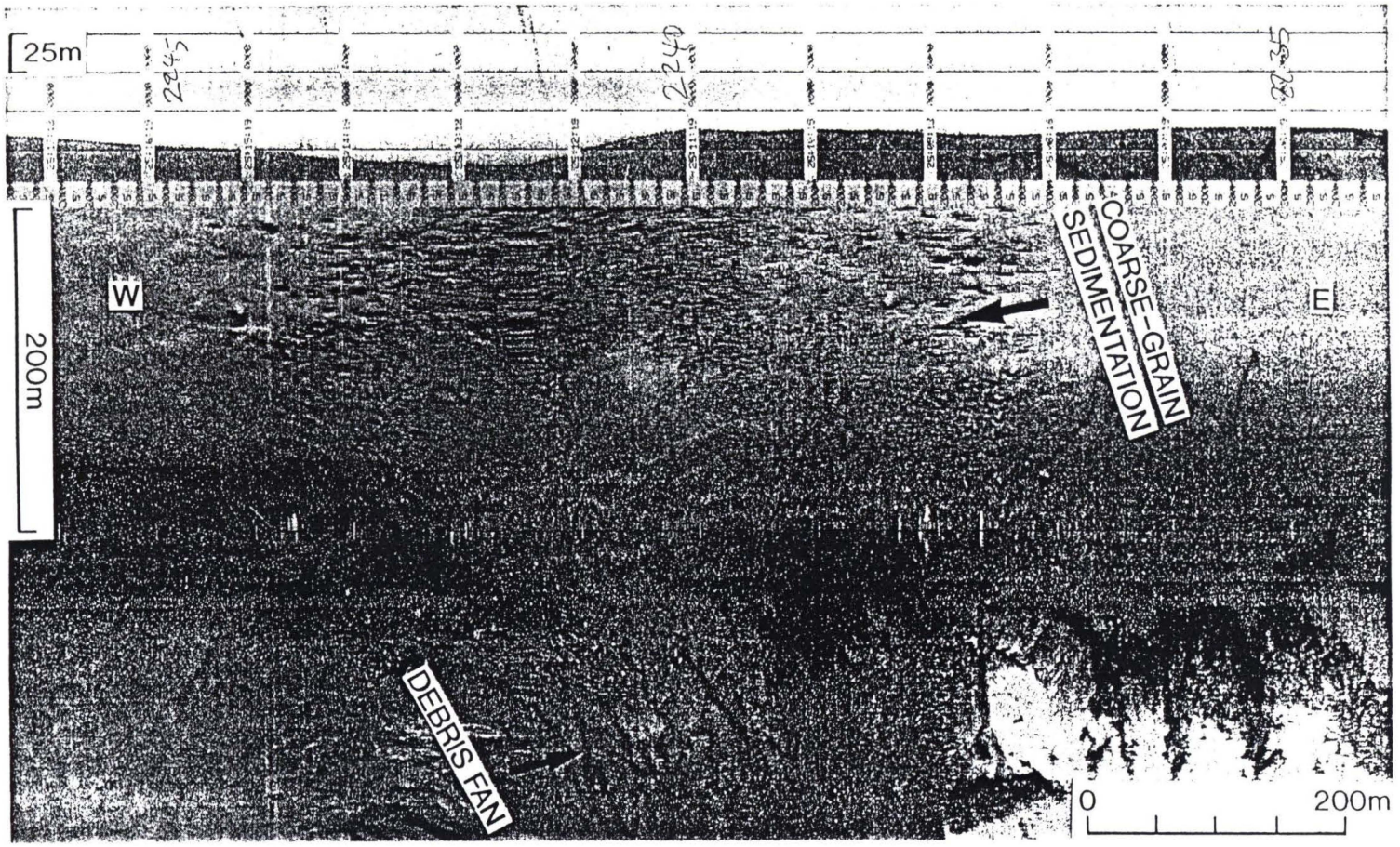

Figure 28. Sidescan sonograph showing debris fan features and coarse materials deposited on the lower part of the fan.

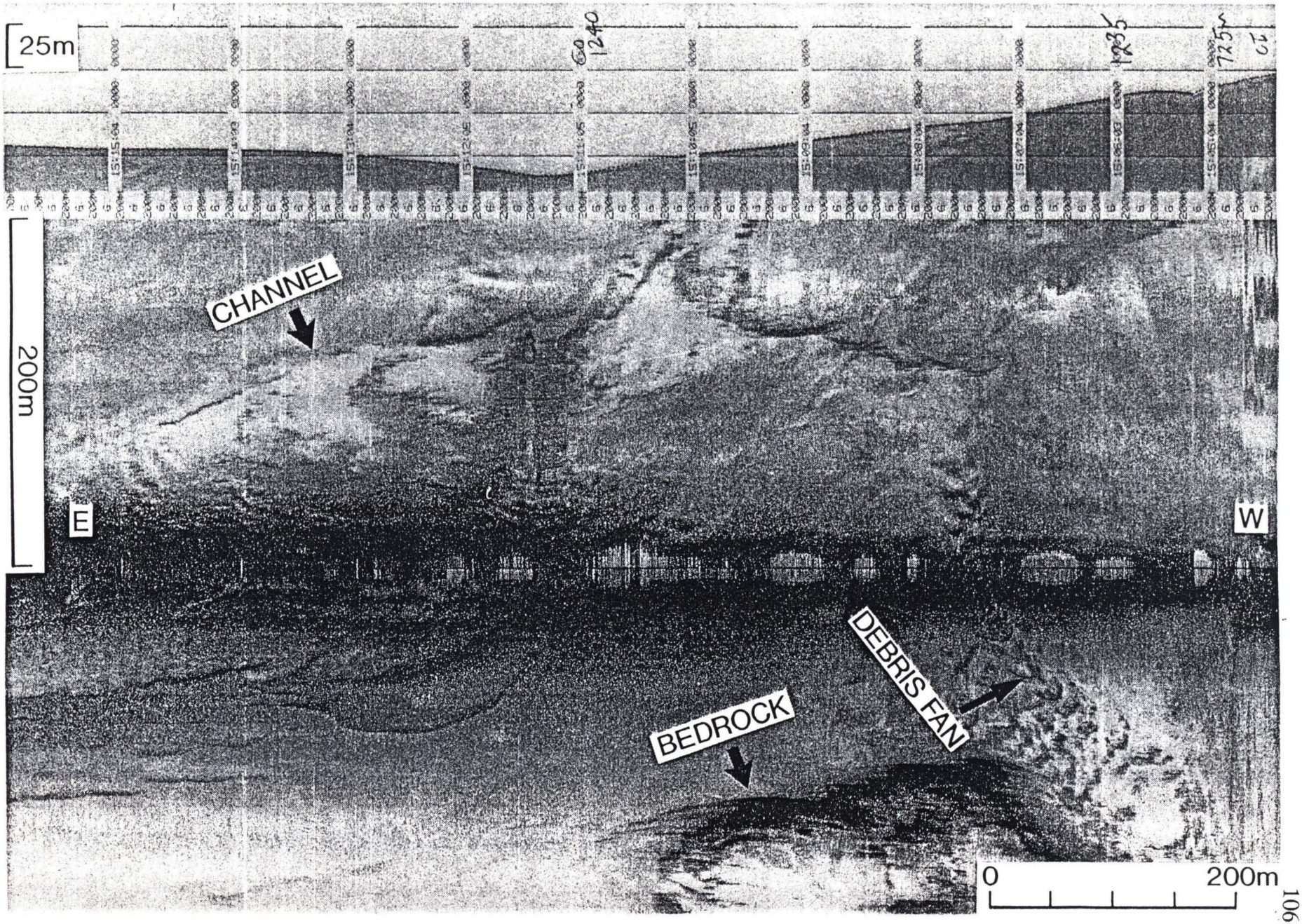

Figure 29. Sidescan sonograph displaying another debris fan feature.

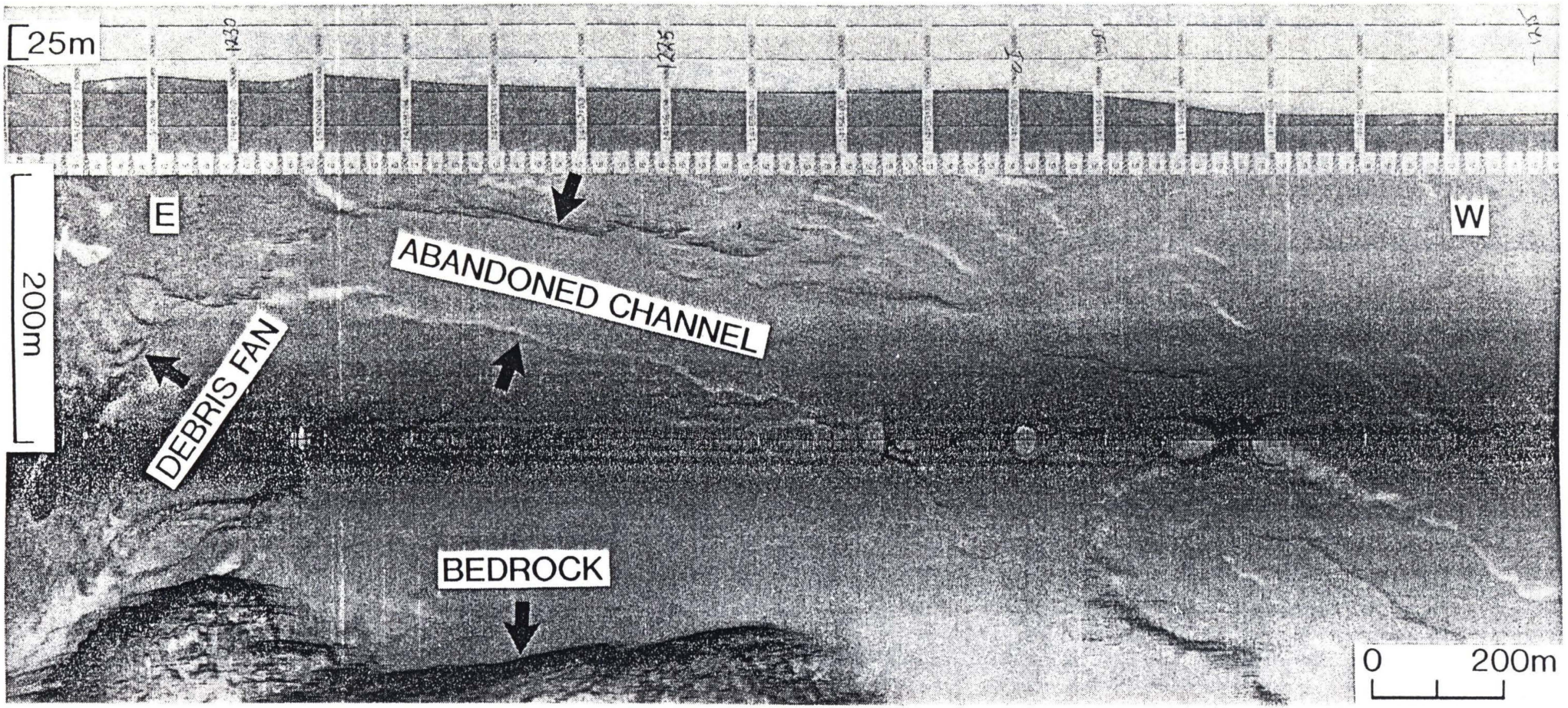

Figure 30. Sidescan sonograph showing an abandoned channel.

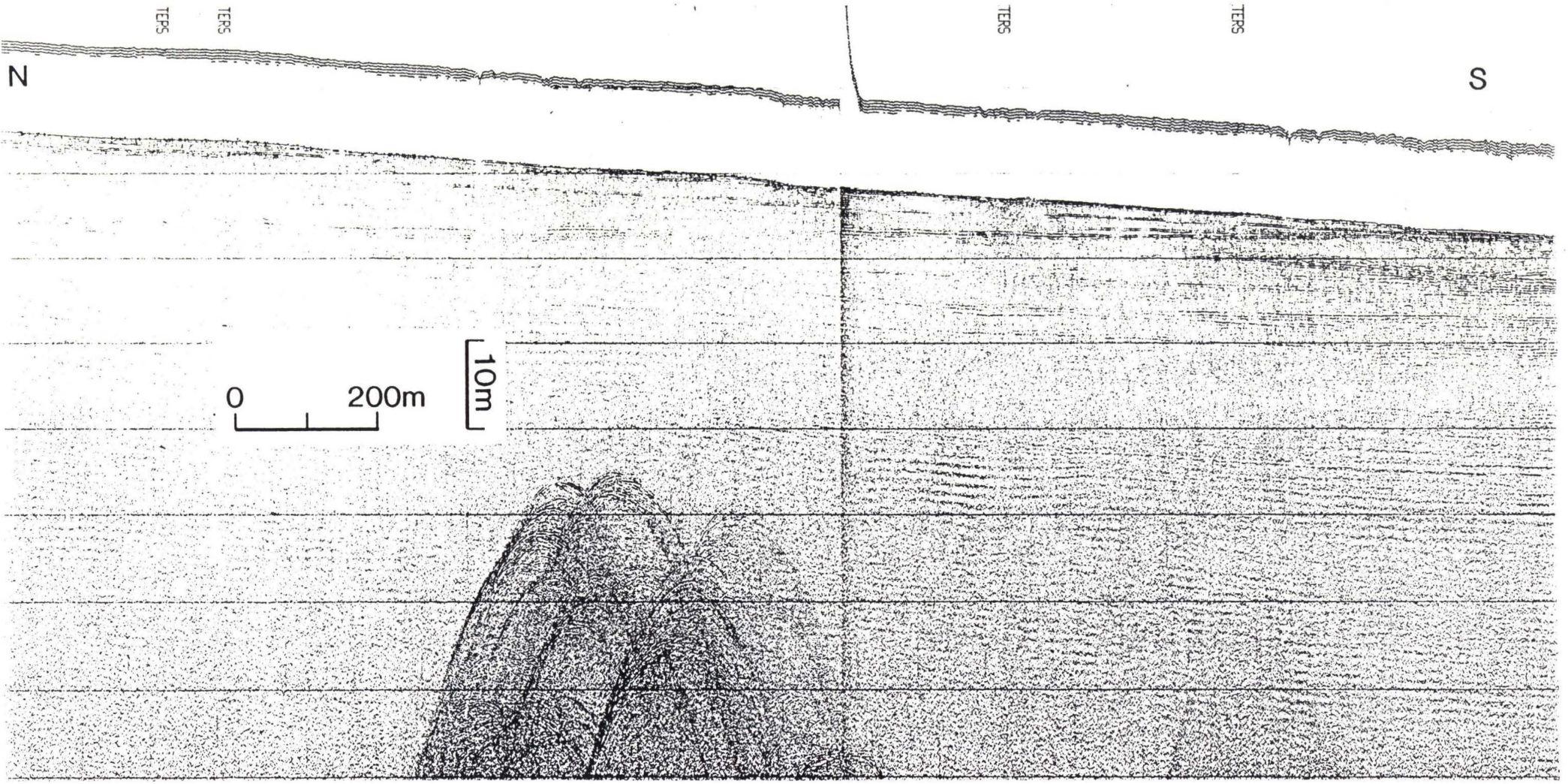

Figure 31. Echosounding profile displaying the smooth and gentle seafloor in Zone Four .

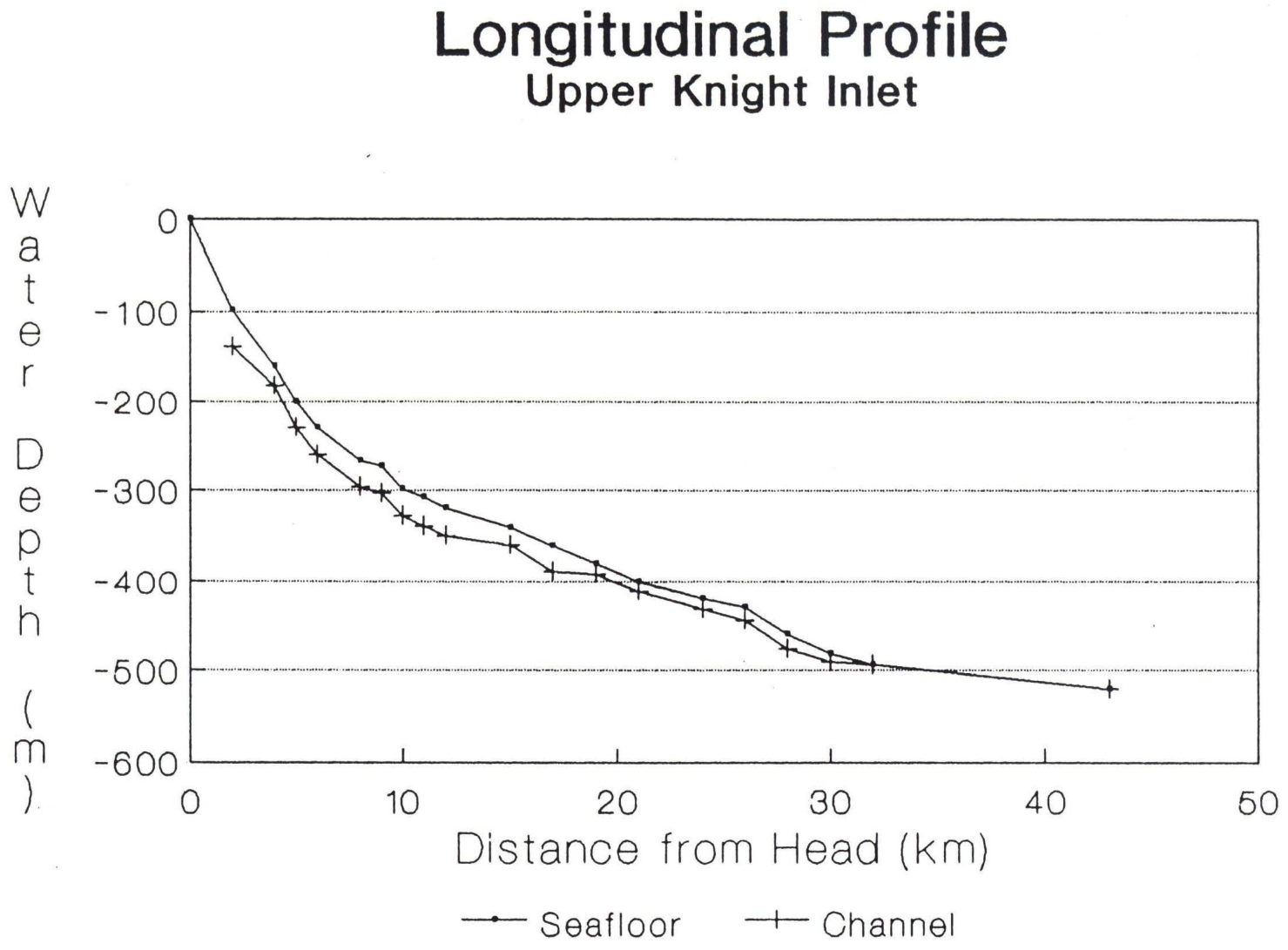

Figure 32. Longitudinal profile through upper Knight Inlet both within and outside the channel.

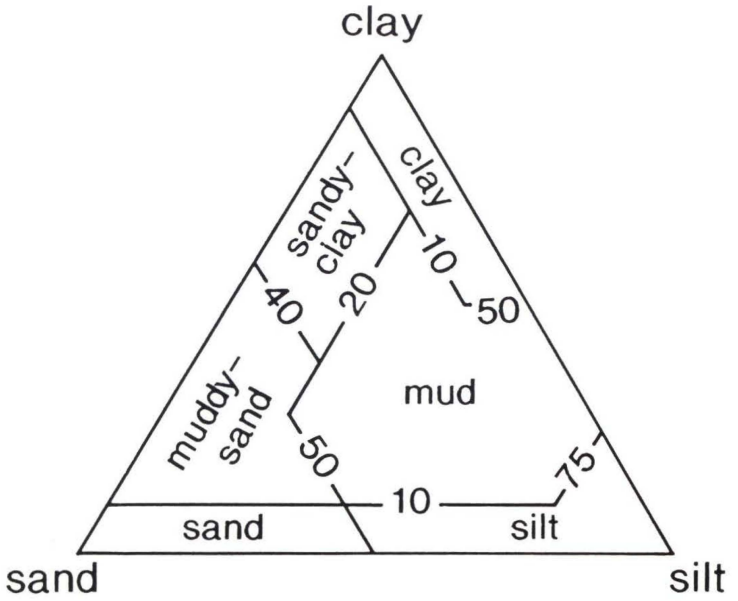

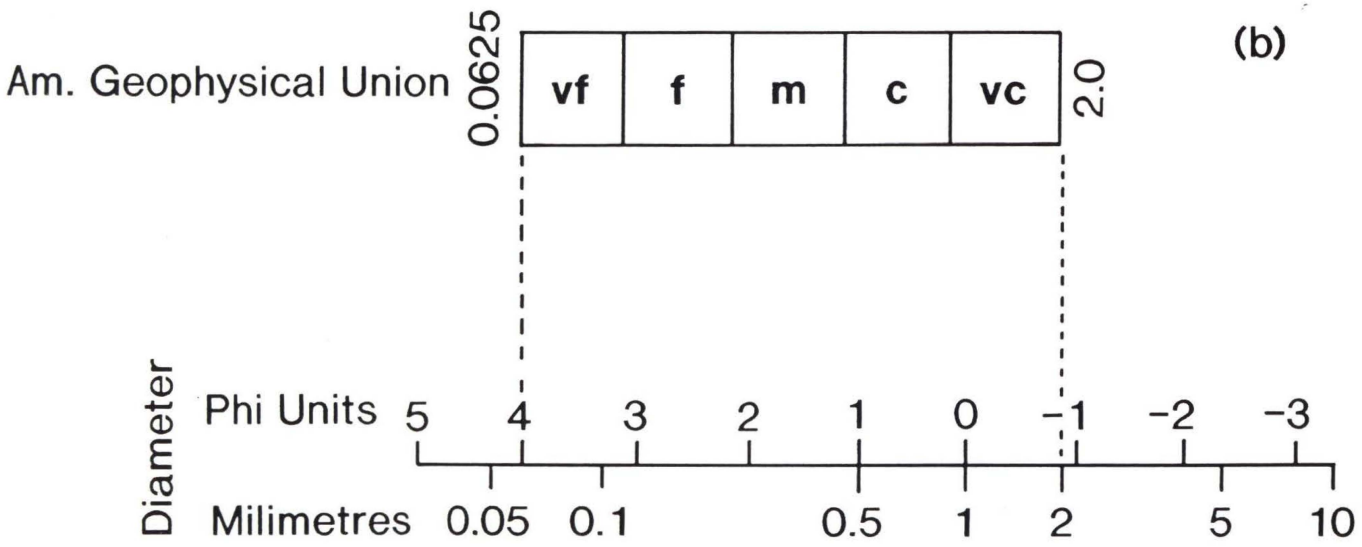

Figure 33. (a). Size limits of sand (vf = very fine; f = fine; m = medium; c = coarse; vc = very coarse); (b) Classification scheme of mixed clastic sediments (after Pettijohn et al., 1972).

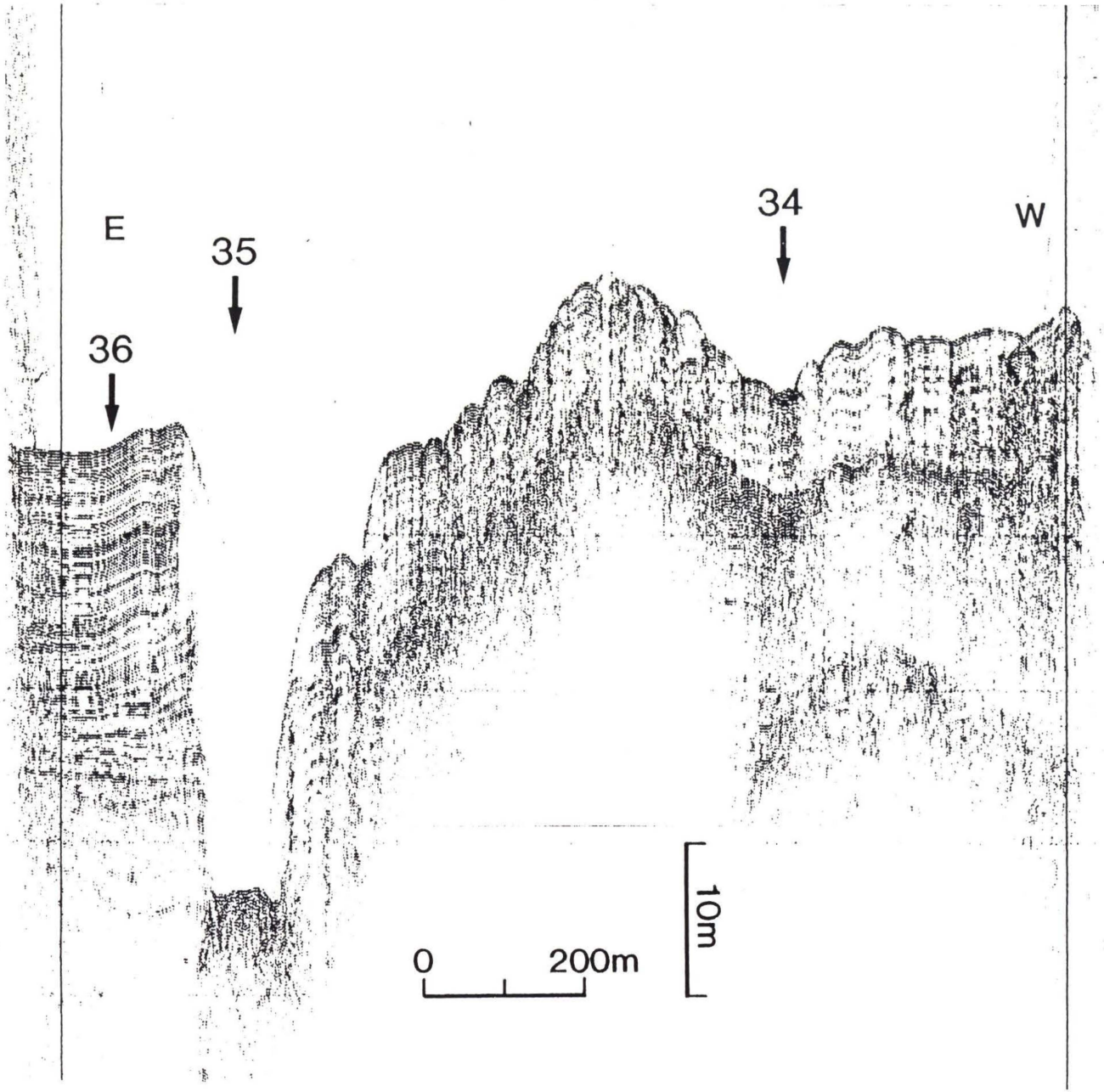

Figure 34. A typical example of grab samples taken from within and outside the channel.

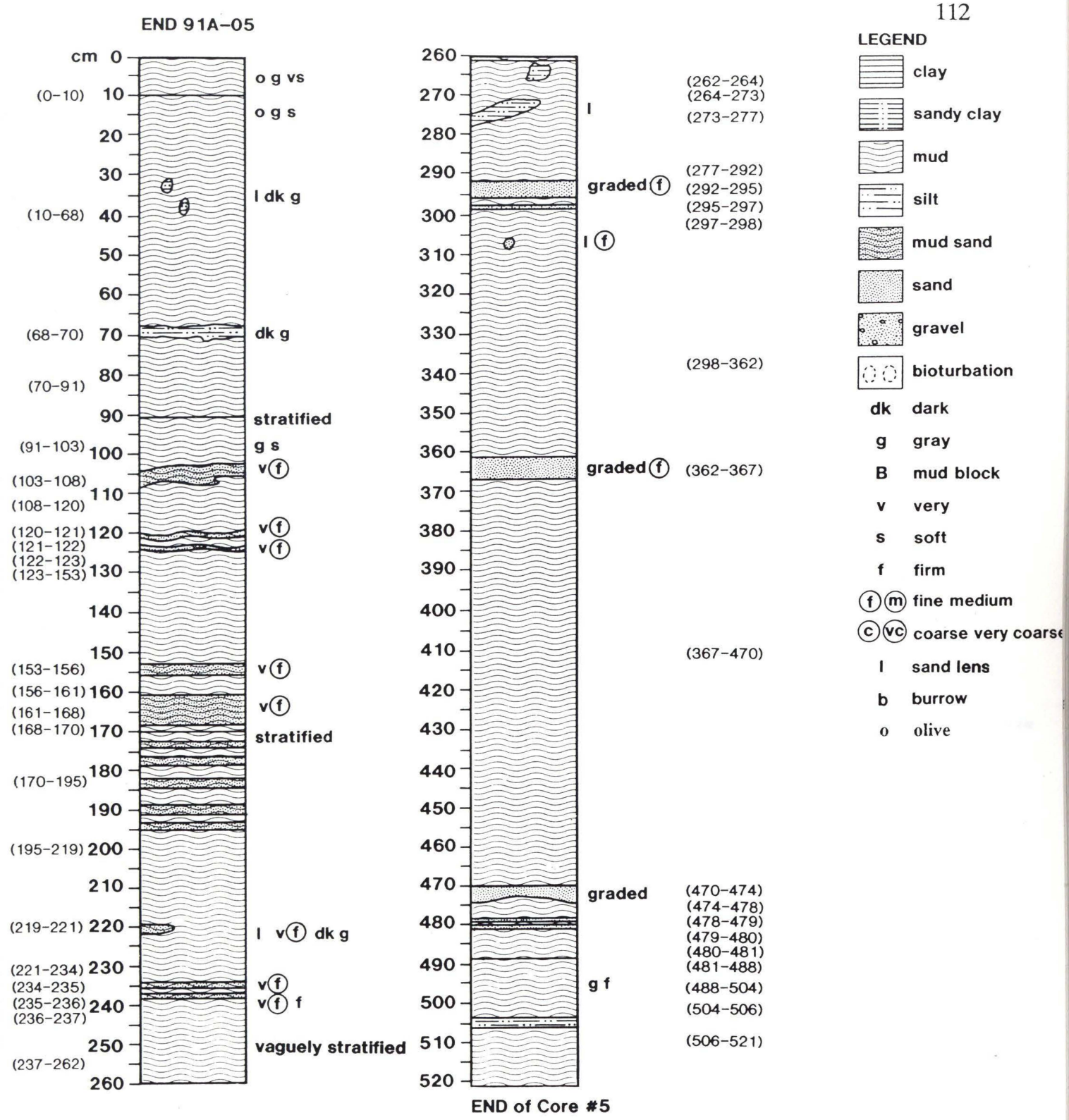

Figure 35. Graphic logs of piston core #5 taken on Knight Inlet, location is shown in Figure 2 and 5.

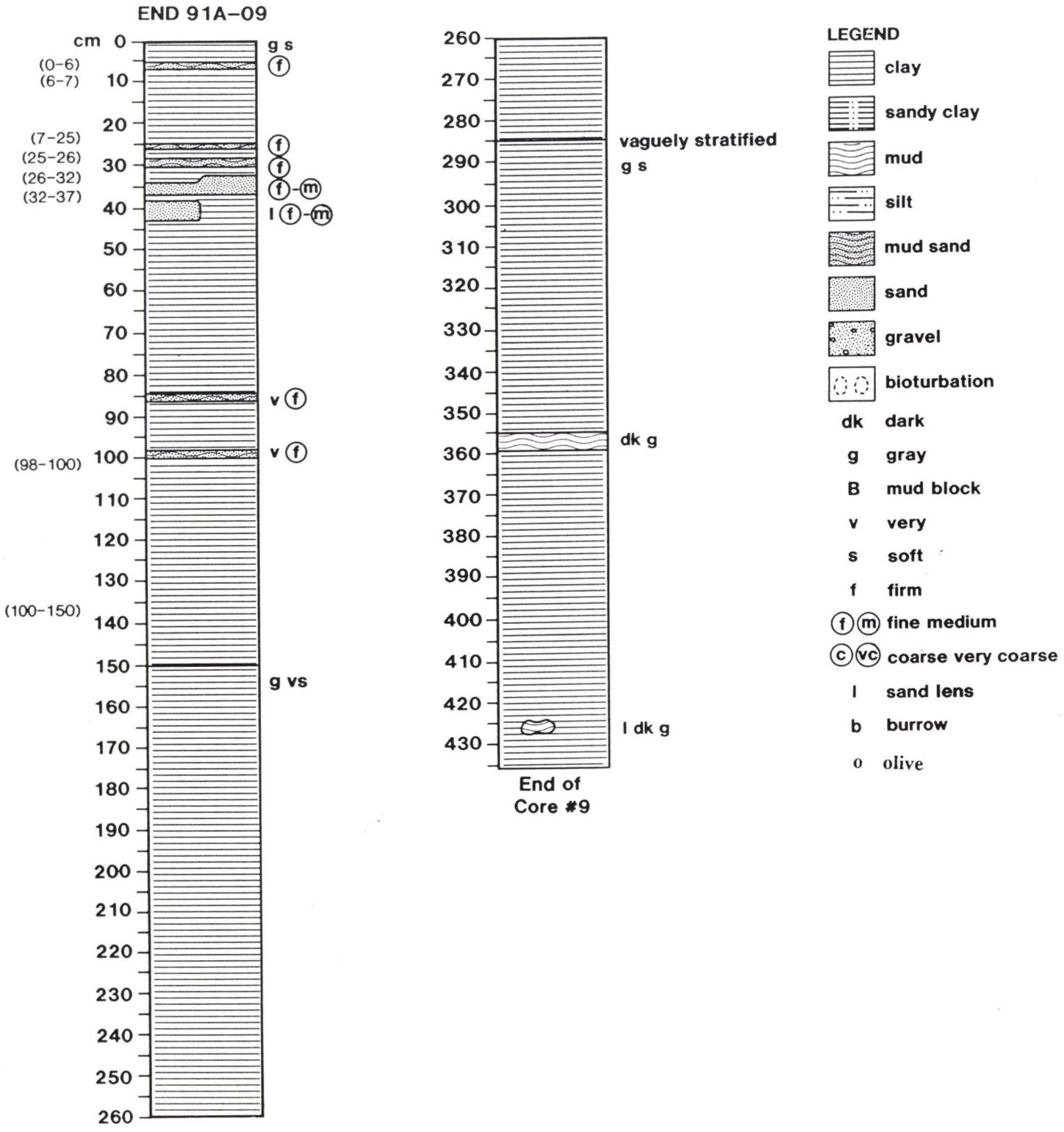

Figure 36. Graphic logs of piston core #9 taken on Knight Inlet, location is shown in Figure 2 and 5.

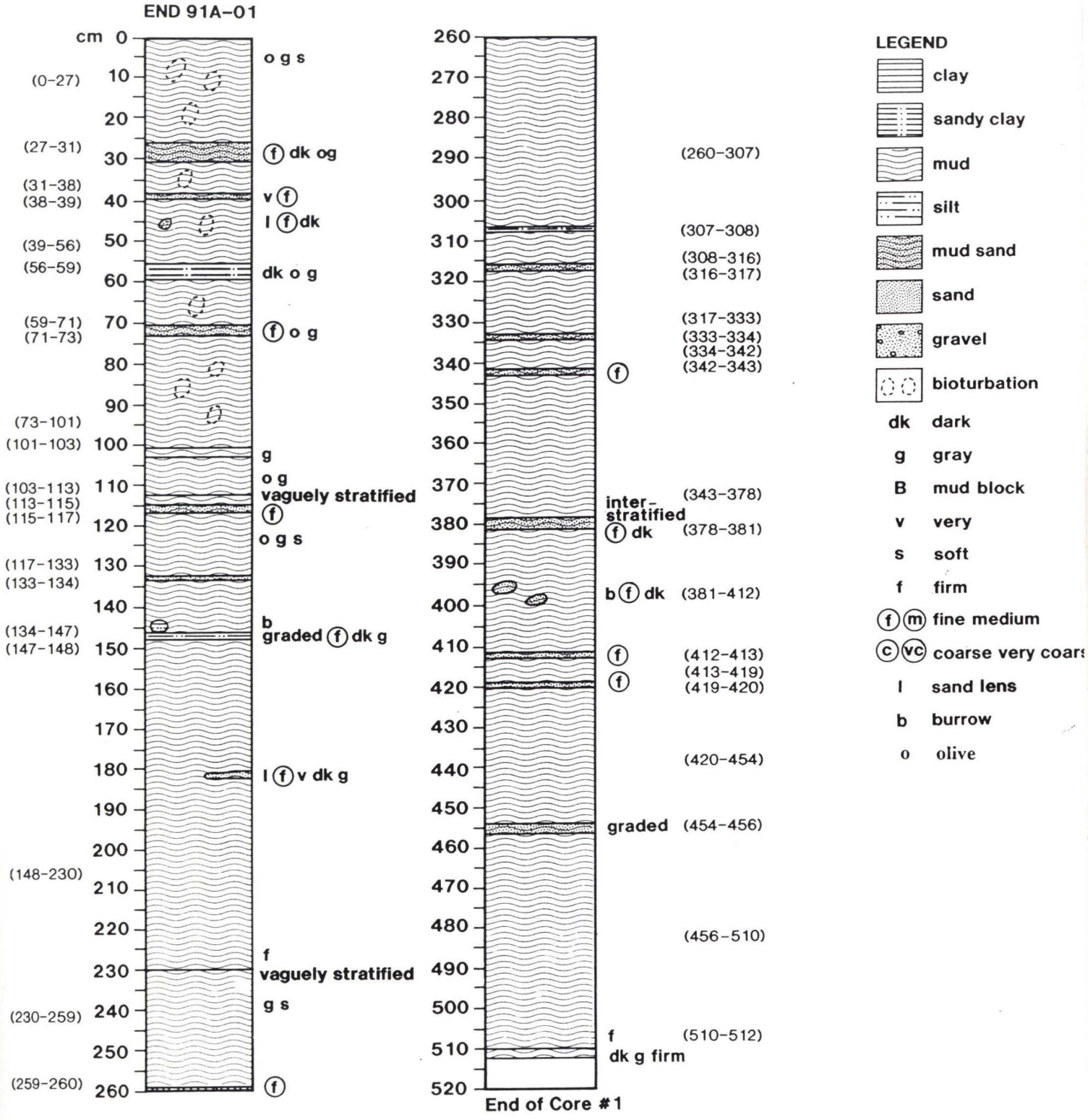

Figure 37. Graphic logs of piston core #1 taken on Knight Inlet, location is shown in Figure 2 and 5.

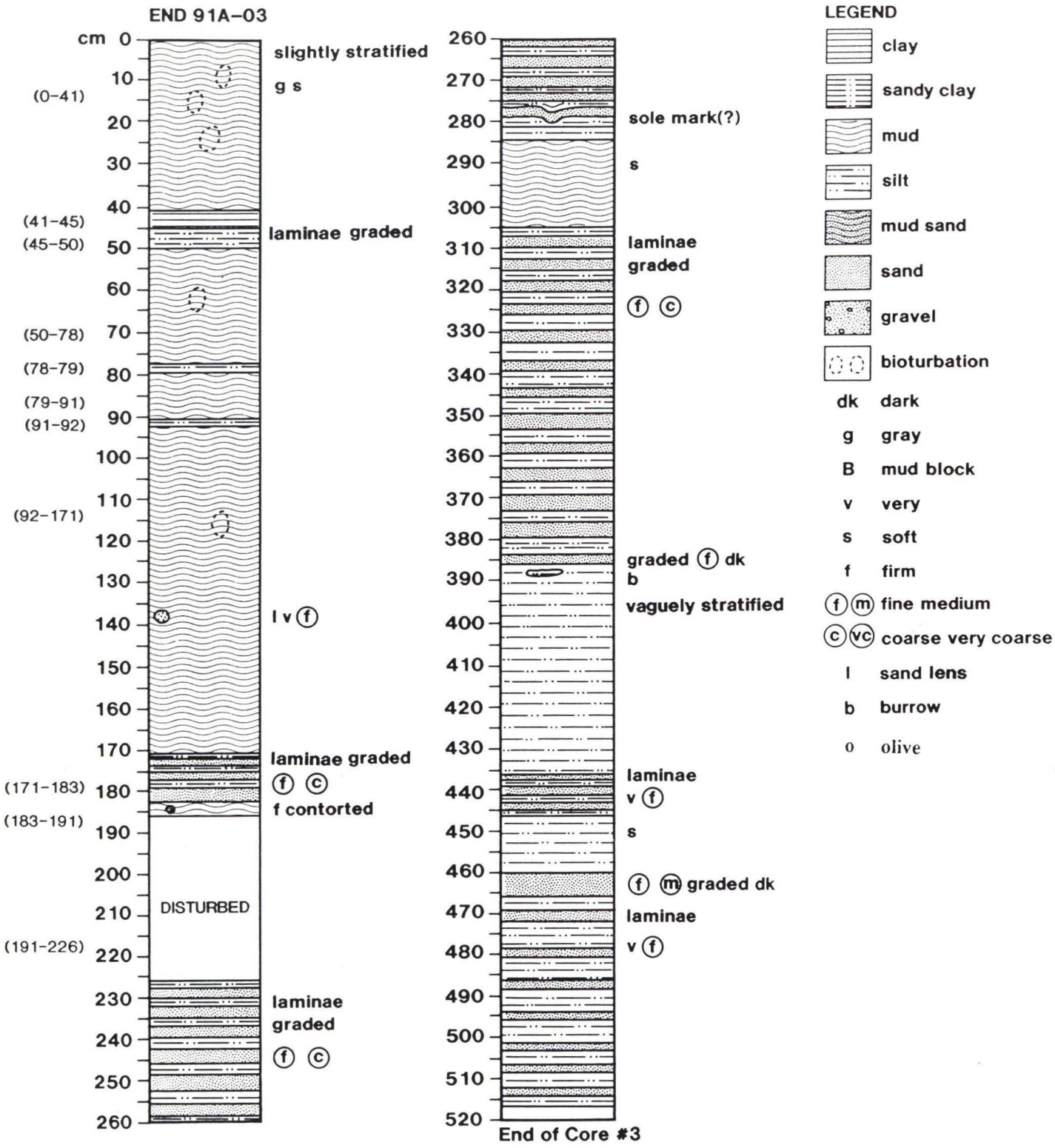

Figure 38. Graphic logs of piston core #3 taken on Knight Inlet, location is shown in Figure 2 and 5.

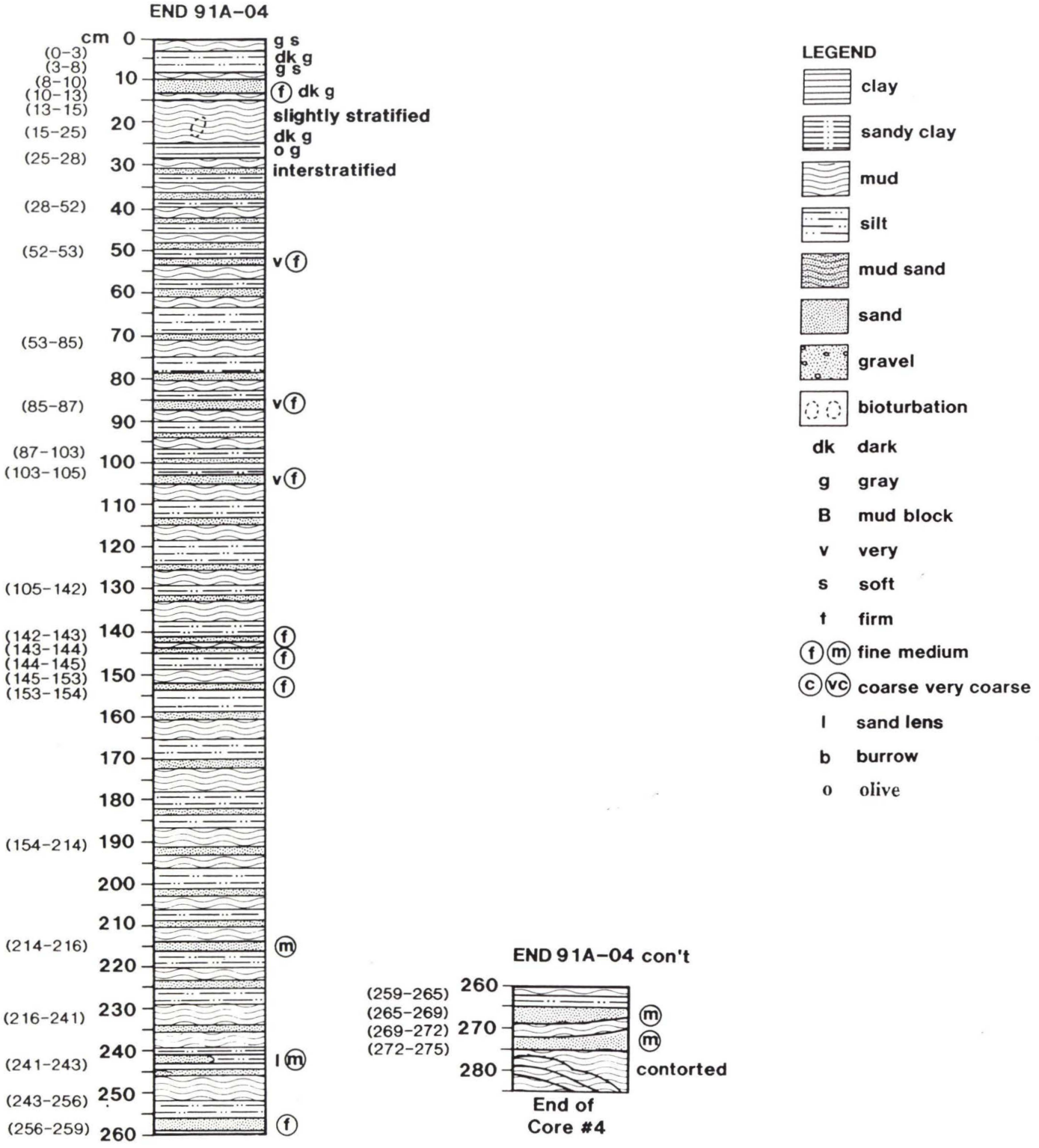

Figure 39. Graphic logs of piston core #4 taken on Knight Inlet, location is shown in Figure 2 and 5.

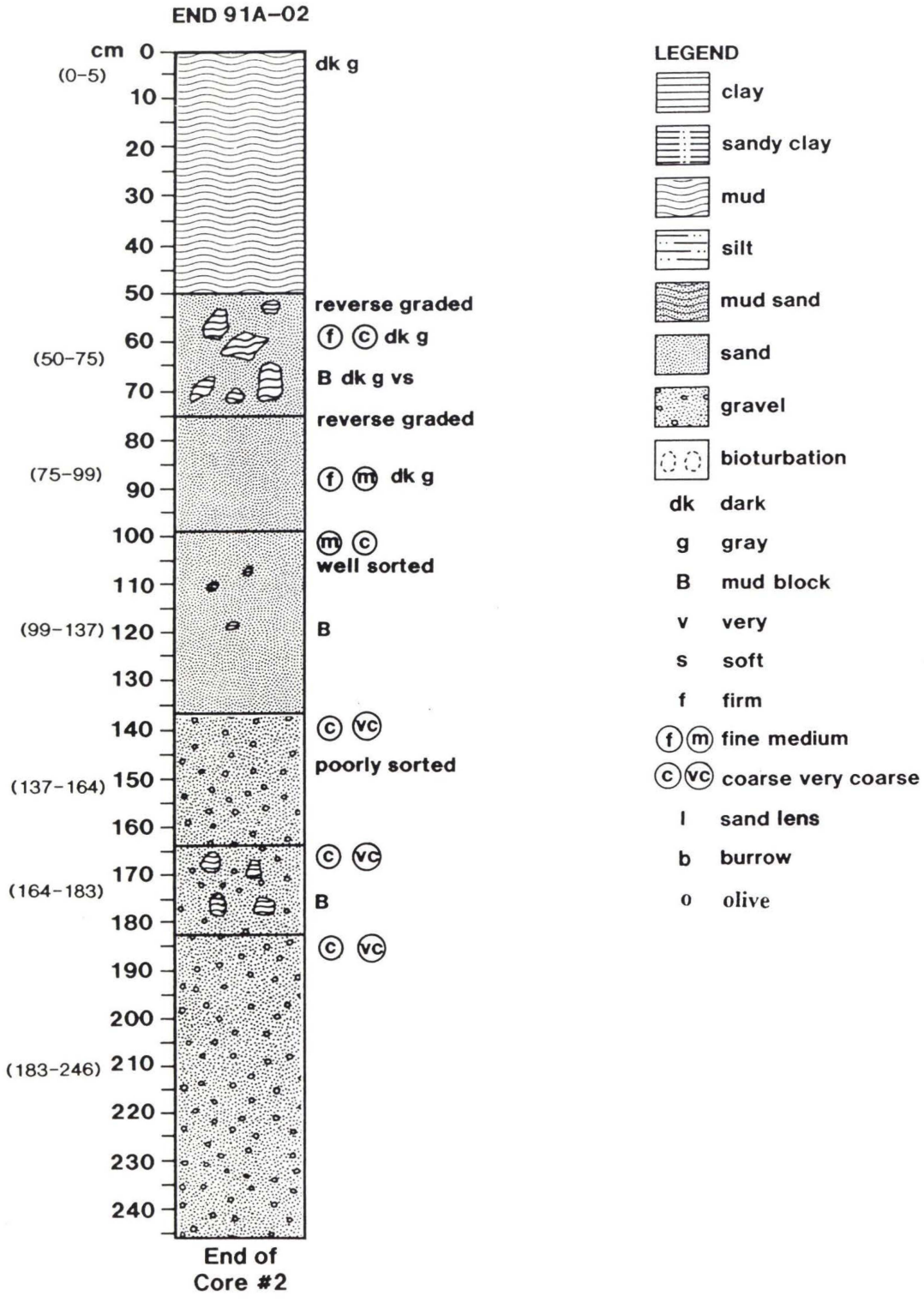

Figure 40. Graphic logs of piston core #2 taken on Knight Inlet, location is shown in Figure 2 and 5.

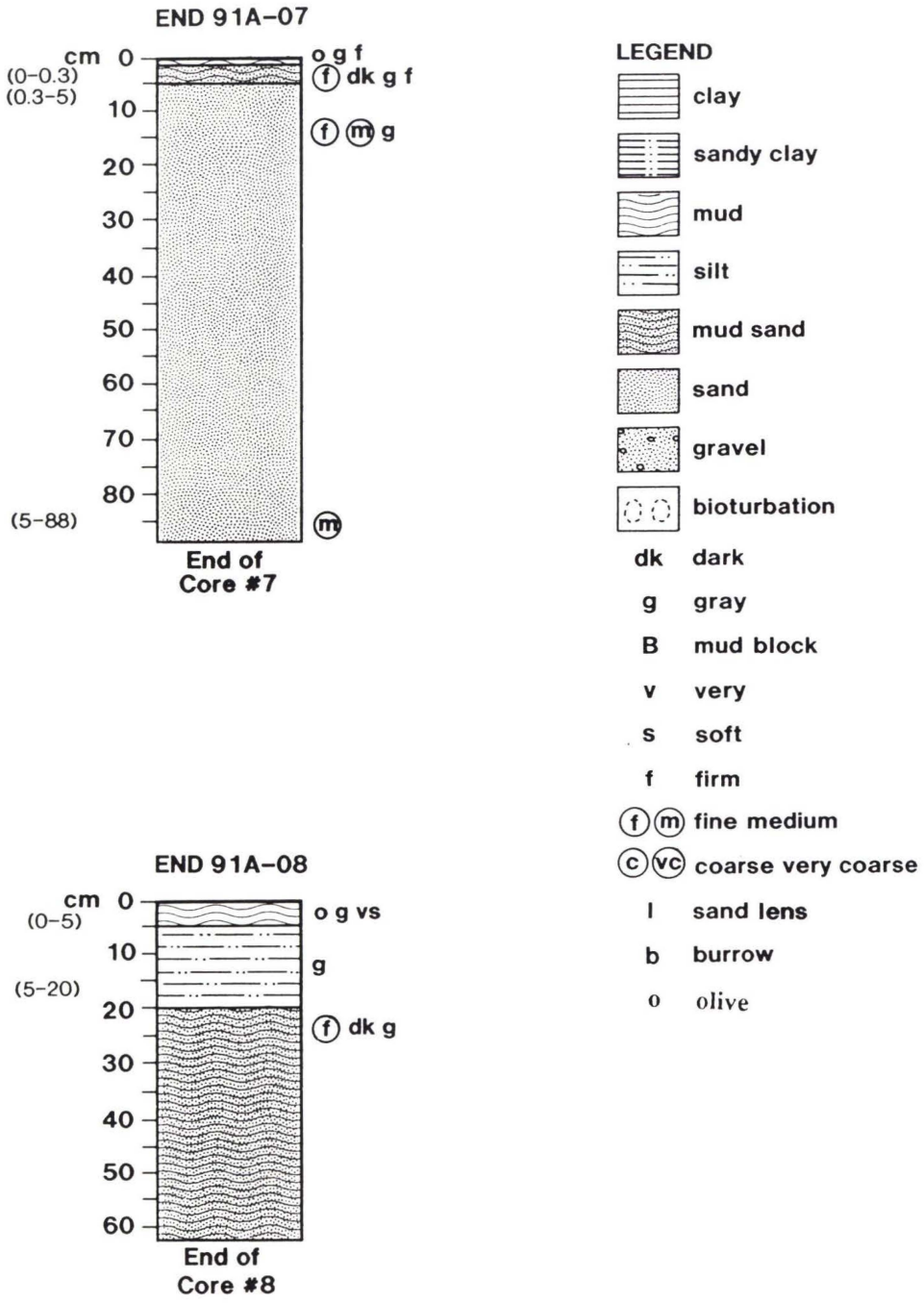

Figure 41. Graphic logs of piston core #7 and #8 taken on Knight Inlet, location is shown in Figure 2 and 5.

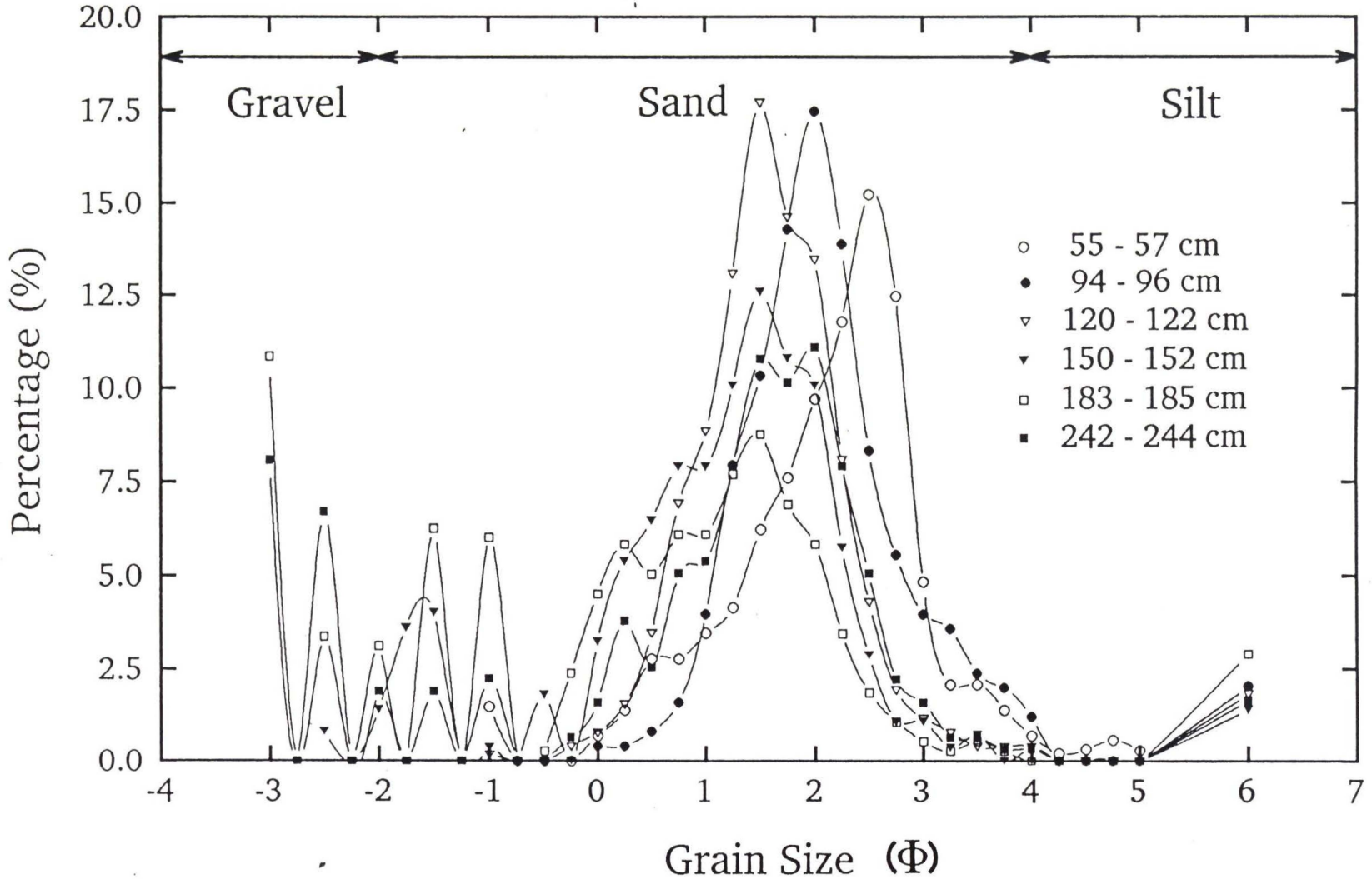

Figure 42. Sediment distributions within core #2 with the depth.

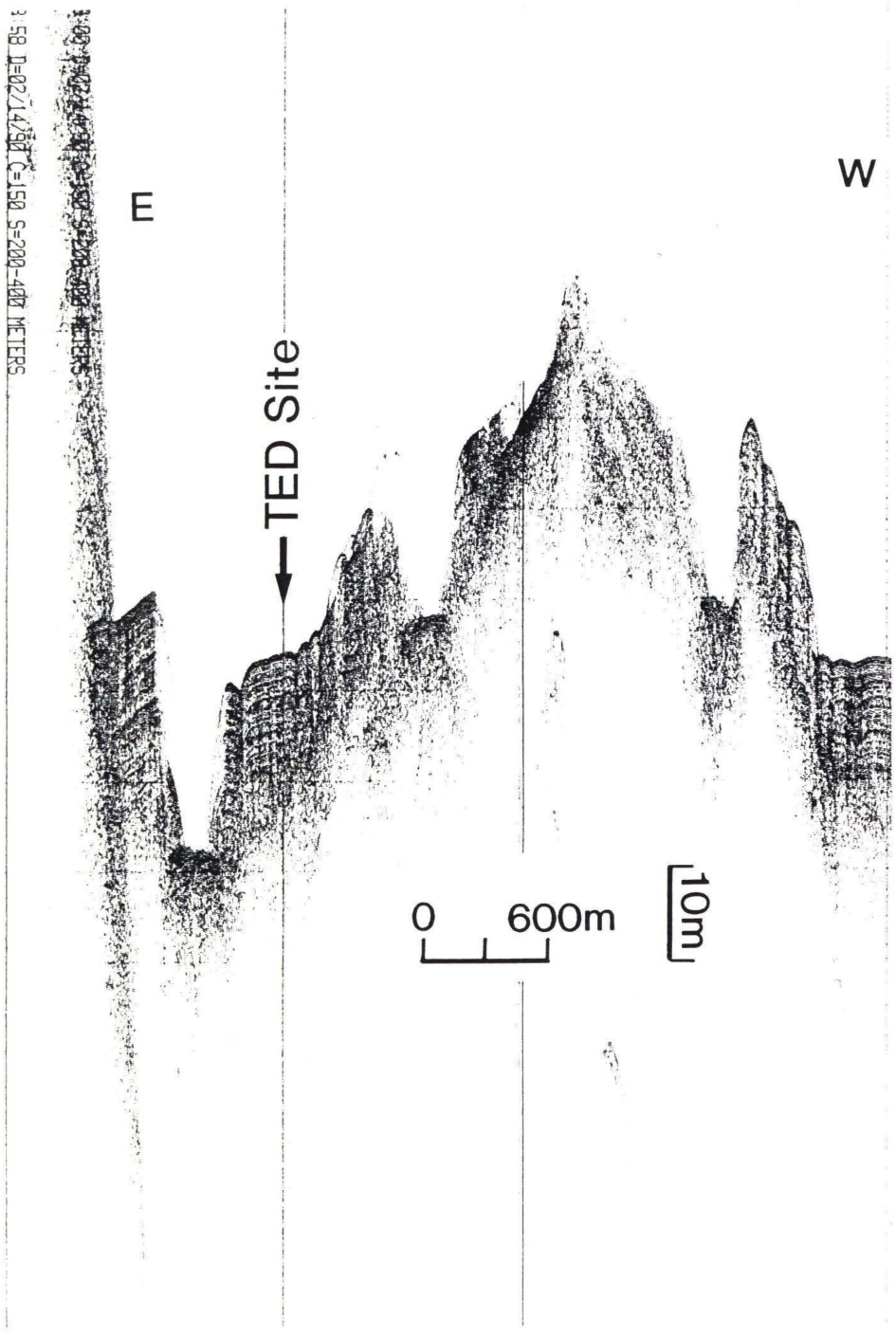

Figure 43. The site of Turbidity Event Detector (TED) installation shown on echosounding profile.

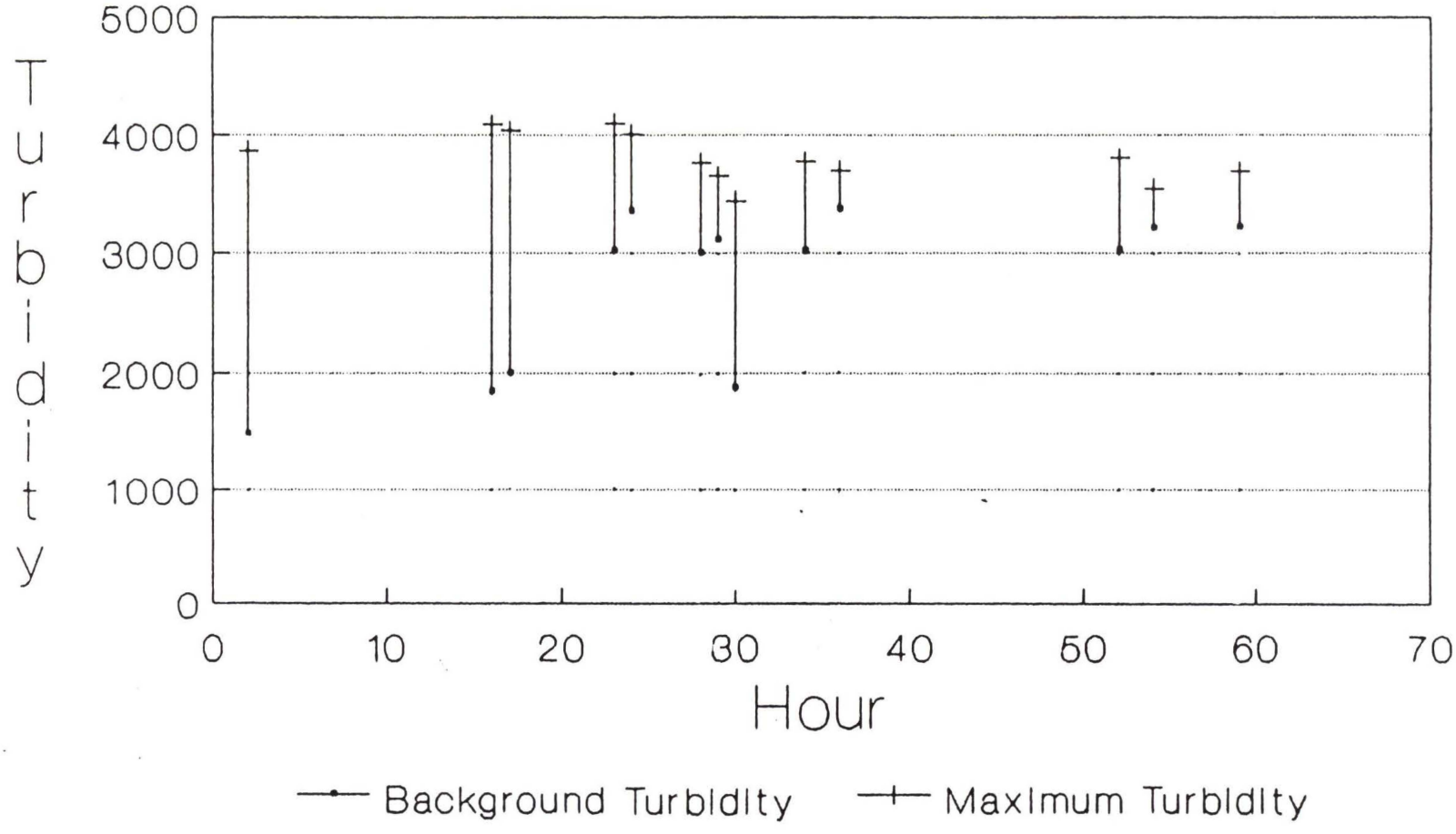

Figure 44. Turbidity events recorded during August 8 to 11, 1991 in Knight Inlet

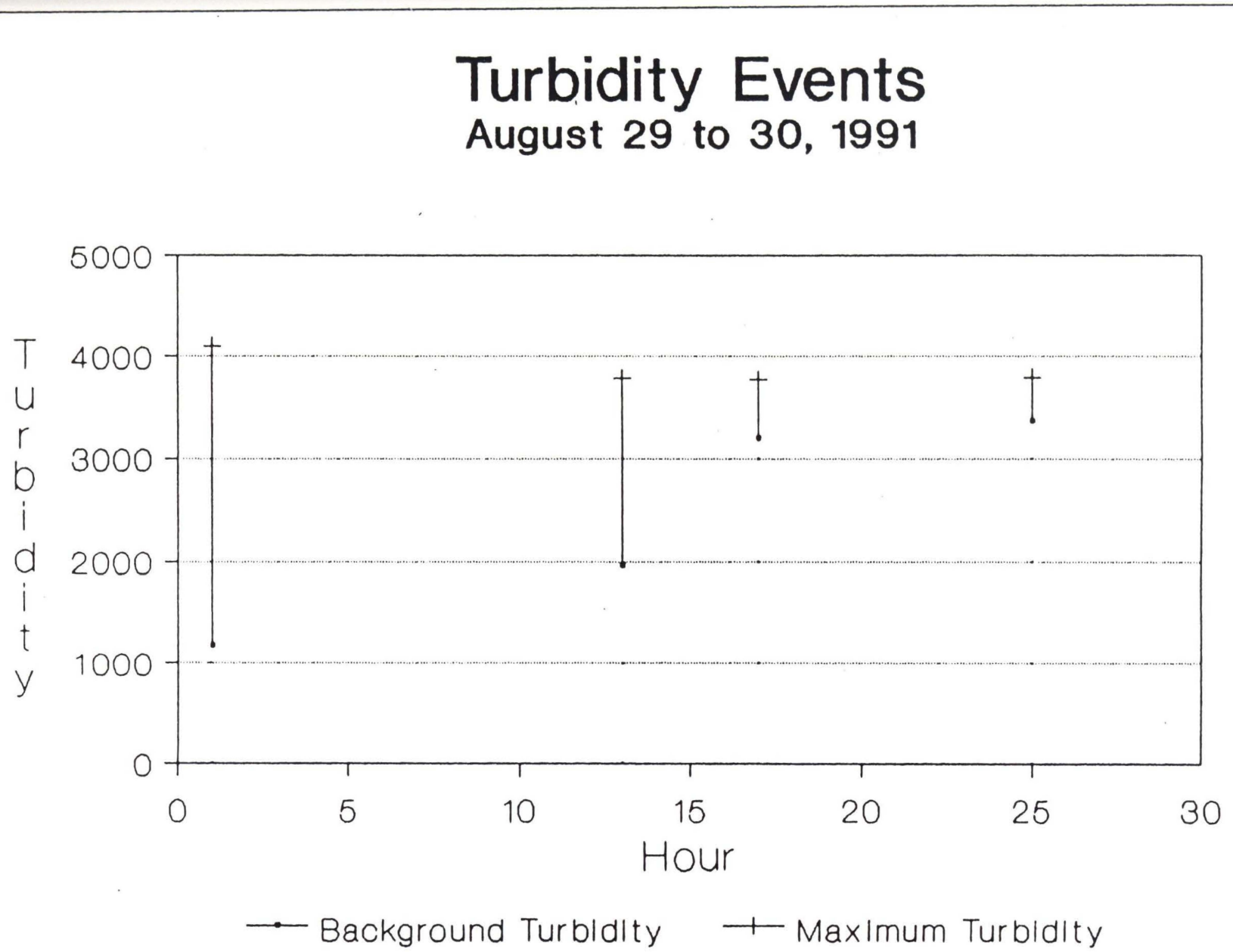

Figure 45. Turbidity events recorded during August 29 to 30, 1991 in Knight Inlet.

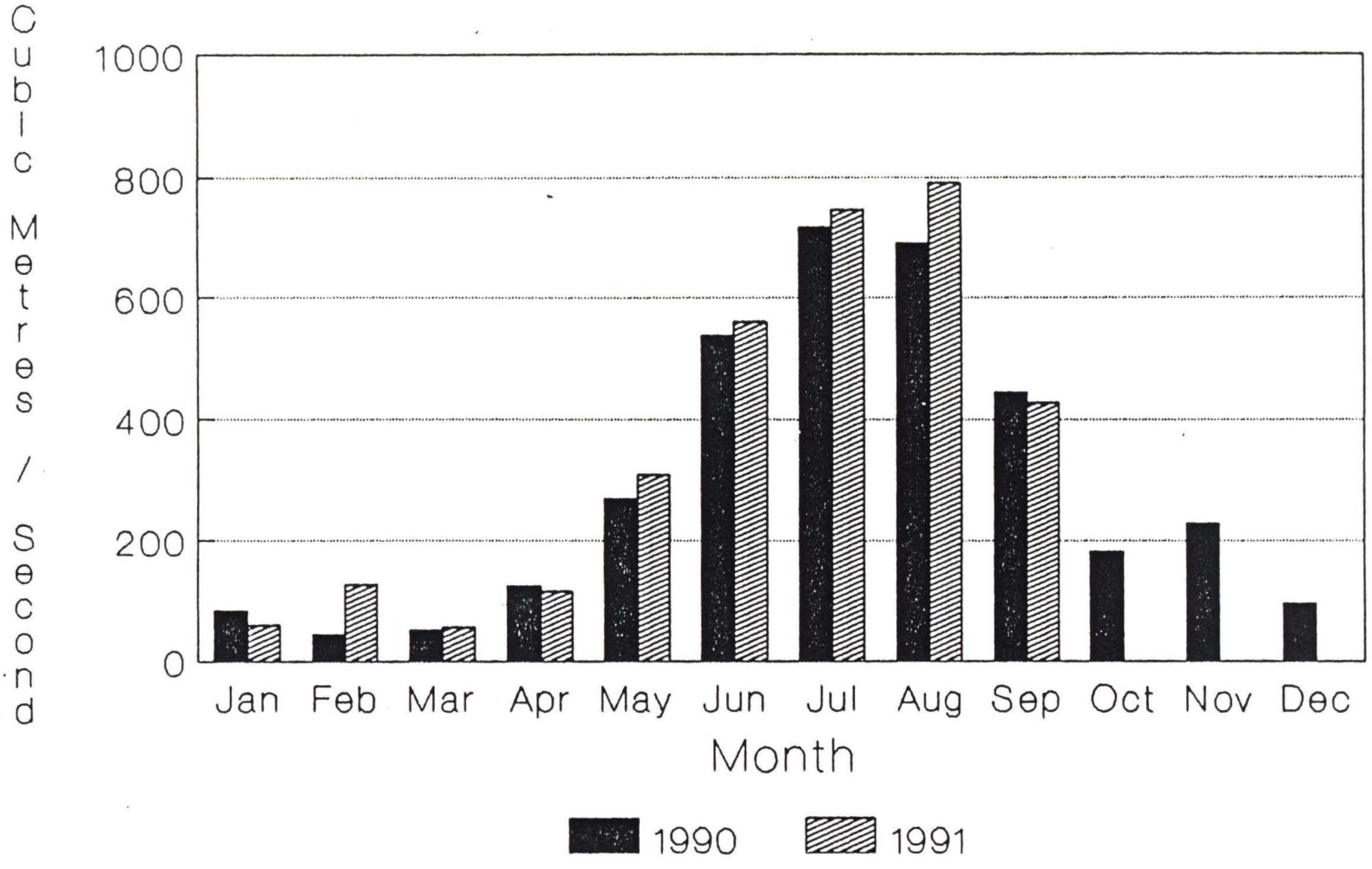

Figure 46. Klinaklini River discharge in 1990, 1991 (monthly average).

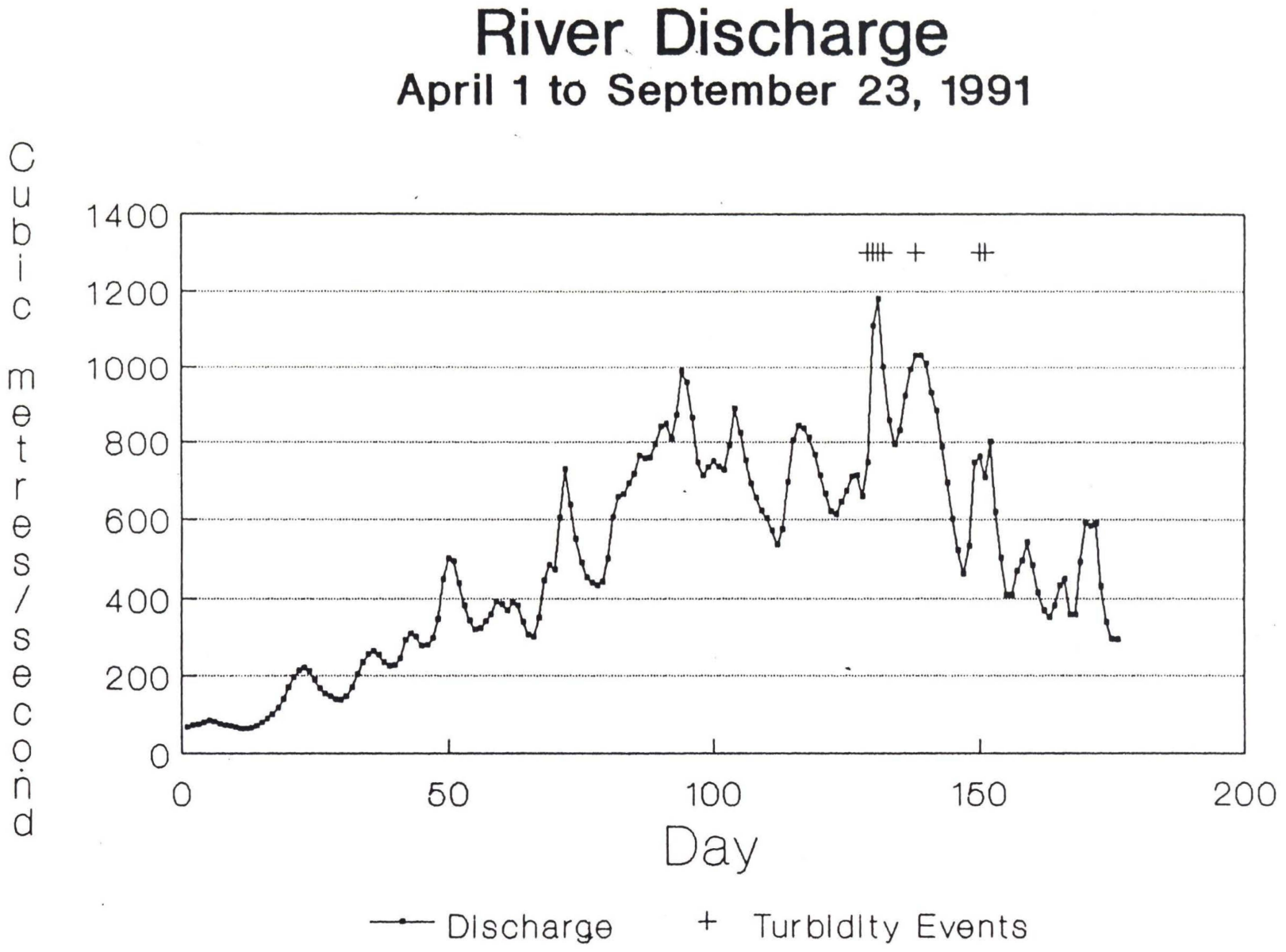

Figure 47. Daily river discharge from April 1 to September 23, 1991 in Knight Inlet.

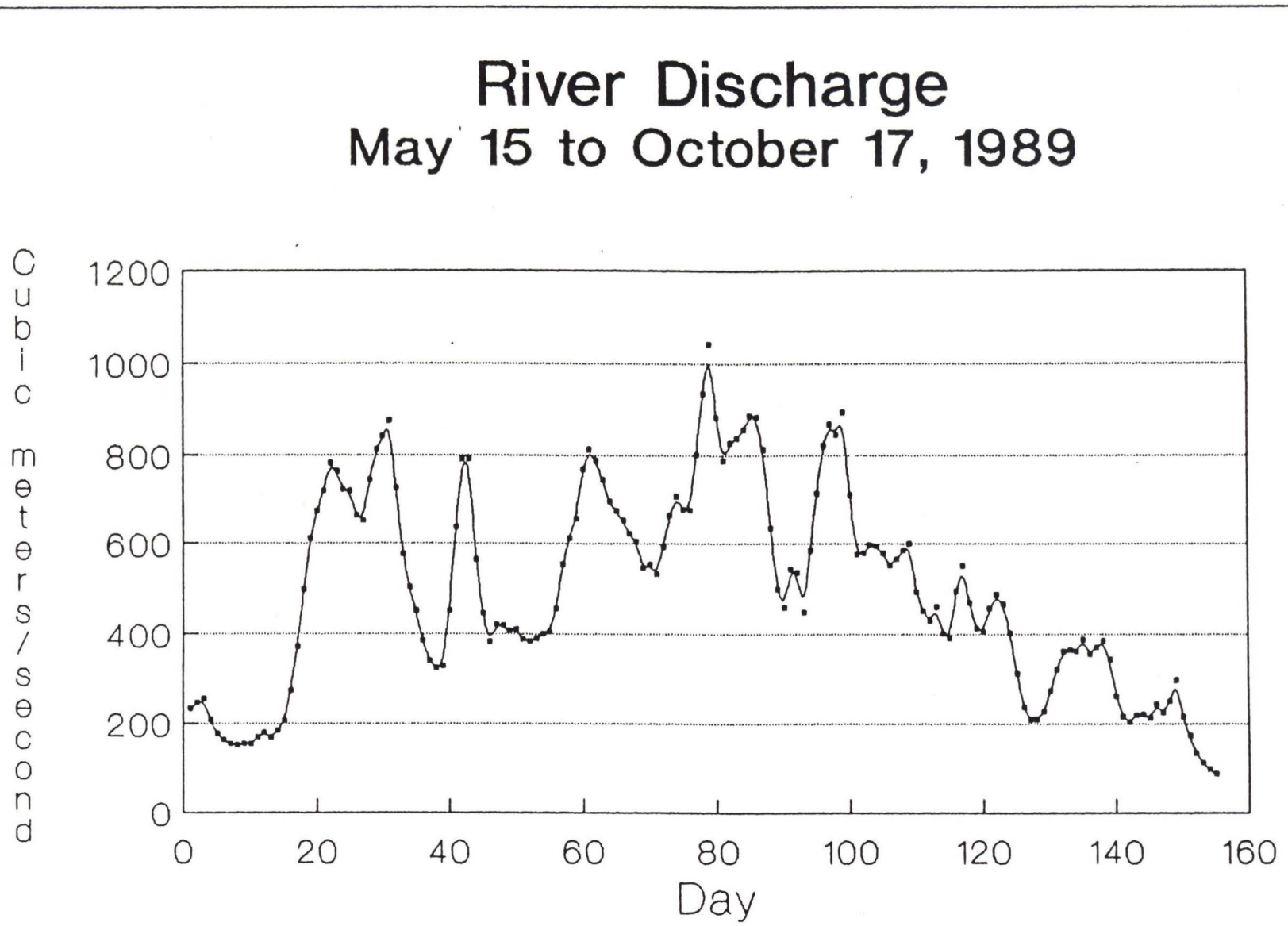

Figure 48. Daily river discharge from May 5 to October 17, 1989 in Bute Inlet.

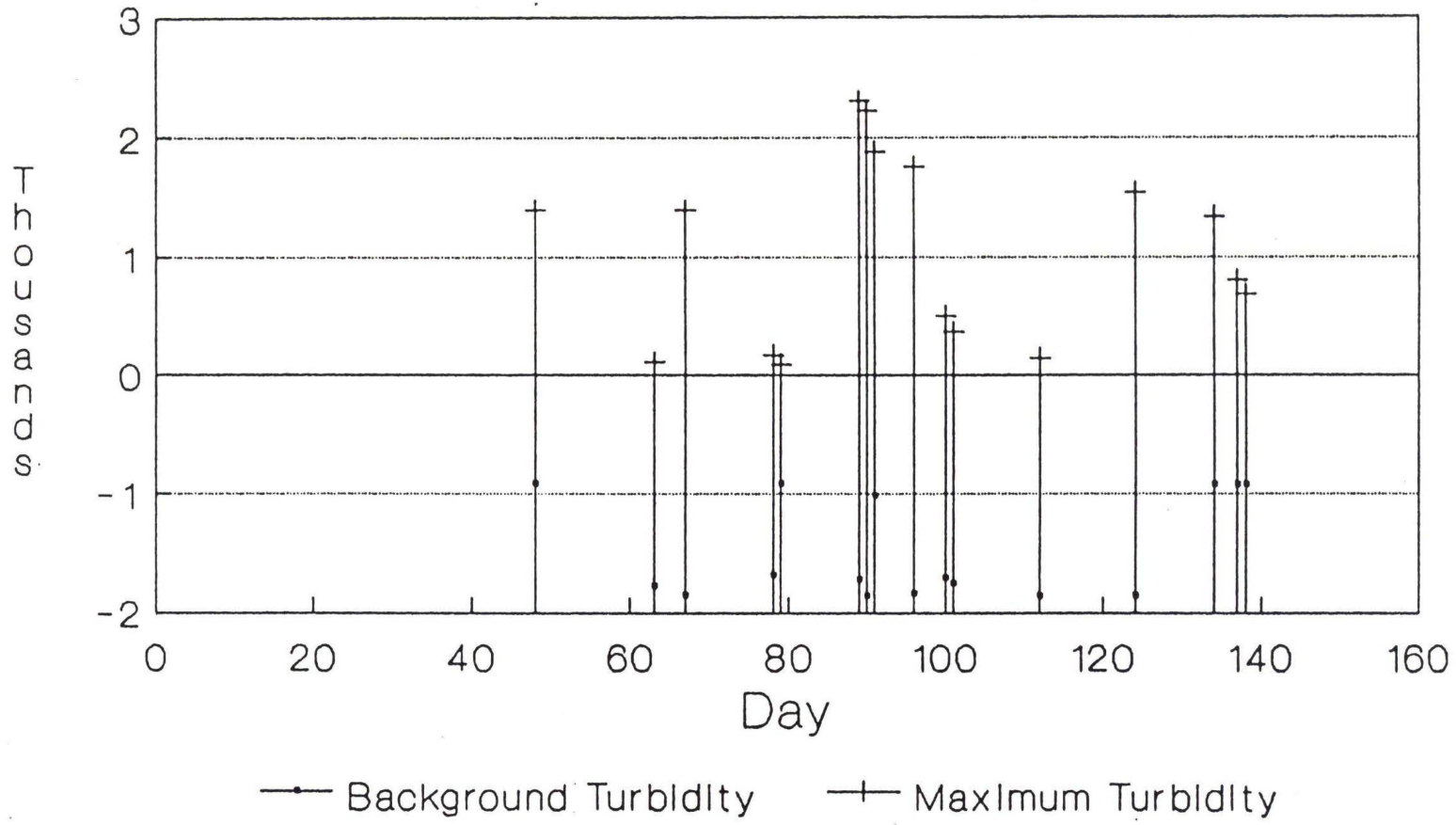

Figure 49. Turbidity events recorded during May 5 to October 17, 1989 in Bute Inlet.

VITA

Surname: Ren | Given Names: Ping

Place of Birth: Shanghai, China | Date of Birth: May 24, 1960

Educational Institutes Attended:

Hangzhou University	1978 to 1982
University of Victoria	1989 to 1992

Degrees Awarded:

B.Sc.	Hangzhou University	1982

PARTIAL COPYRIGHT LICENSE

I hereby grant the right to lend my thesis (or dissertation) to users of the University of Victoria Library, and to make single copies only for such users or in response to a request from the Library of any other university, or similar institution, on its behalf or for one of its users. I further agree that permission for extensive copying of this thesis for scholarly purpose may be granted by me or a member of the University designated by me. It is understood that copying or publication of this thesis for financial gain shall not be allowed without my written permission.

Title of Thesis:

Seafloor Morphology and Sedimentary Processes
in Knight Inlet, British Columbia

Author [redacted]
(Signature)

PING REN

August 7, 1992

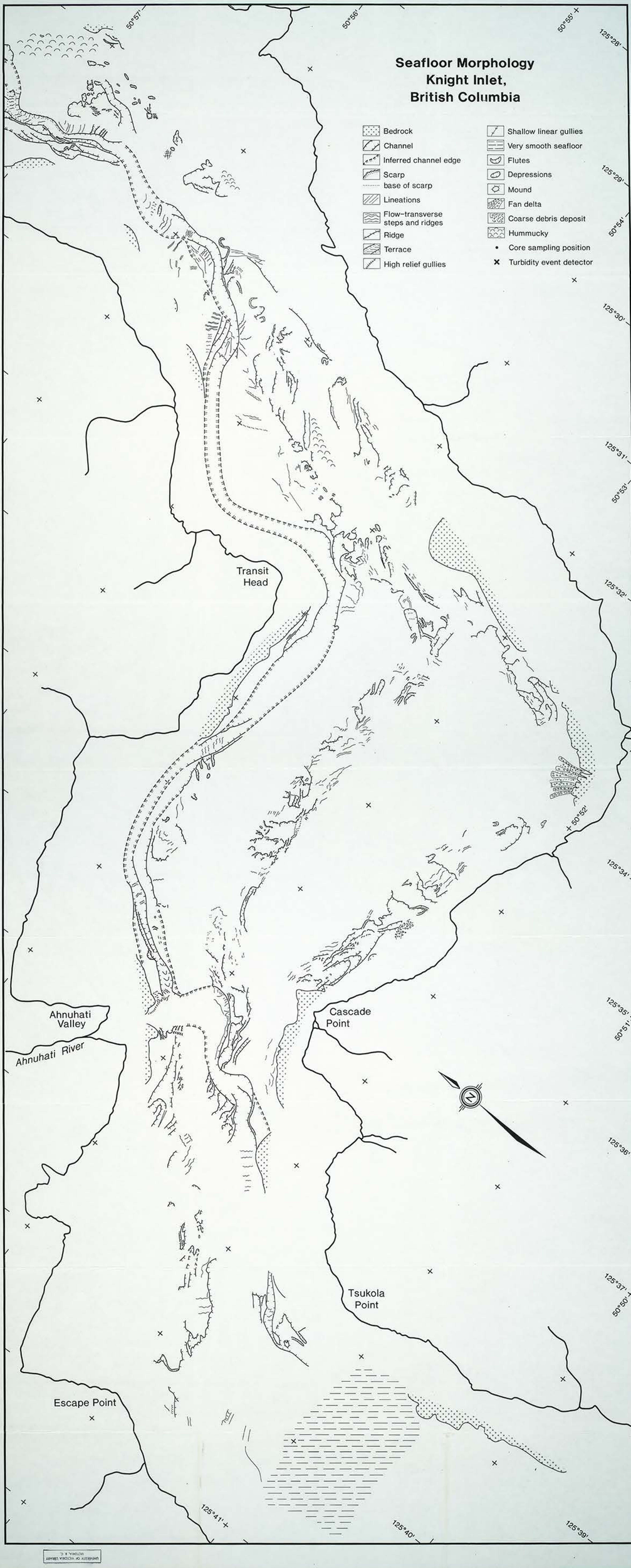

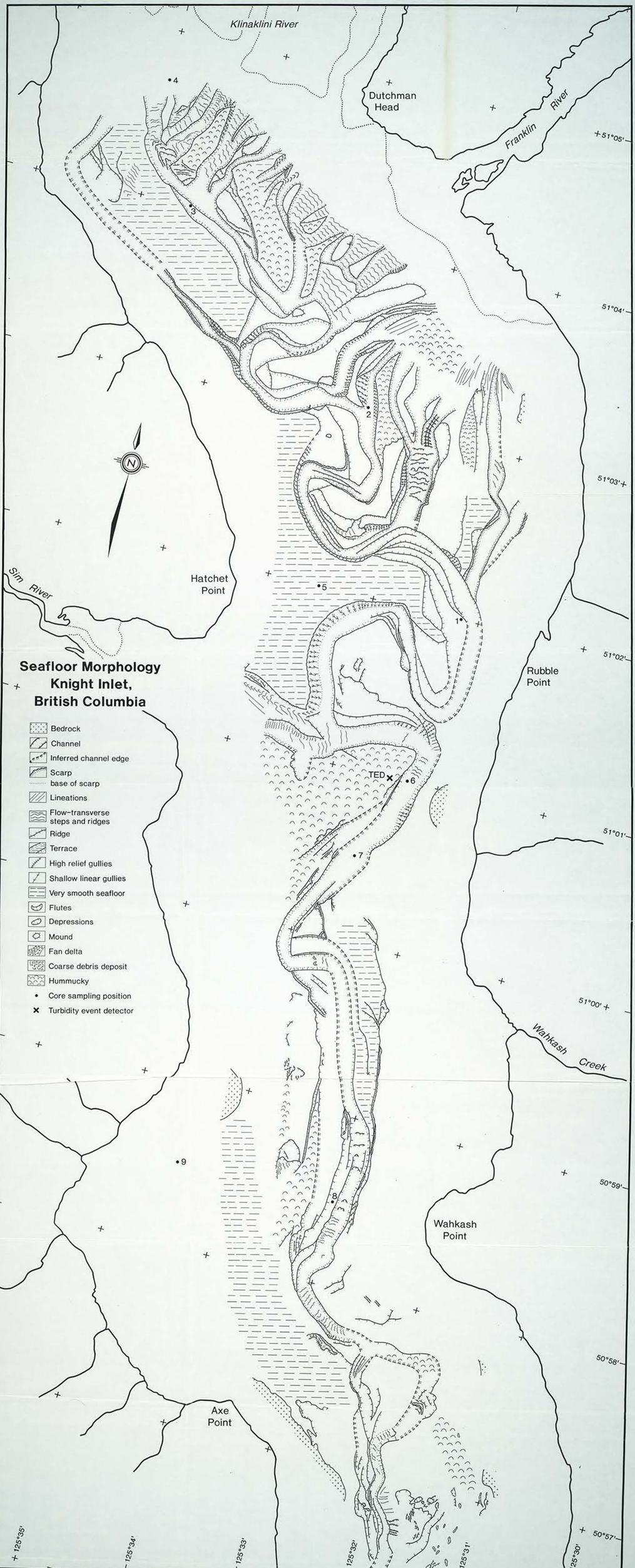

Seafloor Morphology Knight Inlet, British Columbia

- Bedrock
- Channel
- Inferred channel edge
- Scarp
  base of scarp
- Lineations
- Flow-transverse steps and ridges
- Ridge
- Terrace
- High relief gullies
- Shallow linear gullies
- Very smooth seafloor
- Flutes
- Depressions
- Mound
- Fan delta
- Coarse debris deposit
- Hummucky
- • Core sampling position
- × Turbidity event detector